Title

Template-based syntheses for shape controlled nanostructures

Authors

Pérez-Page, M

Yu, E

Li, J

et al.

Publication Date

2016-08-01

DOI

10.1016/j.cis.2016.04.001

Peer reviewed

Advances in Colloid and Interface Science 234 (2016) 51–79

Contents lists available at ScienceDirect

Advances in Colloid and Interface Science

journal homepage: www.elsevier.com/locate/cis

Template-based syntheses for shape controlled nanostructures☆

María Pérez-Page [a], Erick Yu [a,b], Jun Li [a], Masoud Rahman [a], Daniel M. Dryden [a,b], Ruxandra Vidu [a,b], Pieter Stroeve [a,*]

[a] Department of Chemical Engineering, University of California Davis, Davis, CA, 95616, United States
[b] Department of Materials Science and Engineering, University of California Davis, Davis, CA, 95616, United States

ARTICLE INFO

Available online 20 April 2016

Keywords:
Template-based synthesis
Nanostructured materials
Template-filling methods
Nanoporous membrane templates

ABSTRACT

A variety of nanostructured materials are produced through template-based synthesis methods, including zero-dimensional, one-dimensional, and two-dimensional structures. These span different forms such as nanoparticles, nanowires, nanotubes, nanoflakes, and nanosheets. Many physical characteristics of these materials such as the shape and size can be finely controlled through template selection and as a result, their properties as well. Reviewed here are several examples of these nanomaterials, with emphasis specifically on the templates and synthesis routes used to produce the final nanostructures. In the first section, the templates have been discussed while in the second section, their corresponding synthesis methods have been briefly reviewed, and lastly in the third section, applications of the materials themselves are highlighted. Some examples of the templates frequently encountered are organic structure directing agents, surfactants, polymers, carbon frameworks, colloidal sol–gels, inorganic frameworks, and nanoporous membranes. Synthesis methods that adopt these templates include emulsion-based routes and template-filling approaches, such as self-assembly, electrodeposition, electroless deposition, vapor deposition, and other methods including layer-by-layer and lithography. Template-based synthesized nanomaterials are frequently encountered in select fields such as solar energy, thermoelectric materials, catalysis, biomedical applications, and magnetowetting of surfaces.

Contents

☆ Dedicated to Professor Eli Ruckenstein on the occasion of his 90th birthday.

* Corresponding author.
E-mail address: pstroeve@ucdavis.edu (P. Stroeve).

http://dx.doi.org/10.1016/j.cis.2016.04.001
0001-8686/

1. Introduction

Nanostructured materials have attracted considerable attention in recent years. Control over size, shape, and morphology of nanostructures is the most important advantage of template-based synthesis and can produce chemical and physical properties that differ markedly from those of the bulk materials. Many different template materials are available, and depending on their type and structure, a wide range of nanomaterials can be synthesized. The general mechanism for template synthesis includes three principal stages, the template preparation, directed synthesis of the target material using the template, and template removal [1].

Covered in this review are a variety of template-based methodologies that govern the synthesis of some notable nanostructured materials, including zeolites, mesoporous silica, semiconducting nanoparticles, nanowires, nanotubes, and thin films. Although template-based syntheses encompass a tremendously broad range of methodologies, they share striking similarities in regard to their underlying principle and mechanism. The types of templates, ranging from organic molecules to membranes, are discussed, along with their corresponding common synthesis methods and applications.

Two classic examples of heavily template-controlled nanomaterials are mesoporous silica and zeolites. Both owe their nanoporous structure to the templates used to produce them. Characterized by their high surface area and uniform porous structure, mesoporous silica nanoparticles (MSNs) have an incredible degree of variability in their synthesis, and as a result, final structure, due to the multitude of parameters in templates. MSNs can be synthesized into a variety of shapes, including solid and hollow spheres, rods, and irregular forms often named differently from one source to another (e.g. “doughnut”). Likewise, the crystalline structure, such as hexagonal, cubic, and irregular frameworks, introduces a broad diversity into MSNs. The combinations of the physical shape with variations in porous structure are astonishingly widespread as documented in literature. The principle behind MSN formation is very straightforward. The widely used surfactant-template method to synthesize MSNs was discovered originally by scientists at Exxon Mobil in 1992 [2]. Since its discovery, the sol–gel method for synthesizing MSNs, as it is named aptly due to the semi-solid and liquid state during which the silica framework formed, became the basis for which MSNs were produced. The sol–gel synthesis method in principle requires two constituents, a silica source and a templating agent. The former provides the silica, which forms the framework around the pore-determining template. While the silica sources are typically tetraorthosilicates such as tetraethyl orthosilicate (TEOS), other sources including silica fume [3], ash [4], and electronic waste [5] have been used successfully. The templating agent and its impact on the MSN structure are discussed in greater depth in Section 3.1.

Zeolites are nanostructured, crystalline aluminosilicates containing pores and cavities of molecular dimensions. Many occur as natural minerals, but it is the synthetic varieties, which are among the most widely used sorbents, catalysts, and ion-exchange materials in the world. Zeolite crystals are porous on a molecular scale with their structures revealing regular arrays of channels and cavities (3–15 Å), thus creating a nanoscale labyrinth, which can be filled with water or other guest molecules. Zeolites are aluminosilicates with tetrahedrally connected framework structures based on corner-sharing aluminate (AlO_4) and silicate (SiO_4) tetrahedrons [6,7]. These tetrahedrons can arrange themselves in many unique ways, giving rise to the many different types of zeolites. The aluminum exists in Al^{+3} oxidation state bonded to four oxygen atoms, resulting in a net negative charge for each aluminum atom to the framework. Silicon exists in Si^{+4} oxidation state bonded to four oxygen anions, each shared between two silicon atoms, resulting in no net charge. The overall charge of the framework depends on aluminum content only. A high Si/Al ratio gives to the zeolites a high thermal stability [6,7]. The first zeolite was prepared in 1950s under hydrothermal conditions in basic aqueous media and using inorganic cations as charge-balancing species [8–10]. Since then, many approaches have been made which have enabled the discovery a large number of new zeolite framework types. Detailed historical perspectives on the evolution of zeolite synthesis have been written by Flanigen et al. [11] and some years later by Cundy et al. [9,12]. Many zeolites can be made using only inorganic reactants, and all the phases studied up to 1961, such as the classical synthetic zeolites A, X, and Y, were synthesized in this manner. However, in the 1960s the use of organic compounds, particularly quaternary ammonium salts, to make zeolites increased. These organic compounds are often referred to as templates since the zeolite structure appears to form around them, in some cases encapsulating them with a very close fit between the organic groups and the pore walls. Currently, zeolites can be synthesized from small organic structure directing agents (OSDAS), ionic surfactants and liquids, non-

ionic and amphiphilic surfactants, carbon frameworks and natural templates.

Metallic and semiconducting nanostructures including nanowires, nanotubes, and unusual nanomushrooms have been subjects of intense research across many applications including electronics [13], photonics [14], magnetics [15], and biological sensing [16]. Their uniform and large aspect ratio provides a range of intriguing quantum size effects, while maintaining classical behavior in the axial direction. Template methods for nanowire synthesis were first demonstrated in the 1970s and achieved widespread popularity in the 1990s and onward, with template materials ranging from porous bulk media [17] to self-assembly of macromolecules [18] and biological species [19]. While bulk, one-dimensional nanowires and nanotubes can be produced via deposition techniques onto existing nanowires and nanofibers, it is often advantageous to use well-ordered templates to direct the synthesis or fabrication of nanowire/nanotube two-dimensional arrays. In particular, templates such as anodic alumina oxide (AAO) and polycarbonate track-etched (PCTE) membranes have widespread usage in producing highly uniform arrays of nanowire and nanotubes as a result of deposition into the porous channels of the membrane. Control over the final geometry and size depends on the porous membrane, with AAO and PCTE membranes ranging from 1 to 1000 nm in diameter and lengths upwards to 100 μm in length. In other instances, nanomushroom morphologies, usually a result of overgrowth on a porous template, provide a convenient means for in situ or ex situ functionalization of individual nanowires [20], useful in measuring their properties or creating single-wire devices.

2. Nanostructures and their templates

In the following section, different nanostructured materials, classified under zero, one, or two-dimensional geometry and examples of the templates used to produce such structures are outlined. One-dimensional nanostructures here specifically describe nanoparticles on the order of 10–1000 nm diameter while the one-dimensional terminology addresses geometries such as nanowires, nanocables, and nanotubes. Two-dimensional nanostructures include nanodisks, nanoflakes, and nanosheets. Nanowire and nanotube arrays, although two-dimensional in nature, are not specifically addressed in this section and instead, are considered as part of their individual component, the one-dimensional feature. However, in the Synthesis Methods section, arrays are considered a unique nanostructure produced through its own set of synthesis and fabrication protocols.

2.1. Zero-dimensional structures

2.1.1. Small organic structure directing agents (OSDAS)

The need for increasing the Si/Al ratio of the zeolites led Barrer and Denny [21] to popularize the use of small OSDAs such as quaternary ammonium compounds in zeolite synthesis, resulting in ZSM-5 type and beta zeolites with high silica content. Zeolites produced by larger OSDA templates have high framework Si/Al ratios exceeding 10. When the OSDAs are removed from the structure, open pores are produced in the material. The use of OSDAs has been decisive for the discovery of zeolites with different topologies, especially for the synthesis of AlPO-type zeolites, which contain high-silica content [6].

The main characteristics of OSDAs which determine its suitability for the synthesis of a certain zeolite structure are its polarity (hydrophobic/hydrophilic character), size, charge, shape, and rigidity [22]. Concerning the polarity of the OSDA, a compromise has to be achieved, as the organic molecule must be soluble in water, but it should not form complexes with the solvent, at least to a large extent. For example, in the case of quaternary ammonium compounds used as OSDAs, an adequate C/N^+ ratio ranges between 11 and 16. These molecules have the right polarity for being used as OSDAs in the synthesis of high-silica zeolites. The size to charge ratio of the OSDA will determine the final framework charge density.

One of the most important synthetic zeolites is ZSM-5 due to its pore structure, as well as the high stability and high acid strength that are derived from its high Si/Al ratio. This zeolite is synthesized using tetrapropylammonium ion (TPA^+) as the OSDA. The structure of ZSM-5 is built up from 5 to 5-1 secondary building units (SBUs). These join to form chains, which in turn link to form sheets. The ZSM-5 structure results when these sheets are linked across a center of inversion, with TPA^+ cations at channel intersections. ZSM-5 has a pore system consisting of interesting straight and undulating medium pore channels of pore diameters between 5 and 5.5 Å [23]. A more complex di-quaternary cation $[(H_3C)_3N(CH_2)_nN(CH_3)_3]^{2+}$ was used to produce the structures EU-1 [24] and NU-87 [25].

The influence of different templates to synthesize ZSM-5 zeolite has been studied by Fouad et al. [26] The template sources employed were tetramethylammonium hydroxide (TMAOH), tetraethylammonium hydroxide (TEAOH), tetrapropylammonium hydroxide (TPAOH), and tetrabutylammonium hydroxide (TBAOH). The variation of template affects the crystallinity of the ZSM-5. The crystallinity percentage of the produced ZSM-5 increased in the following order TMAOH < TEAOH < TBAOH < TPAOH and 0.537 < 0.43 < 0.333 < 0.215.

Most of the typical OSDA templates used for zeolite synthesis are usually toxic and not environmentally friendly. Moreover, calcination at high temperatures is necessary to remove the organic templates in order to produce the porous structure in the zeolites. This combustion required is accompanied by the release of polluting gases, mainly NO_x and CO_2 [27]. The organic templates used for synthesizing crystalline microporous aluminophosphate zeolites, have relatively high toxicity in comparison with the organic ammonium cations, which are used by aluminosilicate [28,29]. Wang et al. [30] reported a method for identifying low-toxicity organic templates for the synthesis of aluminophosphate zeolites, such as AlPO-5. The nontoxic and inexpensive organic compounds containing nitrogen atoms such as tetramethylguanidine (TMG), which can be found in the products of animal metabolism could be suitable for templating microporous aluminophosphate zeolites.

Another problem that OSDA templates have is that most of them are costly, and the calcination for removing them would result increased cost for the production of zeolites. In order to avoid this problem, new low-cost OSDAs have been used in the synthesis of zeolites. Zones et al. [31] have developed a new approach for preparation of zeolites using multi-organic amines instead of expensive organic templates. Typical MWW-type zeolite is produced from hexamethylenimine in aluminosilicates gels but Zones et al. [31] used isobutylamine together with a small amount of aminoadamantane to template SSZ-25 (MWW). Also, zeolites such as SSZ-13 (CHA), SSZ-33 (CON), SSZ-35 (STF), and SSZ-42 (IFR) have been prepared in the same manner. Important EMT-type zeolites that usually are templated by the toxic 18-crown-6 [32], recently have been produced successfully using the poly(diallyl dimethyl ammonium) chloride (polyquaternium-6), which is a component of shampoo [33]. One of the most important applications of the zeolite Cu-SSZ-13 is as catalyst in the reaction of reduction of NO_x by ammonia and would benefit greatly from reduced cost in its synthesis. Ren et al. [28] have synthesized units of SSZ-13 zeolite with a series of inexpensive inorganic or organic compounds. They also found that a low-cost copper complex (Cu^{2+} coordinated with tetraethylenepentamine, Cu-TEPA) was successfully used to synthesize the zeolite Cu-SSZ-13.

2.1.2. Ionic surfactants and liquids

The templates frequently used in MSN syntheses are surfactants due to their innate tendency to form micelles. As a result, the silica source tends to aggregate and form silica networks around these micelles. Selection of the template dominates the final porous structure of the MSN and as such, is the center of attention for many MSN syntheses

studies. The two major crystalline structures observed in MSNs as a result of ordered pore formation are hexagonal and cubic. Disordered and random structures are also possible. Surfactants typically used are either ionic or non-ionic, but in more complex MSN systems, such as hollow MSNs (HMSNs) mentioned in Section 2.1.4, a secondary or dual template is needed.

Ionic surfactants direct MSN templating through strong electrostatic interactions between the surfactant micelles and the silicate source. Both anionic and cationic surfactants can be used, although different reaction conditions are required for each case. For silica, the isoelectric point is approximately 2, where below this value; the surface is positively charged and above, negatively charged. The silicate precursor is typically negatively charged at most experimental conditions and as a result, cationic surfactants are much more widespread in order to promote the electrostatic bonding between the template and the silica source (see Fig. 1). To abbreviate the different pathways possible, typically notations such as S^- or S^+ denote the anionic or cationic surfactant, N^- or N^+ for any co-surfactant, and A^- as the anionic silicate source. An example of the S^+–A^- combination frequently found in literature is hexadecyltrimethylammonium bromide (CTAB) and tetraetil ortosilicato (TEOS). Hexadecyltrimethylammonium chloride (CTAC) is another commonly used cationic surfactant.

Due to the small hydrodynamic radii of ionic surfactants, pore size control is limited by only changing the template. However, there are multiple instances in literature that demonstrate differences in cationic surfactant size will induce directly correlated pore sizes in mesoporous silica. The classical examples are MSNs produced by CTAB and CTAC with varying alkyl chain lengths. Defined alkyl chain lengths for these surfactants have been used as studies have shown direct correlation between the length of the chain and the final pore size of the MSN [34]. In addition to quarternary ammonium surfactants, additional cationic species such as small organic amines (SOAs) can be used complementarily to assist in formation of the porous structure [35]. While these do not solely template the micellar framework for the pores, they disrupt and promote cationic surfactant micelles to preferentially bind together, resulting in a worm-like porous structure.

Synthesis of zeolites also uses this type of template. Quaternary ammonium polymers represent a special class of organic cations in that a growing crystal must accommodate not just a single cation but also a complete, linked chain of defined structure. It was with this thought in mind that a series of polymers was prepared and studied for effects in zeolite crystallization [36]. A controllable route for the synthesis of hierarchical mesoporous zeolites template from a mixture of cationic polymer and small organic ammonium salts has been developed. The route involves a one-step hydrothermal synthesis, and the template mixture is homogeneously dispersed in the synthetic gel. Hierarchical mesoporous beta zeolite was crystallized in the presence of TEAOH, which is the general organic template for the synthesis of this zeolite, and a mesoscale cationic polymer, polydiallyldimethylammonium chloride (PDDAC). The molecular weight of the cationic polymer lies in the range 1×10^5–1×10^6, and its sizes estimated at 5–40 nm, which is in good agreement with the dimensions of the mesopores obtained [37].

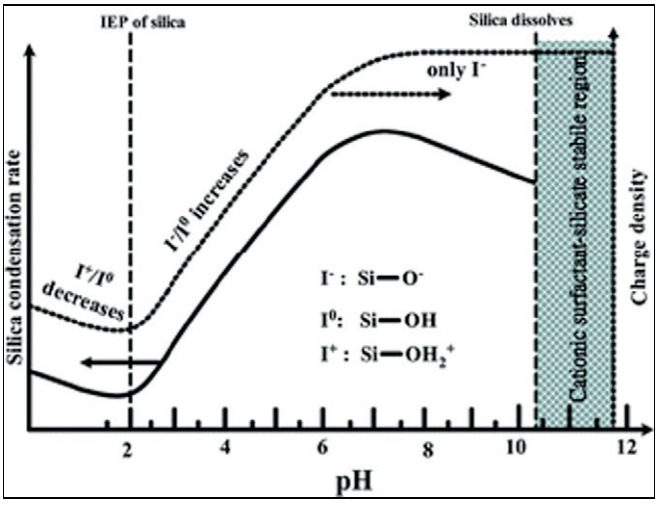

Fig. 1. Effect of pH on MSN formation in typical cationic surfactant template governed syntheses [511].

Although not as common their cationic counterparts, anionic surfactants are used as well. Due to the anionic nature of silicate precursors, an intermediate or co-silica source with cationic behavior is needed in order to adapt the anionic surfactant templating method. In one example by Yokoi et al. [38] a charge neutralization effect is achieved when the negative anionic group of sodium dodecyl sulfate (SDS) interacts with the positively charged ammonium site of (3-aminopropyl)triethoxysilane APTES, in addition to TEOS present. Another similar example by Che et al. [38] utilizes a similar electrostatic approach using a variety of anionic surfactants with APTES or N-trimethoxysilylpropyl-N, N, N-trimethylammonium chloride (TMAPS). The resulting structure is highly uniform, can be cubic or hexagonal, and have pore sizes ranging from 2.3 to 5.2 nm.

Ionic liquids (IL) have also been used to template mesoporous silica nanoparticles. As with ionic surfactants, ionic liquids behave similarly in electrostatically interacting with the silicates to form porous networks. In particular, 1-alkyl-3-methylimidazolium (C_nMIM) has been used multiple times in literature to produce MSNs under near identical alkaline conditions with TEOS acting as the silicate precursor [39]. Even short chain IL templates, which do not preferentially form micelles, still generated mesoporous silica structures, although with random, worm-like porosity [40].

2.1.3. Non-ionic and amphiphilic surfactants

Non-ionic and amphiphilic templates are just as abundantly used to synthesize MSNs as their ionic counterparts. The most widely used classes of these templates are tri-block polymers, specifically polyethylene oxide-polypropylene oxide-polyethylene oxide (PEO–PPO–PEO) with the BASF trademark name of Pluronic®. Due to the hydrophilic nature of the PEO tails and the hydrophobic nature of the PPO, Pluronics behave as amphiphilic surfactants, with varying strength in relation with the polymer chain length and ratio of PEO:PPO components. Typically Pluronics with high molecular weight, such as P123 or F127, are used due to their greater stability and structure-directing ability. One of the earliest MSN synthesis methods involving non-ionic surfactants was done by Zhao et al. [41] at the University of California, Santa Barbara, from which their SBA-15 (Santa Barbara Amorphous) was named. Typical SBA-15 type MSNs since then have been produced using PEO–PPO–PEO triblock polymers with both the original hexagonal and later seen cubic crystalline structures. A tremendous range of non-ionic surfactants exist, with trade names such as Brij®, TWEEN®, Tergitol®, Triton®, and Span®, in addition to the tri-block PEO–PPO–PEO Pluronics. A comprehensive study [42] investigated mesoporous silica structures synthesized with a range of non-ionic surfactants at acidic conditions.

As observed with Pluronic syntheses in acidic conditions, the cubic phase is predominately favored. The mechanisms through which non-ionic surfactants direct MSN synthesis is similar to those found in ionic surfactants, and can produce as equally uniform hexagonal crystalline structures. However, as noted by Zhao et al. [41], the formation of uniform porous crystallinity is sensitive to all reaction parameters, including the template concentration, pH, and temperature. At non-optimal conditions, amorphous, disordered, or even no silica is formed. The results indicate that both the electrostatics between the template and silicate source, as well as the self-assembly of the template itself, are crucial parameters that vary with the reaction environment and ultimately govern the porous crystallinity during the sol–gel formation.

In addition to the predominantly found hexagonal mesoporous structure, cubic structured MSNs were also synthesized shortly after the former's discovery. When using PEO–PPO–PEO as the template, it was noted that greater PEO content resulted in the cubic structure [41]. MCM-48 (belonging to the same M41S family as MCM-41) also shares the cubic structure as with other later developed varieties, SBA-1, SBA-16, KIT-5, and KIT-6. The cubic porous network has advantages over hexagonal networks as theorized by Monnier et al. [43] With the intertwined porous structure, diffusion and transport within the mesoporous network is not hindered with pore blockage as it is seen in the well-ordered hexagonal crystalline structure. The synthesis of cubic MCM-48 observed by Kim et al. [44] was produced with both pure CTAB as a template, but only seen with higher stir speeds and low surfactant to silicon ratio. Presence of a co-solvent, ethanol, also drives the conversion of hexagonal to cubic symmetry as well [45]. Excluding the extremities of synthesis parameters possible in both ionic and non-ionic methods, disordered mesoporous silica structures produced from non-ionic templates also exist, as those observed in KIT-1 [46] and MSU-X [47] type MSNs. Bagshaw et al. [47] attributed the irregular and disordered porous network to the silicate formation around the stable worm-like micelles of longer amphiphilic templates.

2.1.4. Secondary templates

For dual-templated systems, such as those found in hollow MSNs (HMSNs), hierarchal MSNs, and other hollow organic/inorganic nanoparticles, a secondary template is used in addition to the pore-governing one. Frequently this is a colloid of polymeric nanoparticles that function as the core, such as polystyrene [48,49] or other polymers including poly(methylacrylic acid) [50] and poly(methyl methylacrylate) [51,52]. For dual-templating MSNs, polystyrene latex has been a widespread choice due to its homogeneous synthesis, commercial availability, nanoscale diameter, and thermal degradability during calcination [53]. Negatively charged polystyrene beads provide strong electrostatic interactions with cationic surfactants and thus serve as highly stable templates for HMSNs [54]. Fig. 2 shows the versatility of PS, performing both as a template for the larger, hollow core, and smaller surface pores. The effect of the latex core on the porous structure and orientation was also observed [55] but the relationship between the two was not explicitly explained. The reverse is observed as well, with inorganic materials such as solid silica [56–59] or ZnO [60] having been used to template hollow polymeric nanoparticles. An important criterion for the template is the ability to be selectively removed, and as a result, polymeric templates are most commonly used as they can be removed through calcination, leaving the silica structure intact. With silica cores, solutions of hydrochloric or hydrofluoric acid are used instead.

Besides HMSNs, a “yolk-shell” structure has also been frequently studied in context of core–shell, dual template MSNs. Advantages of this system allow for encapsulation of inorganic nanoparticles within the permeable silica shell, allowing for targeted delivery, imaging, catalysis, or nanoreactor applications. Wu et al. [61] used a dual-surfactant template of lauryl sulfonate betaine (LSB) and sodium dodecyl benzenesulfonate (SDBS) to form micelles around silica, gold, or iron oxide cores. Afterwards, APTES and TEOS were used to form the mesoporous silica shell as described earlier. Similar to the LSB/SDBS system, fluorocarbon surfactants have also been used to form micelles around inorganic cores, followed by normal mesoporous silica synthesis for the shell [62].

2.1.5. Carbon frameworks

The major drawback of zeolites is the small size of channels and cavities with diameters of 0.8 nm and between 0.3–1.5 nm respectively. This fine microporosity also has disadvantages because diffusional limitations impose high back pressure on the flow system. To minimize diffusion problems, efforts have explored the synthesis of zeolites with controlled particle morphology and porosity. Although generally successful in terms of improved diffusion, a reduction in pore-wall crystallinity is often observed, resulting in reduced catalytic activity [63,64]. One approach to overcome these limitations is to decrease the zeolite crystal size to the nanometer scale, consequently increasing external surface area while reducing the diffusion path length. Although various strategies have been proposed to design and produce zeolites, template-directed synthesis is currently the most widely used method.

Different carbon frameworks have been used for the synthesis of mesoporous zeolites [63,64]. Jacobsen et al. [65] synthesized zeolites on carbon nanoparticles as the porous matrix. They use an excess of a zeolite gel in the system so that the zeolites fully encapsulate and form around the carbon particles template. Subsequently, large zeolite single crystals are formed. Removal of the carbon matrix by combustion leads to isolation of large zeolite single crystals with a mesoporous

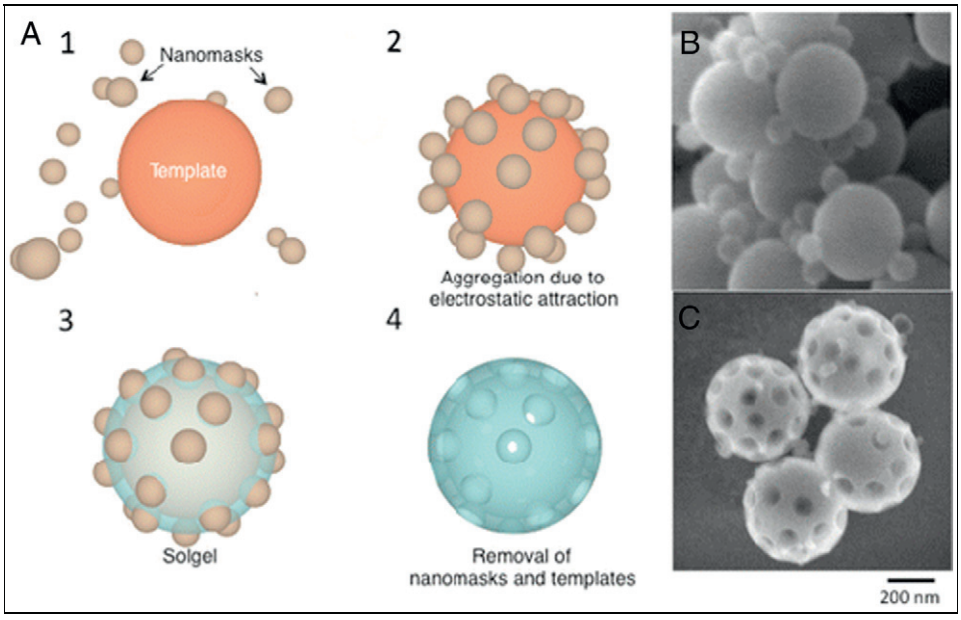

Fig. 2. One example of HMSN synthesis using polystyrene nanoparticles as templates for pore and hollow structure formation. [467].

system. By the proper choice of carbon matrix it is possible to influence the mesoporous system.

Multiwalled carbon nanotubes (MWCNT) were also used as a template to form mesoporous zeolites [66,67]. Zeolites with mesoporous were prepared by sequential impregnation of MWCNT with a 40 wt.% aqueous solution of TPAOH and TEOS. The sample was crystallized at 175 °C for 24 h. After the hydrothermal crystallization, the MWCNT were completely removed by calcination in air at 600 °C for 20 h. The diameter of the carbon nanotubes varies closely around a 12 nm average with walls consisting of 6–8 graphene layers. Zeolite crystal is grown around the carbon nanotube. The individual zeolite crystal has partly encapsulated the MWCNT material during growth. The uniform mesoporous penetrate the zeolite crystal. The use of MWCNT as templates offers a high degree of control over the diameters and spatial arrangement of mesoporous in zeolites crystals. Carbon nanofibers (CNFs) were also employed as templates for the synthesis of the mesoporous zeolites. This carbon material yields zeolite crystals whose pores vary widely in diameter, some particles can have pore diameters similar to CNFs, 20–40 nm, while others have much larger diameters [63].

Aluminosilicate molecular sieves (RMMs) synthesized using carbon mesoporous molecular sieve (CMK) as a carbon template and ZSM-5 as a precursor resulted in the formation of zeolite nanocrystals on the external surface of the carbon template. For this synthesis the carbon template was treated first with TPAOH and then aluminosilicates were introduced, followed by crystallization. If the materials were prepared by CMK-1 templating possessed uniform pores with cubic patterns and if they were prepared by CMK-3 hexagonal patterns were obtained [63,68,69].

Carbon aerogels (CAs) [63,70–74] are obtained in monolithic form and their structures and properties depend on the agglomerate structures of uniform spherical carbon particles [63,73,75]. CAs show an adsorption isotherm type IV, which is typical from mesoporous materials [63,76]. This type of isotherm means that the adsorption in this material proceeded via multilayer adsorption, followed by capillary condensation taken place in mesopores, resulting in an increased amount of adsorption at higher relative pressure. Capillary condensation is a secondary process that requires the preformation of an adsorbed layer on the pore walls formed by multilayer adsorption [77]. Using shrinkage of RF aerogels during the pyrolysis can control the pore size from CAs and they have developed as templates for the preparation of mesopore-modified zeolites [63,78,79]. The synthesis of zeolites with mesopores consists of three different steps. In the first step, the zeolite precursor was introduced into mesopores of carbon aerogel, then the zeolite was synthesized in the inert mesopores, and finally, the zeolite was separated from the aerogel [63].

2.1.6. Biological templates

Macroscopic bacterial threads produced from the mutant *FJ7* strain of *Bacillus subtilis* [80] have been used as template of zeolite fibers with hierarchical structure by Baojian et al. [81]. TPA-Silicalite-1 nanoparticles, which were synthesized previously from clear solution by reflux and aqueous solution containing TEOS and TPAOH, can be infiltrated into the ordered void spaces of a bacterial template where they can be used as building blocks for the construction of macroporous inorganic templates. Removal of both molecular (TPA^+) and micrometer scale (multicellular filaments) templates by thermal degradations gives the zeolite fiber hierarchical porosity that might have technological advantages owing to the high surface area and uni-directionality of the patterned architectures.

Mesoporous silica nanoparticles have also been templated by *B. subtilis* [82]. As seen with zeolite fibers, mesoporous silica fibers have been produced using bacterial threads dipped into a mesoporous silica sol–gel. Due to the anionic surface charge of the Gram positive bacteria, the anionic silica readily phase separates from the bacterial strands and forms a superstructure. Additionally, starch has been used as a template for both zeolite and silicate nanostructures. Pores ranging between 0.5–50 μm were produced by varying the starch ratio in the sol–gel [83].

2.2. One-dimensional structures

2.2.1. Nanowires

Nanowires (NWs) are a key building block of nanotechnology and, are at the core of research efforts integrating them into novel devices. Metallic nanostructures provide a broad range of functionalities in electronic applications [84,85], magnetism [86–88], catalysis [87,89,90], biological tagging [91], photonics and plasmonics [92,93], and controlled self-assembly [94]. Integrating nanostructures into devices has many advantages such as a better utilization of precious metals, better control over the structure and thickness of adlayers, more effective electron pathways, and improved mechanical support. Template synthesis has proven useful in the controlled synthesis of highly uniform nanowires and nanowire arrays. Nanostructure synthesis in a template offers the possibility to grow nanostructures with complex compositions [95,96], high aspect ratio and integrated junctions, such as nanocable structures with integrated p-n junctions [97,98]. Numerous interesting properties have been identified in relation to the nanoscopic dimension (the diameter) of the materials with high aspect ratio [99]. More importantly, template synthesis offers the direct integration of nanostructures into electronic devices. Once the template is created, nanostructures can be produced by either chemical (electroless deposition), electrochemical or physical methods. After the nanostructures were synthesized, the template may be removed to expose the nanostructure arrays. Nanocables with radial junction can also be produced (e.g. Au/Te [100–102]). Electrochemistry can be used in combination with electroless deposition, where slow electroless plating (no mass transfer limitations) allows for a uniform metallic film. The metal deposition occurs uniformly at the pore walls creating hollow metallic nanotubes inside the pores [103–108]. For multiscale nanostructures such as nanotubes, nanofibers, and nanocables, it is important to know which characteristic length scale, nm or μm, governs the deposition process [109]. For the μm scale, diffusion limitations can be important if the surface deposition processes are relatively fast.

Electrochemical deposition, or electrodeposition, is a process in which an external potential is applied to a sample substrate in a solution of ions, along with a counter electrode to complete the circuit, usually a noble metal such as Au or Pt, and a reference electrode to provide a reference potential at a known half-cell potential. In the case of metals, the working electrode acts as a cathode, injecting electrons into the reaction, which reduce cations in solution, causing them to deposit in or on the attached template. The technique of growing very fine wires into a porous template was first demonstrated like Possin [110], and was popularized by Martin et al. [111] and Preston et al. [112] Commonly used templates include nanoporous anodic aluminum oxide (AAO) and polycarbonate track etched (PCTE) membranes which have been modified with a conductive back layer, such as sputtered gold. Walter et al. [113] have also demonstrated the electrodeposition of metallic nanowires at the step-edges of oriented graphite. Electrodeposition may be used for the deposition of a wide array of metals, including noble metals, iron-group metals, Pb, Zn, Sn, In and Bi [87,88,110]. Codeposition of metallic alloys is also possible (see Section 2.1), as is the electrodeposition of many compound semiconductors, wherein the anion is deposited from the reduction of a complex cation containing the anionic species [95]. The use of porous membranes facilitates the inexpensive growth of large arrays of nanowires with tight control over nanowire size and aspect ratio. Furthermore, the use of pulsed electrodeposition allows for nanowire growth with excellent length uniformity [87,114] and controllable crystallinity [115] allowing for the growth of highly uniform segmented nanowires [87], or nanowires containing monolayer molecular junctions [84]. Hurst et al. provide a detailed review of segmented nanowire template growth [87].

Templated nanostructures may also be grown via electroless deposition into or onto a template. This method substitutes a reducing agent in solution, such as a citrate, oleylamine or polyol, for the external potential used in electrodeposition [116]. This process is best understood for metallic films, though chemical pathways for the electroless deposition of compound semiconductors are also known [117]. A template is surface-functionalized with a group that binds well to the depositing cation, such as a thiol- or amine-terminated self-assembled monolayer (SAM); the adsorption and galvanic reduction of cations on the template surface then proceeds spontaneously, with the deposited film conforming to the shape of the functionalized surface. The process has been successfully demonstrated for a wide range of materials, including Au, Ag, Pt, Cu, and Ni–P and Co–P alloys.

Many nanoporous materials and membrane templates may be used as templates, including PCTE, AAO, mesoporous zeolites, nanochannel array glass, polypeptide tubules, and surface relief grating (SRG) templates [118–121]. For example, SRG patterns can be used as a template for colloid self-assembly and nanowire fabrication. Titania nanowires have been fabricated using a spin-on process on one-dimensional (1D) SRG patterned and flat substrates of epoxy-based azobenzene functionalized polymer (AFP) templates [119–121]. The two most common template materials used are AAO and PCTE (see Fig. 3). AAO membranes consist of a highly regular array of uniform pores with pore densities as high as 10^{11} cm^{-2} [87], diameters from 5 nm to 250 nm, and lengths in the micrometer range. They may be produced electrochemically via a two-step anodization process established by Masuda et al. [122] and described in detail by Kovtyukhova et al. [123] or purchased commercially. AAO pores have the benefit of high pore density, uniform and parallel pores, and durability; however, they are much more difficult to dissolve than polymeric membranes, requiring NaOH to fully remove the membrane [124]. PCTE membranes are produced by bombarding a polycarbonate film with ionizing radiation followed by UC sensitization and chemical etch to widen the damaged area into a pore [125]. They are available commercially, and have uniform pores ranging from 10 nm to 2 μm and a pore density of approximately 10^{9} cm^{-2} [87]. The ion bombardment process results in randomly distributed and occasionally intersecting pores, which may lead to issues in the processing of highly uniform or complex structures. However, PCTE membranes are inexpensive, large-area, and readily dissolved in solvents such as dichloromethane, easing handling and processing procedures.

Multisegmented nanowires were developed to fill in need for different chemical functions along a nanowire, which will allow them to perform several tasks simultaneously [126]. Multifunctional/multisegment magnetic nanowires with modulated electrocatalytic and bioelectrocatalytic responses were adapted for on-demand operation/switch of microchip device, electrochemical sensors, magnetic stimulus, which will lead to the 'smart' devices. Fig. 4 presents a few examples of multifunctional/multisegment nanowires including their fabrication by template- assisted electrochemical synthesis, which is the main technique used to create multi segment nanowires. Sequential template- assisted electrochemical synthesis offers spatial control over the segment composition. Therefore, a combination of different materials or compositions is possible to be achieved into a single nanowire. Individual segments have different reactivity and can be functionalized by molecular linkages that bind specifically to different segments along the nanowires [126]. Having a high aspect ratio, nanowires exhibit unique magnetic properties. Furthermore, multisegment ferromagnetic nanowires bring additional size and compositional effect benefits to their coercivity and remanence along the magnetic easy axis, parallel to the wire axis [127]. Additional tuning can be achieved by controlling the nanowire diameter since coercivity, remanence and Curie temperature depend on nanowire size.

2.2.2. Nanocables

Nanocables are core–shell type structures that combine interesting properties induced by the difference in structural growth (longitudinal vs axial) characteristic of the core and shell. Electrochemical template synthesis is by far the technique of choice used to obtain arrays of nanoelectrodes [95,96,128–131]. Both axial and longitudinal growth of nanocables with p-n junctions can be produced. Starting with a nanoporous polycarbonate tract-etching (PCTE) membrane as a template, Au nanotubes were fabricated by electroless Au deposition inside the nanopores of the PCTE membrane [128]. Using the Au nanotube membrane as a second template, Te was deposited on the surfaces of the Au nanotubes by slow electrochemical deposition, taking advantage of underpotential deposition (UPD) [132]. The deposition rate was sufficiently slow to radially grow Te nanotubes coaxially within the Au nanotubes to form nanocables.

There are several advantages associated with nanoelectrode arrays. They exhibit a small potential drop, which make the electrochemical measurements possible when a low electrolyte concentration is used. The small size of the nanoelectrodes array maintains a steady-state current and has a high current per unit area (i.e. high ratio of signal to noise). This property is mainly used in sensors, where the sensitivity of the device could increase more than 100 times. Furthermore, one of the many advantages for preparing multilayered nano-sized materials is that the electrodeposition can be performed on flexible substrates and at room temperature, which is very important for systems in which undesirable interdiffusion occurs between the adjacent layers.

However, more recent developments have suggested that a more sophisticated architecture of the nanocable arrangement cannot be achieved using commercial templates. More complex nanocable or nanowire configurations for certain applications in can use other technologies to create particular design nanostructured array for nanoelectrodes, such as nano-imprinting. Another way to create complex structures is to use nanocable arrays as template for bimetallic nanotubes [133]. An electrochemical template assisted method was developed for functional Pt nanostructures to improve their electrocatalytic activity by controlling the shape and the size of Pt. Nanowires of ZnO

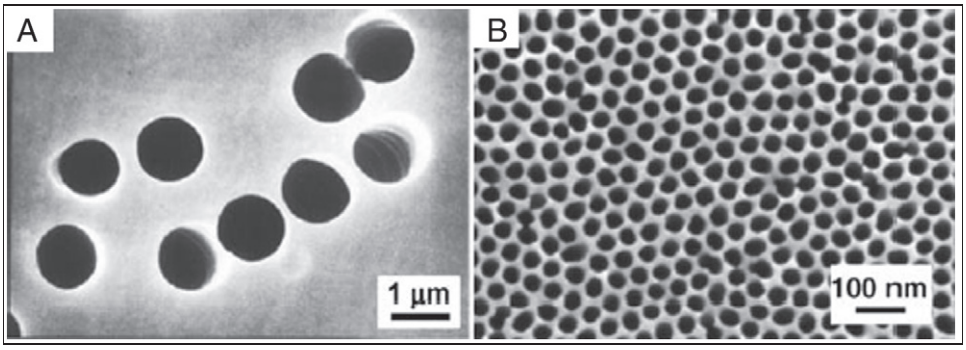

Fig. 3. a) Track-etched PCTE membrane and b) AAO membrane. Figure reproduced from Hurst et al. [140].

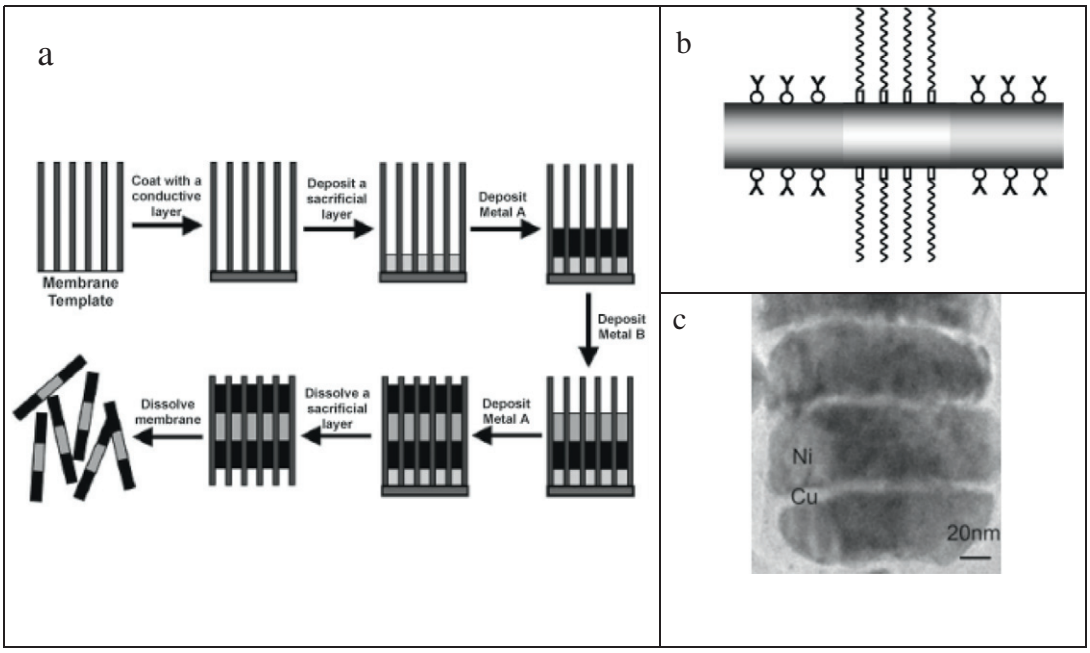

Fig. 4. a) Schematic description of the membrane-template electrochemical preparation of multisegment nanowires, and b) Selective functionalization of a multisegment metal nanowire [126]; c) TEM image of a 140 nm diameter nanowire with 40 nm Ni layers and 5 nm Cu layers [127].

were used as a template for growing porous Ni–Pt core–shell nanotube arrays [133]. Uniform layers of Ni and Pt were electrodeposited on ZnO nanorods (see Fig. 5). Then, dissolving the ZnO template, porous Ni–Pt core–shell nanotube arrays were obtained.

2.2.3. Nanotubes

Due to the two-dimensional structure and their hollow interior, nanotubes have specific properties such as one-dimensional electron transport, light trapping, and novel photonic properties. There are two types of templates that can be used for the synthesis of the nanotubes and hollow fibers. The first method is based on the internal diameter control. In this case wires or rods will be used as a template and the diameter of the template will determine the internal diameter of the nanotube. The second approach is based on the external diameter control. In this case cylindrical wells will be the substrate for the deposition and the diameter of the cylindrical wells will determine the external diameter of the resulting nanotube/fiber.

The most common method of synthesis of nanotubes is by employing nanofiber or nanowire templates. The templates will be removed after deposition of the interested materials and hence provides with a hollow interior. The template removal can be performed by thermal or chemical methods. The ideal template for nanotubes should be removed at fairly low temperatures and should not leave any residue that would interfere with the final product or its application. The pyrolysis of the template and the byproduct exhaust gas or expansion should not disrupt the structure of any surface layer of the material as well.

Due to these factors, cellulosic fibers are one of the more attractive thermally removable templates. Cellulose nanofibers have been used for production of inorganic nanotube structures, including hollow TiO_2 fibers [134,135], SnO_2 nanotubes [136,137], Fe_2O_3 nanotubes [138], and SiO_x nanotubes [139]. The main advantage of cellulosic fibers is that long fibers (in the range of 10 μm) can be produced with this method. By controlling the diameter of the cellulosic fibers, the internal diameter of the hollow fibers can be controlled. Solution-based techniques such as sol–gel and layer-by-layer self-assembly (LbL) are commonly used to synthesize nanotubes. The LbL techniques provide the ability to deposit nanoparticles on the surface of the cellulosic fibers and hence, the nanostructured hollow fibers will be produced. The nanostructured fibers are important for application which high surface area and electrolyte diffusion are important such as batteries and solar cells [134]. Ghadiri et al. [140] used sol–gel process for deposition of TiO_2 on the surface of the cellulosic fibers. After removal of the template, the remaining hollow fibers showed the electron collection efficiency of a dye-sensitized solar cell. High surface area and the electron transportation are both important in

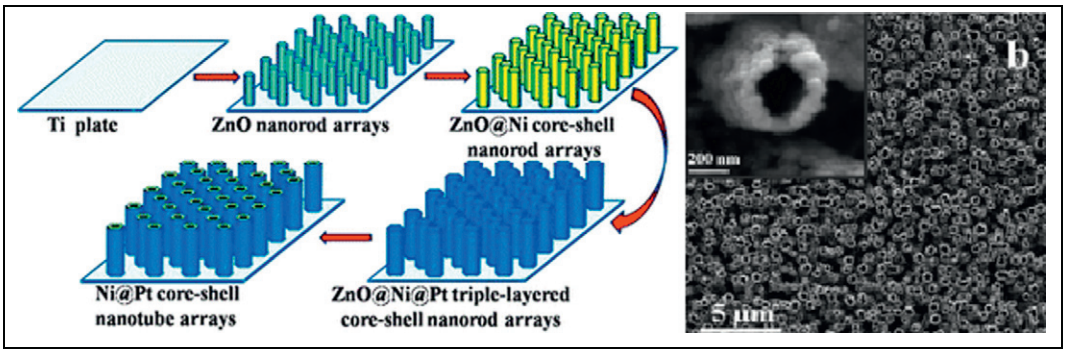

Fig. 5. Schematic illustration for the synthesis of Ni@Pt core–shell nanotube arrays (left) and Ni@Pt core–shell nanotube arrays after etching ZnO nanorods(right) [133].

the gas sensors. Therefore, the nanotubes with mesoporous structures are suitable candidates. Huang et al. [137] used cellulose fibers as templates and prepared tin oxide nanotubes by sol–gel method.

Cellulose fibers often require some treatment to improve their dispersion. However, in the many instances for templating nanotubes, commercial cellulosic membranes and loose fibers are used, which are random in structure and vary from micrometer [141] to nanometer [142] to aerogel varietals [143]. Treatments done in order to improve the dispersion of cellulosic fibers, but obtaining the nanofibers as suggested is quite unpredictable and difficult to achieve in the sense of a supported template membrane [144]. Instead, the treatment, typically acidic/ultrasonication modification, are used to for nanofibers of cellulose, which are either processed into membranes or aerogels, or at times used directly for deposition of the matrix material [145].

Along with cellulosic nanofibers, carbon nanofibers are widely used to template a variety of inorganic nanotubes as well, including ZrO_2, Al_2O_3, and SiO_2 [146], and then removed through calcination at elevated temperatures (1023 K) TiO_2 [147] and SnO_2 nanotubes [147] produced using carbon nanofibers are highly similar to those produced from cellulose templates. Polymeric fibers and other natural organic species can also be used as thermally removable templates. Polymeric membranes can be prepared with electrospinning which provides accurate control on the diameter and porosity of the fibers [148]. Polypropylene hollow fibers have been used for preparation of zirconia hollow fibers [149]. The polypropylene was removed at 873 K for four hours. Peptide amphiphiles, which self-assemble into long nanofibers, were used to produce silica nanotubes [150,151]. Lastly, inorganic nanofibers can be used to template nanotubes, although less commonly due to their difficult removal. Jun. et al. [152] used a sacrificial Mn_3O_4 nanofiber template to produce conductive polyaniline nanotubes. Similarly, V_2O_5 nanofibers served as templates for polypyrrole nanotubes [153]. During the polypyrrole polymerization process, the V_2O_5 nanofibers were consumed and removed, eliminating any need for rigorous post-synthesis template removal.

As noted in templates used for nanowire syntheses, formation of nanotubes using porous membranes such as AAO or PCTE requires an additional step to induce the hollow geometry of the final nanotube. In some instances, this can be a simple methodology of simply absorbing away the contents of the nanopores, as done using AAO membranes sandwiched between filter paper [154] to produce nanotubes of Cu_2ZnSnS_4 after immersing the AAO membrane in the precursor sol-gel. More elaborate methods such as controlled polymerization are applicable for the synthesis of organic nanotubes. Nanotubes of polyaniline and poly(2-methoxyaniline) were prepared inside the polycarbonate membranes by chemical in situ deposition, although poly(2-methoxyaniline) was clearly more uniform in nature, and formed regular nanotubes, whereas polyaniline nanostructures were not clearly nanotubes [155]. With a spin-casting technique and AAO as the template, polymer nanotubes of either polystyrene or poly(methyl methacrylate) or both could be produced after removal of the AAO template with 1 M NaOH [156]. Using AAO or PCTE membranes, several metal oxide nanotubes can be produced, including TiO_2 [157], ZnO, FeO(OH) [158], WO_3 [159] Co [160].

The important factor for formation of the desired nanotubes is selection of a coating method with precise control over the thickness of the deposited layer inside the pores. As with electrodeposition and electroless deposition techniques discussed earlier, control of the deposition rate and quantity can limit growth of the nanowires to have hollow cores intact. Example methods include electroless gold deposition [161] or a layer by layer method [162] which is based on the alternative immersion of the AAO pores inside the precursors of α,ω-diorganophosphonate/Zr.

2.2.4. Nanomushrooms

Mushroom cap morphologies result most commonly from the overgrowth of nanowires grown in porous templates by electrodeposition [163] though similar morphologies have also been achieved through reflux growth [164] or interference lithography [165]. While template overgrowth is generally considered unfavorable when growing nanowires, mushroom cap morphologies have proven useful in increasing electrical contact reliability in functionalized nanowires [166,167] as well as in monitoring and automating nanowire growth by using mushroom cap electrical contact to an electrode grid on the top side of the growth substrate to detect the location of single nanowires or terminate nanowire growth [20,168]. Single-crystal GaN nanowires templated on catalyst seeds and grown via vapor–liquid–solid growth have also been intentionally coalesced to form a low-defect semiconductor film on a highly mismatched substrate [169], with the nanowire stems providing strain relaxation. Similar structures have also proven useful for plasmonic applications [165]; templated deposition might provide an inexpensive and scalable method for creating such structures.

The growth regimes of the mushroom cap may differ from those present in the nanowire growth, as the physics of adsorption, available growth surface, and cation mass transfer differ on the mushroom cap compared to within the nanopore. The shape and aspect ratio of the mushroom cap depends strongly on the energy balance of adsorption of metal cation complexes on the template surface compared to the deposited metal, as well as the relative interfacial energies of the template and mushroom cap with the cation solvent (usually water). If adsorption and wetting of the metal on the substrate surface is favorable, the mushroom caps may grow in a layer by layer (Frank–van der Merwe) regime; however, if adsorption is not favorable, the mushroom caps will exhibit layer-island (Staranski–Krastanov) growth, not readily coalescing with

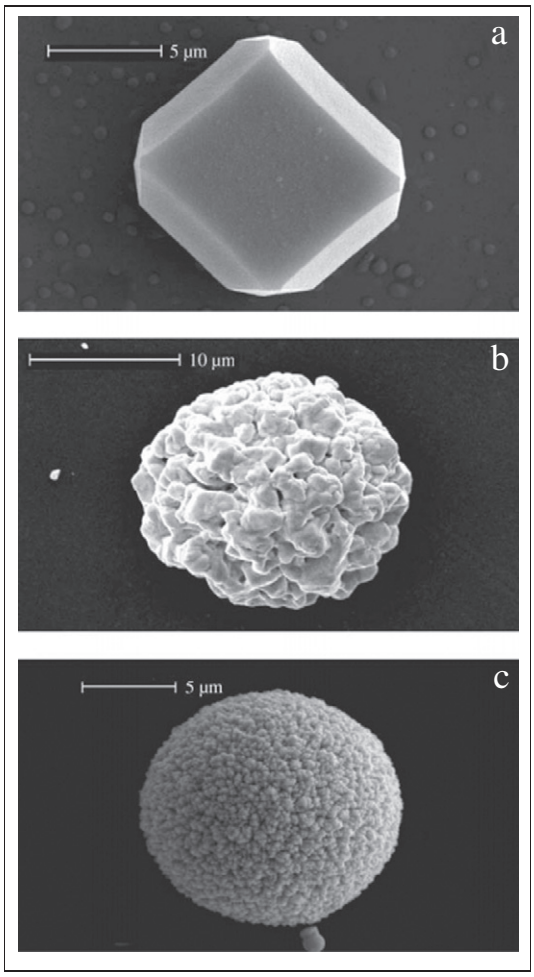

Fig. 6. SEM of Au mushroom caps showing a) monocrystalline faceting, b) large grains, and c) fine grains. Reproduced from Karimi et al. [125].

each other but instead forming rough nanopillars [163]. When single-crystalline wires are grown, the caps demonstrate strong faceting, as opposed to the rough surfaces seen in polycrystalline wires (Fig. 6) [125].

2.3. Two-dimensional structures

2.3.1. Nanodisks, nanoflakes, and nanosheets

Planar structures with their thickness in the nanometer range can be categorized to nanodisks, nanoflakes, and nanosheets. One simple approach for the synthesis of the nano-disks is by coating the surface of large spherical particles such as polystyrene and then removing the substrate. Polystyrene mesospheres have been used as the templating structure for the synthesis of silver nanodisks [170]. In this research aqueous colloidal polystyrene spheres functionalized with carboxylate were used as the template. In this method proper selection of the precipitation or grow of the desired material on the surface of the polystyrene is very important.

The uniform cylindrical pores of membranes such as AAO can also be used to produce polymeric curved nanodisks, such as polystyrene ones produced by Chi et al. [171] By using polystyrene nanospheres and depositing them on the inner pore walls of AAO, during subsequent drying and annealing steps, the nanodisk is formed. Similar results are seen with poly(methyl methacrylate) and acrylonitrile-butadiene-styrene polymers.

Biological templates are no exception to function as templates as well. Ferritin, a uniform spherical protein, is often used due to its biomineralization capability of iron. As a result, iron oxide is deposited onto surfaces from the ferritin template. Uniform sub-10 nm silicon nanodisks were produced using ferritin as the template [172]. By using a smaller biological template, Listeria-Dps, silicon nanodisks of approximately 4.5 nm can be produced [173]. With stabilizers added to the ferritin template, such as PEG, the spacing of ferritin on surfaces can be controlled, and utilized to produce uniform nanodisk arrays, as shown with InGaAs done by Yoshikawa et al. [174].

Similar to nanodisks, nanoflakes have near identical geometry but are frequently observed in clusters or agglomerates. As such, nanoflakes are usually produced to increase the surface area of their templates. Supramolecular templates are candidate templates for the synthesis of nanoflakes. Shen et al. [175] reported the synthesis of metal nanoflakes by deposition on functionalized fullerene prepared as the template. Although this method is simple, the method does not provide accurate control over the size of the nanoflakes. Carbon nanotubes also are frequently used as templates for nanoflake synthesis as well, as observed by Chen et al. [176], where graphitic nanoflakes were grown onto carbon nanotubes.

Novel porous nanosheets can be produced with several templates. Precursor chemicals, which can form lamellar complexes, can be used as soft templates [177] while hard templates such as metal oxides or graphene also are viable [178]. For solid nanosheets, narrow phase separation cadmium halide and diamine can form diamine bridges and hydrogen bonds in the form of an alternating layered structure. This method has been used for large scale production of CdSe nanosheets with less than 2 nm thickness [179]. In other instances, deposition and growth onto templates such as graphene oxide, can produce ultrathin nanosheets of silicon [180].

3. Synthesis methods

It has been established that there are a wide variety of templates capable of templating zero-dimensional, one-dimensional, and two-dimensional nanostructures. In this section, we only briefly discuss three categories of synthesis methods involving the templates and their respective final nanostructured products. For a majority of nanoparticles, such as MSNs or semiconducting nanoparticles, emulsion synthesis is a versatile and efficient method to produce homogeneous nanoparticles. For one and two-dimensional nanostructures, such as nanowires, nanotubes, and nanostructured arrays, template-filling methods are used to form the final product around an appropriate template through differing techniques including electrodeposition, vapor deposition, and melt/sol–gel deposition. Due to the incredible variety of templating methodologies, other techniques such as layer-by-layer and lithographic syntheses are also discussed briefly, but potentially many newer, novel methods have not been covered in-depth. The different synthesis methods are discussed here, with a focus on their capability, feasibility, and potential extension.

3.1. Hard and soft templating syntheses

The majority of nanoparticles are produced through hard and soft templating methods, which can be categorized roughly into deposition onto colloidal suspensions and emulsions respectively. In the former, hard templates such as polystyrene nanoparticles are used as the core for a target material deposition, while in the latter, emulsions are a straightforward method to similarly deposit material onto micelles or phases within a solution. The basic principle for emulsion systems is the phase separation of two media from which preferential micelles or nanoparticles will form. As the target material deposits onto the micelles of one phase, typically either water or oil, the nanostructure develops and is finalized once the template is removed. Due to this mechanism, colloidal solutions can also be used as emulsion templates, such as those comprised of polystyrene latex, a common template for this method [181]. As described earlier, the majority of template reagents used for MSN syntheses, such as TEOS and trimethylbenzene (TMB), are already candidates for oil-in-water emulsion methodologies and as such, HMSNs are frequently produced through emulsion syntheses. In this instance, the oil phase forms micelles and functions as a template in determining the shape and structure of the target material deposited on it. The reverse micelle method, or water-in-oil, is another suitable way for obtaining the uniform and size controllable particles [182]. Reverse micelles are small, dynamic aggregates or surfactant molecules surrounding a polar, typically aqueous, core dispersed in a nonpolar continuous oil phase. Reverse micelle solutions are clear and thermodynamically stable, as water is added to a reverse micelle solution, a microemulsion is formed that contains nanometer-sized water droplets dispersed in continuous oil phase [183]. Several reverse micelle systems, especially AOT ternary water-in-oil system, have been used for preparing nanoparticles. This surfactant can form reverse micelles in nonpolar fluids without addition of a co-surfactant [183] however there are studies that indicate that with the assistance of co-surfactant, the size of nanoparticles prepared in quaternary reverse micelle system is more controllable [182].

After nanoparticle formation, typically a stable complex is formed but in many cases, demicellization is an issue that will cause incomplete formation of the porous or nanoparticle structure. Empirical studies [184] have qualitatively demonstrated how adjustment in the temperature, reagent ratios, etc. will affect the structure of the MSN formed, but a strictly kinetic investigation of the emulsion mechanism is not well known. Yao et al. [185] interestingly demonstrated the inherent variability and instability in emulsion based syntheses involving TMB and CTAB (TMB being the oil phase). Summarized in a phase diagram, it can observed that dimicellization occurs upon the introduction of (3-mercaptopropyl)trimethoxylsilane (MPTMS) resulting in a phase shift from cylindrical pores to vesicular phase. Other MSN syntheses that select TMB as the oil phase template for hollow MSNs have noticeably seen the effect of adsorption onto the template micelles and its effect on the MSN structure [186]. Similar results can be seen where high concentrations of CTAB convert hollow MSNs to solid silica nanoparticles with the collapse of the micelle oil phase [187]. In addition to altering the oil–water surface, solvent selection is a critical factor in determining emulsion stability. In the previous case, decreasing or increasing the ethanol to water solvent beyond an optimum range resulted in unstable droplets which form solid silica nanoparticles, likely due to the oil

phase, TEOS, being unstable in either a completely miscible or immiscible solvent, respectively. Using hexadecane as the oil-phase, Tsou et al. [188] reaffirms the basis that solvent selection is a significant factor in driving the collapse of hollow MSNs during synthesis.

The sensitivity of emulsion stability is also seen in the variation of water and the alcohol content to synthesize of CdS nanoparticles as seen by Curri et al. [189] They used a quaternary water-in-oil emulsion formed by CTAB/n-pentanol/n-hexane/water. The alcohol has two effects on the interfacial properties of the microemulsion that can be described as microstructural and dynamic issues. From a microstructural standpoint, the alcohol modifies the surfactant packing parameters by adsorbing to the interfacial film and thus influencing the radius of curvature of microemulsion droplets. This effect is particularly relevant in systems with use CTAB because it cannot form reverse micelles in n-hexane without the assistance of pentanol, due to its unfavorable packing parameter. A dynamic role is also played by pentanol, since a droplet formed in these conditions does not show the same interface rigidity observed in ternary microemulsions, where the plain presence of the surfactant makes the interfacial film more compact.

3.1.1. Inorganic nanoparticles

Hollow inorganic nanoparticles, ranging from metals such as gold [190] and silver [191], to ceramics such as titania [192], silica [193], and hydroxyapatite [194] can be produced through oil-in-water emulsion templates using commonly used oil phase media including alkanes to less frequently seen ones such as beeswax. Typically hollow nanostructures, with diameters ranging from 100 nm to 100 μm are produced as the oil phase naturally leads to uniform spherical cavities once the material is deposited and formed around it. In some instances, such as that with titania, microfluidic arrangements can be used in conjunction with the emulsification to rapidly and uniformly produce hollow nanoparticles. In recent years, HMSNs have become increasingly popular [195] as the empty core of the nanoparticle allows for greater pore volume, more flexibility in the loading species, such as the possibility of dual-delivery [196], as well as the functionality as a nanoreactor [197] within the nanoparticle itself. Emulsion techniques can also be employed to produce HMSNs or materials with larger porous microstructure. Multiple co-surfactants are frequently used to mediate the process. In the case of Schmidt-Winkel et al. [198], TMB was used as an oil-phase in order to pore-expand MSNs with an existing template done with Pluronic P123. Typically the pH adjustment and surfactant are done prior to silicate addition, but when done in reverse, TEOS acts as an oil phase with the surfactant assembling at the oil–water/ethanol phase boundary [187]. Fine adjustment of the ethanol: water ratio and CTAB concentration is needed in order to control the shell thickness. A more traditional method using kerosene as the oil-phase with Span® 80 as the surfactant template also yielded HMSNs [199].

Typical templating methods of producing hollow nanostructures use either hard or soft templates, with both versions requiring multiple steps or dual templating methodology where the core is selectively removed, thus rendering the nanoparticle hollow. Several approaches in recent years have demonstrated these synthesis methods. The hard templating as seen in Yang et al. [200] utilized polystyrene spheres as a foundation for the mesoporous silica growth onto its surface. Calcination done afterwards removed the polystyrene core, leaving behind a hollow mesoporous silica shell. Modification to the polystyrene through copolymerizing with poly(2-vinyl pyridine-*b*-ethylene oxide) allowed for further electrostatic interaction with CTA+ ions [201]. The concept of removing an interior core also is adopted by Fang et al. [202] where a solid silica core was selectively etched after formation of a mesoporous silica shell. A more uniform hollow MSN was developed by Chen et al. [203] through a selective, secondary etching treatment with sodium carbonate. A solid silica core was first synthesized, and then CTAC and TEOS were used to form the mesoporous shell.

Soft templating methods involve emulsions where the oil-phase (or reverse) or co-surfactant forms larger droplets within the solvent and the silica framework forms around them. TMB is frequently seen for this application, as seen in one study done by Botterhuis et al. [204] The reverse water-in-oil emulsion method done by Yu et al. [205] shows similar HMSNs produced as well. Tailoring the hollow core diameter depends on the oil phase in emulsion techniques. With kerosene [199] or octane [206] as the oil phase, larger micrometer scale HMSNs are produced, but with the same mechanism.

It is worth noting that TMB is also added after the sol–gel process in order to expand the pores templated by the surfactant. Due to the hydrophobic nature of TMB, preferential diffusion into the hydrophobic interior of the micelles allows for pore diameters up to 30 nm [41] when used with SBA-15 MSNs, with preserved crystallinity. On the other hand, Kim et al. demonstrated the effect of severely expanding the porous structure with hydrothermal treatment and TMB [207]. The resulting structure no longer retains the original uniform crystallinity found in typical M41S based nanoparticles, as was originally used prior to pore-expansion. Achieving large-pore mesoporous silica structures (9–12.1 nm) was also done using TMB combined with anionic sodium dioctyl sulfosuccinate (AOT) and Pluronic F127 systems [208].

Recently, the shift toward developing hierarchical MSNs has led toward an influx of complex porous structures well documented by Du et al. [209] To achieve the multi-level structures seen in hierarchical MSNs, typically additional co-templating agents are involved in conjunction to the primary pore determining agent. MSNs with hierarchical porous networks include those with several, homogeneous pore distributions or radially oriented pores, with a gradient of pore diameter.

To achieve distinctly multimodal pores in MSNs, nanoparticles, such as silica or polystyrene are used during the MSN formation to produce secondary or tertiary pores. Iskandar et al. [210] demonstrated the ability of various sized polystyrene latex spheres to introduce uniform large pores into silica nanoparticle formation. Later, through simultaneous polystyrene formation during silica formation, complex porous structures were formed [211]. Due to the polystyrene polymerization done in situ with the silica condensation reaction, a more irregular and heterogeneous porosity is produced.

Radial hierarchical porous structure MSNs are obtainable through co-templates as well. Through the addition of ethyl ether, which has a low boiling point of 34 °C, MSNs with radial pores are generated as it is continuously gasified and escapes during the silica condensation around CTAB-stabilized ethyl ether nanodroplets [212]. This structure is seen elsewhere with other synthesis methods, as seen by Moon et al. [213] using cetylpyridinium bromide as the templating agent in an oil-in-water emulsion synthesis. This “wrinkle” or “flower-like” structure has been observed later [214] with similar oil-in-water emulsion systems.

3.1.2. Polymeric nanoparticles

As observed with inorganic hollow nanoparticles, polymeric nanoparticles are also templated through hard templates or emulsion synthesis methodologies and produce either hollow, core–shell [215], or other hierarchal, hollow nanostructures [216] due to the removal of the core phase template. The varying hard templates used is seen with the synthesis of hollow polyaniline, a conductive polymer, nanoparticles which have used gold [217], silica [218], and polystyrene [219] as cores. Other hollow polymeric nanoparticles are typically widely used in the biomedical field, and include polypyrrole/chitosan [220–222], chitosan/dextran [223], and carbohydrate-derived, carbonaceous nanoparticles [224].

For soft templating methods, in traditional emulsion, a self-assembly of micelles comprised of a secondary phase produces the fluid template upon which the target material deposits on. In the case of polyaniline polymer hollow nanoparticles [225] the oil phase of the emulsion contains the monomer and is removed during the process of polymerization, resulting in a one-step process that requires no removal of the template. Other emulsion-based methods to produce polymeric nanoparticles include microfluidic injection and membrane-injection

systems. Microfluidic arrangements incorporating oil-in-water droplets have been demonstrated to template hydrophobic nanoparticles-in-oil [226] to produce hollow colloidosomes, or nanoparticles comprised of smaller colloidal nanoparticles. Similarly, AAO membranes can function as the injection membrane to form nanoparticles as oil phase containing the target material is passed through and enters an aqueous phase [227].

3.1.3. Semiconducting nanoparticles

Semiconductor nanoparticles are crystalline clusters of hundreds to a few thousands atoms. The shape is somewhat spherical and the size is in range of 1–10 nm in diameter [228]. Since the nanoparticle size range is of the same order of magnitude as the Broglie wavelength of electrons and holes at room temperature, the movement of the electrons and holes in the nanoparticles are confined in all three dimensions and thus quantum confinement effect can be observed. Semiconductor nanoparticles, therefore, are often called quantum dots, QDs. Due to the quantum confinement effect, the bandgap of the semiconductor nanoparticles can be controlled simply by changing their sizes [229].

QDs can be synthesized from a variety of different materials and in several different surroundings, most of which are carried out in aqueous solutions and in organic solutions. The principle of this technique was demonstrated by Murray et al. [230]. The process involves the decomposition of molecular precursors, which are molecules that deliver the monomers of the nanoparticles, at relatively high temperatures. The proposed surfactants including tri-n-octylphosphine oxide (TOPO) and tri-n-octylphosphine (TOP) are still extensively used. Since QDs are expected to be the key component of nanoscale electronic devices and also the electronic energy levels of QDs are radically affected by their sizes, there is a large demand for reproducible methods for making and handling the same size quantum dots [231]. Besides widely used emulsions and reverse micelles methods, other template synthesis techniques, such as bio-templates and electrodeposition in carbon frameworks or mesoporous silica, have also been developed.

Emulsion techniques are one of the most important template methods to synthesis of nanoparticles, as explained earlier. This synthesis has been developed to make HgSe quantum dots by the application of emulsion liquid membrane system, which use templates to control the sizes of quantum dots in internal-aqueous phase solution [232]. To improve the crystal phase of the products, it is necessary to use relatively high temperatures and long reaction times [233]. The combination of other techniques such as ultrasound [234] or microwave [235] with microemulsion is suitable for the synthesis of CdS nanoparticles. This combination could be useful for controlling of crystal phase, morphology, and the size of nanoparticles. Entezari et al. [234] studied a combinatory method of ultrasound and microemulsion for the synthesis of CdS nanoparticles. They obtained nanoparticles with a hexagonal structure at a low temperatures (60 °C), short time, and fast transition phase. The microemulsion was a quaternary oil-in-water formed by CTAB/1-butanol/-xylene/water. Caponatti et al. [235] also reported that microwave assisted synthesis in microemulsions can be a rapid and well suited methodology for the production of materials for specialized purposes. Reverse micelle is another template method used for the synthesis of QDs. Zhang et al. [182] studied quaternary CTAB/n-hexanol/n-heptane/water reverse micelles which they used as effective microreactors to prepare uniform and size controllable CdS nanoparticles. Since the cosurfactant affects the droplet microstructure and dynamic process during the reaction, the size of CdS nanoparticles can be controlled more accurately than in any other ternary reverse micelles.

3.2. Template filling syntheses

Template filling method provides a straightforward route to synthesize nanostructures of metals [236], oxides [237,238], semiconductors [239,240], and polymers [241,242]. An important advantage of this template filling method is that both the dimensions and compositions of the nanostructures can be easily controlled by choosing proper templates and varying experimental conditions. The pioneering work of Martin and co-workers has demonstrated the versatility of this method in preparation of nanowires and nanotubes by complete filling and incomplete filling the void spaces within the nanoporous membrane templates, respectively [243]. Among all the templates that have been explored, anodic aluminum oxide (AAO) membranes [244] as well as track-etched polymer membranes [243] are most common and successful. Some other nanoporous materials, such as nanochannel array glass [245], mesoporous zeolites/silica [41,246], proteins [247] and carbon nanotubes [248,249] have also been used as templates.

3.2.1. Electrodeposition

The majority of template filling fabrication methods for nanostructures fall into two categories: electrochemical deposition and electroless deposition. These methods have been extensively used to prepare a variety of metallic and semiconducting nanowires/nanotubes, QDs, polymers, etc. [238,250] First, metallic nanostructures can be easily synthesized using electrodeposition methods. Metallic nanowires and nanotubes provide a broad range of functionalities in electronic applications [84,85], magnetism [86–88], catalysis [87,89,179], biological tagging [91], photonics and plasmonics [92,93], and controlled self-assembly [94]. Nanowires grown by electrodeposition often show a pronounced crystalline texture often as a result of the crystalline orientation relative to the substrate reducing mismatch stress [115]. Crystallite size may also be controlled; growth at a lower overpotential is generally slower, and favors the growth of existing grains rather than the nucleation of new crystallites, resulting in a coarser grain size within the nanowires or even single-crystal growth. Higher temperatures may also favor single-crystal growth or large grain size by accelerating the diffusion kinetics of the deposited species [115]. The choice of electrolyte, as well as the addition of additives to the deposition solution also affects the grain size [125].

Co-deposition of alloys in solution is also achievable, though a number of factors affect the composition of the nanowires grown, including the deposition potential relative to the reduction potentials of each individual cation species, the concentrations of each cation species in the bath, the adsorption kinetics of each species at the depositing interface, and the rate of mass transfer of each species within the solution, which is in turn affected by pore diameter and length. Deposition must occur at an overpotential relative to both species, but more strongly favors the deposition of the species with the larger relative overpotential. The adsorptivity of each species plays a large role in the alloy composition, with certain combinations of elements exhibiting anomalous deposition wherein the material with the smaller overpotential deposits disproportionately; this is most commonly seen in iron-group elements [88]. While the mechanism differs by material, anomalous deposition is generally related to the formation of metal hydroxides in solution, which may differ strongly in both adsorptivity and dissociation constant from their elemental cationic forms [251]. Pore size and depth affects solution mass transfer, with more slowly diffusing or less concentrated cation species depositing more slowly as pore aspect ratio increases [88]. In spite of these limitations a wide range of alloys was reported with good control over composition [88,252–256].

A wide range of morphologies is achievable through the choice of template shape and material. Hollow spheres and core–shell structures may be grown via electroless deposition on a spherical template composed of silica [257], polystyrene [89], or polymethyl methacrylate (PMMA) [258]. The template may either be left in place in order to form a metal-dielectric interface, or dissolved to form hollow metallic shells. The process may be used with equal efficacy to form individual nanoparticles or 2D and 3D colloidal crystals [257].

Biological templates provide an array of unique and tunable substrate morphologies for templated deposition, as discussed in detail by Dickerson et al. [259] Certain proteins contain charged or polar residues

such as cysteine and tyrosine that readily adsorb metal complexes [259], making them excellent candidates for electroless deposition templates. Bovine serum albumin (BSA) makes an excellent template due to its favorable surface chemistry. It may be used to form hollow Au nanospheres; when Au ions are incorporated into a BSA-based surfactant-like foam, a disperse array of irregular Au nanoparticles may also be grown. Highly linear biomolecules also make excellent templates for the growth of metallic nanowires and nanotubes. Tobacco mosaic virus (TMV), a linear helical virus consisting of repeating protein subunits, makes an excellent template for the electroless deposition of highly organized Pt and Au colloidal clusters [259,260]. Similarly, collagen fibrils, flagellin proteins, helical peptide microtubules, and DNA have also been demonstrated as templates for the electroless deposition of linear metallic nanoparticles [259,261,262].

Templating methods can also rely not on the initial shape of a template but instead on the anisotropic surface energy of its facets. Feng et al. showed that Pt, Pd, Ru and Ir grown on highly twinned Au seed particles deposited preferentially in certain directions, leading to unique dendritic nanoparticle shapes. Similarly, Habas et al. showed that Au deposited on Pt nanocubes did not grow conformally, instead favoring linear growth due to a combination of lattice mismatch between the Pt and Au and twinning within the nucleated Au sections [263].

Second, electrochemical deposition can also be used to synthesize QDs. Kim et al. [264] reported the use of a nanoporous mask can be a viable means to form a uniform nanostructured film of CdSe quantum dots on the graphene basal plane. They applied a mesoporous silica thin film whose pore structure is composed of about 8 nm sized vertical channels in a hexagonal symmetry (SKU-1) on the graphene surface as a nanoporous mask. The graphene electrodes were synthesized by chemical vapor deposition of methane on thin Ni layers formed on SiO_2/Si substrates. A mesoporous silica film was formed on top of this graphene/Ni bi-layer by spin-coating a precursor solution composed of TEOS and a triblock non-ionic surfactant F-127 followed by aging at 800 °C, and calcination at 400 °C. Drbohlavova et al. [265] have developed a synthesis of QDs by electrochemical deposition through high-ordered nanoporous alumina templates. They use a non-toxic titanium dioxide to get quantum confinement of TiO_2 QDs. Ordered arrays of titania QDs were fabricated by anodization of aluminum and titanium bilayers. The acid provided smaller pore diameter in alumina template compared to other commonly used electrolytes.

Third, a variety of conductive polymers have also been synthesized using electrochemical deposition since they show increased potential to replace inorganic components in many applications, including electronics, optoelectronics and energy storage devices [266–268]. Early studies have demonstrated successful syntheses of polymeric nanostructures, such as polypyrrole [269–271] and polyaniline [241], using electrochemical deposition. Recently, Lee and co-workers investigated electrochemical synthetic mechanism using poly(3,4-ethylenedioxythiophene) (PEDOT). By proper selection of the monomer concentration and the applied potential, both nanowires and nanotubes can be synthesized in a porous alumina template [272]. This process is shown in Fig. 7. More recently, Lee et al. [273] was able to coelectrodeposit MnO_2 and PEDOT into an AAO template. The coaxial nanowires with PEDOT as the shell and MnO_2 as the core showed excellent electrochemical properties for supercapacitor applications.

Due to the versatile nature of electrodeposition technique, a wide class of nanostructured templates can also be adapted to electrodeposition methods for the fabrication of two-dimensional metal oxide and semiconducting materials. Such examples include the self-assembly of colloidal nanoparticles onto substrate surfaces. As observed with the secondary templating for mesoporous silica nanoparticles, polystyrene colloidal particles that have been precipitated and self-assembled on a surface were then dipped in an electrolytic solution and then Ni or Pt electrodeposited onto them [274]. Once the polystyrene was removed afterwards, a highly ordered two-dimensional metallic nanostructure remained. This methodology has been successfully reproduced using

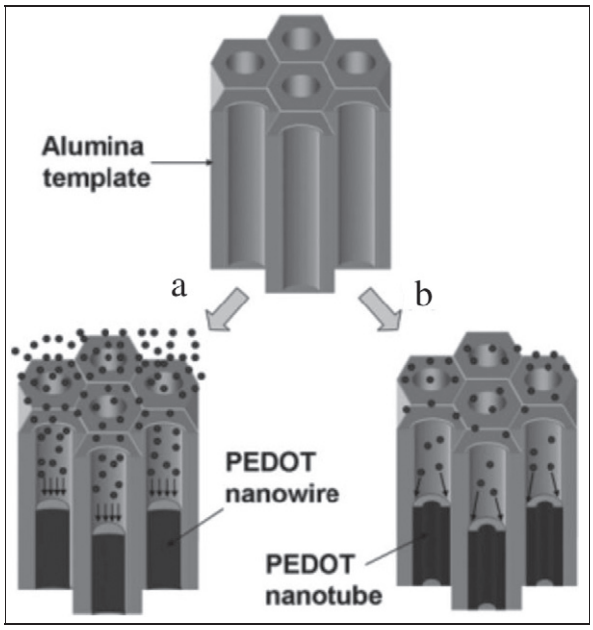

Fig. 7. Schematic of EDOT electropolymerization. Slow and sufficient monomer supply will result in the synthesis of poly(3,4-ethylenedioxythiophene), PEDOT, nanowires (a) and fast reaction rate with low concentration of monomers is required for the synthesis of nanotubes (b) [272].

other metals, metal oxides, and semiconducting materials such as Au [275], Co_3O_4 [276], ZnO [277], MnO [278], CdSe [279], and V_2O_5 [280]. With other two-dimensional structure promoting templates, such as graphene or carbon nanotubes, unusual two-dimensional nanostructures such as Mn nanoflowers [281], ZnO nanoflowers [282], and Co_3O_4 nanoflakes [283] can also be produced through electrodeposition.

3.2.2. Electrophoretic deposition

Electrophoretic deposition (EPD) is another simple and effective method to deposit material onto existing templates. In EPD, material in a colloidal suspension is moved to the target template by means of an applied potential. In principle, electrodeposition operates in a very similar fashion, but typically only refers to the ions in an aqueous solution and charge transfer via ion reduction once deposited. EPD is more versatile and general in that many of these particular requirements are not needed.

For one-dimensional nanostructures such as nanowires or nanotubes, block polystyrene-polyvinylpyrrolidone (PS-b-PVP) templates combined with EPD has been used to selectively deposit modified CdSe into the pores [284]. This approach differs from standard electrodeposition methods which originate with the metal ion in solution and effectively reduce ions as they are deposited onto the target electrode. Other metal oxides such as ZnO [285] and Fe_2O_3 can form nanowires from a colloidal suspension when combined with electrophoretic deposition [286]. EPD more often is used to first deposit the colloidal framework [287], such as polystyrene or latex nanoparticles, on a substrate that is then used to template two-dimensional nanostructures, nanoflakes, or nanodisks. In some instances, graphene or carbon networks are deposited via EPD, as seen with NiO nanoflakes that were grown from a combinatory EPD and chemical bath deposition [288]. Materials such as hydroxyapatite scaffolds can be deposited with EPD as well [289] from which the surface functions as a template for cellular growth or other biomaterial adhesion.

3.2.3. Sol–gel deposition

Sol–gel template filling deposition provides another pathway to achieve desired nanostructures. Similar to the conventional sol–gel

processing, a dispersion of colloidal particles (the sol) is prepared first. The chosen templates are then immersed into the precursor sol for certain amount of time, followed by drying and thermal treatment for templates removal as well as structural densification. Compared with other template filling methods, sol–gel fabrication routes also offer high control of the chemical composition through doping and modification of the precursor sol–gel, in addition to the lower temperatures as opposed to evaporation or deposition methods.

In the early stages, Martin and co-workers [237,238] performed extensive studies on synthesizing nanostructures of various oxides using sol–gel template method, such as TiO_2, WO_3, ZnO, V_2O_5, MnO_2, Co_3O_4, and SiO_2. It is worth pointing out that the shape of the nanostructures can be easily controlled by varying the immersion time. TiO_2 nanowires and nanotubes, for instance, were obtained by simply altering the immersion time from 60 s to 5 s [237]. However, this technique has its own limitations. Since the colloidal content in the sols is very low (~5 vol.%) and the capillary action is the only driving force to fill the templates, the amount of solids packed in the pores is still significantly less than the maximum possible loading, which leads to cracking and defects on the nanostructures.

In order to overcome above-mentioned disadvantages, Cao and coworkers combined conventional sol–gel template filling deposition with electrophoretic deposition to synthesize nanostructures of a variety of oxides materials [290–292]. Fig. 8 shows a schematic of this process. For example, lead zirconate titanate (PZT) nanowires of 70–150 nm in diameter and ~10 μm in length were grown in PCTE membranes [290]. Additionally, fabrication of uniform nanowires with a diameter of 125–200 nm and a length of 10 μm over large areas were also demonstrated using TiO_2, $BaTiO_3$, SiO_2, $Sr_2Nb_2O_7$, and PZT [291,292]. To further reduce the diameters of the nanowires, e.g. down to 20 nm, electrochemically induced sol–gel deposition was introduced recently. Miao et al. [293] fabricated highly ordered TiO_2 single crystalline nanowires with diameters of about 20 nm and 10 nm using AAO templates. The growth mechanism of the TiO_2 nanowires was also proposed.

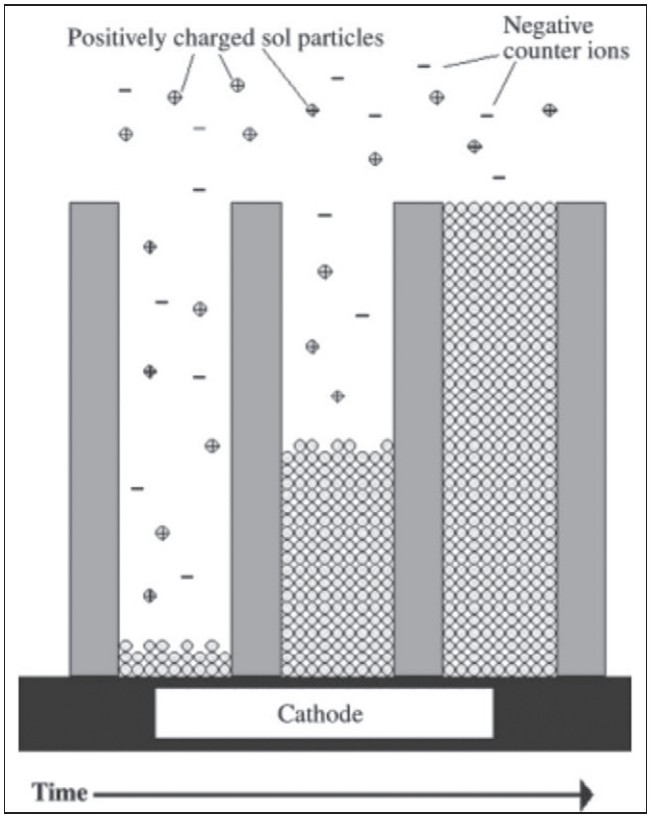

Fig. 8. Schematic representation of the progression of the growth process [290,291].

Two-dimensional structures can be produced in a similar fashion to one-dimensional nanostructures but are heavily dependent on the material itself. Due to preferential crystallographic orientation and growth of the metal oxides, control of the nanostructure is often due to controlled growth kinetics. Examples of this include mesoporous silica sol–gel film [294] produced by dip-coating to yield uniform cubic and hexagonal pores, or intentionally seeding the substrate to align crystal growth, as with ZnO on Si and Al substrates [295]. Through modification of the sol–gel phase as well, structure-directing agents can be used to further adjust the final structure of the material. Diblock copolymers such as polystyrene-polyethylene oxide were added to a ZnO sol–gel, resulting a range of different nanostructures, including wormlike aggregates to spherical granules [296].

3.2.4. Vapor deposition

In addition to solution based deposition methods for fabricating solid nanostructured materials, vapor deposition can be used to form nanostructured materials using a template as the target substrate as well. As with solution based deposition, vapor deposition is highly versatile and can accommodate a variety of species for both the mobile and target material. The primary types of vapor deposition are chemical vapor deposition (CVD), atomic layer deposition (ALD), and plasma vapor deposition (PVD). Inherent to all these methods is that the material to be deposited onto the surface must be atomized and well-dispersed so that uniform monolayer growth can be achieved. There is a tremendous amount of organic and inorganic materials that can be vapor deposited onto templates, primarily porous membranes such as AAO and as seen with other methods to produce one-dimensional nanostructured materials.

Nanowires and nanotubes of metals and semiconducting metal oxides including Si [297], CrO_2 [298], ZnO [299], and CdS [300] can be synthesized using AAO membranes. In these methods, the target material is placed upstream in a reactor tube and deposited downstream onto the template material. Due to elevated temperatures during most vapor deposition techniques, ranging from 260 to 650 °C [297,298], the template material is dominantly AAO for thermal stability reasons. However compared to electrodeposition or sol–gel processes, in some instances, the membrane seems to be ineffective in controlling uniformity with vapor deposition methods, as seen with ZnO [301]. Additionally, precise control over the deposition is required in order to effectively introduce the metal oxide into the pores. While some methods such as shadow evaporation through electron beam vapor deposition [302] are specific toward surface templating, ALD can also effectively deposit alumina into the entire pore depth of the membrane [303].

In addition to carbon nanotubes [304,305] that can be formed through vapor deposition into porous templates, monomers of polypyrrole [306], poly(acrylonitrile) [307] and other polymers [308] have been vapor deposited and then polymerized within the porous channels of AAO. This approach allows for excellent control of the nanotube thickness and uniformity through the monomer feed, as seen by Jang et al. [306]. Other templates besides porous membranes have been used to a lesser extent. Two-dimensional nanostructures such as graphitic nanoribbons have been produced through CVD onto DNA as the template [309]. Through templating with reverse micelles of PS-b-PVP onto silicon substrates, ALD was done to achieve nanotemplated ZnO onto the highly homogeneous and periodic surface [310].

3.2.5. Melt and solution filling

Metallic, semiconducting and polymeric nanowires/nanotubes can also be synthesized by injection of the melt liquid into templates [311]. Huber et al. [311] fabricated nanowires of various metals (In, Sn and Al) and semiconductors (Se, Te, GaSb and Bi_2Te_3) using pressure injection technique. Later, Zhang et al. demonstrated that relatively low melting points metal bismuth (Bi) can also be applied using AAO

templates to prepare ultrafine nanowires (13 nm in diameter) with extremely high packing densities, up to 7×10^{10} cm^{-2} [312,313]. Recently, Steinhart et al. [242] synthesized polymeric nanotubes by filling melt-processible polymers, such as polytetrafluoroethylene (PTFE), polymethyl methacrylate (PMMA) and polystyrene, into ordered porous alumina and oxidized macroporous silicon templates. More recently, other novel templates, such as carbon nanotubes, were extensively utilized for synthesizing nanowires using the same technique [249,314]. Ajayan et al. [248] reported that the molten Pb could fill the carbon nanotubes through strong capillary force, but only ~1% of which were filled. In addition, Kiang et al. [315] used single-walled carbon nanotubes to produce molecular nanowires by filling Bi. It is reported that the percentage of filled nanotubes was increased to 30%. Besides metals, molten oxides, such as PbO_x [248], V_2O_5 [316], and MoO_3 [317], were also reported to be able to fill carbon nanotubes.

In addition to the melt, solution is another media that can be employed to fill the both membrane and nanotube templates, along with chemical reactions. As a typical example, Han et al. [318] successfully synthesized gold, platinum, and silver nanowires using mesoporous silica SBA-15 as a template. To reach this, metal precursors ($HAuCl_4$, $Pt(NH_3)_4(NO_3)_2$, and $AgNO_3$) were first incorporated into mesoporous channels by immersing template into aqueous solutions and subsequently treating with CH_2Cl_2. The metal precursors were then reduced under a H_2 flow to form nanowires.

Furthermore, it is also worth mentioning that a significant amount of syntheses falling into this solution filling category are in situ polymerizations. Similarly, templates such as AAO membranes are immersed into a solution that contains monomer as well as initiator [111] [319,320]. The polymer then nucleates and grows on the walls due to solvophoic and electrostatic interaction between polymer and walls [321]. Parthasarathy et al. [319] showed that the wall thickness of polyaniline (PANI) tubes could be easily altered by controlling polymerization time with longer polymerization times resulting in thicker walls. Nanostructures of other polymers, such as polypyrrole [322–326], poly(3-methylthiophene) (PMT) [323,327], polyacrylonitrile (PAN) [328,329], and poly(3,4-ethylenedioxythiopene) (PEDOT) [330] have also been reported using this in situ polymerizations template filling method.

3.3. Other methods

While template-filling and emulsion/colloid approaches to templating nanostructured materials cover a substantial amount of syntheses, other methods such as layer-by-layer and lithographic techniques also are used to template one-dimensional and two-dimensional nanostructured materials. Both methods involve previously mentioned precursors, such as sol–gel or polymer melts but presented here is an emphasis on the usage of either a multilayer aspect or reproducible, large scale methodology, respectively. It is worth noting that while these two methods compliment template filling syntheses discussed earlier, there are still many other unique methods that are rapidly-evolving and as such, not mentioned here.

3.3.1. Layer-by-layer deposition

The layer-by-layer (LbL) templating method is a simple and effective deposition method for a variety of templates. Being highly popular and versatile, the LbL deposition technique provides a facile to form nanostructures onto an existing template. In principle, LbL encompasses a large span of deposition techniques, often overlapping other very similar template-filling techniques such as electrodeposition and other solution-based methods seen earlier [331,332]. As such, solely examples of specific zero or one dimensional structures uniquely templated by layer-by-layer approaches involving multilayer or hierarchal structures are discussed here [333]. Due to the basic principle that the desired material(s) simply take their final shape and structure from the target template, material affinity and compatibility are the most important factors in successful layer-by-layer depositions.

Multilayered hollow and core–shell nanoparticles are often produced by LbL deposition. In the case for polymeric layer-by-layer approaches, alternating layers of anionic/cationic species, such as such polystyrene sodium salt (PSS) or poly(diallyldimethylammonium chloride) (PDDA) respectively are used. Often a precursor functional group is required to improve adhesion or bonding between the template and the first layer. However, strongly ionic polymers such as PDDA can be used to establish a favorable charged surface to promote further electrostatic bonding without any precursor functionalization [334]. In a similar group of strongly cationic polymers, poly(allylamine hydrochloride) (PAH) and poly(ethyleneimine) (PEI) are also frequently used to alternate with an appropriate anionic polymer such as PSS or poly(acrylic acid) (PAA). The PSS-PAH LbL system has been used in instances to template 0D [335,336] and 1D [337] nanostructures.

The usage of PDDA, PSS, or PAH are frequently seen as precursor modifiers for metal oxide deposition onto carbon nanotubes, which themselves do not allow for facile deposition of inorganic compounds on its surface. Nanotubes of indium-tin-oxide (ITO) [338] Au [339], CdTe [339], TiO_2 [340], Pt/CeO_2 [341], WO_3 [334], and Y_2O_3/Yb/Er [342] have been produced using this method. For the formation of hollow nanoparticles, PS nanoparticles as seen with templating hollow MSNs, are also used in conjunction with LbL to produce hollow nanoparticles of titania, silica, or laponite (synthetic clay $[Na_{0.7}(Si_8Mg_{5.5}Li_{0.3})O_{20}(OH)_4]$) with PDDA/PAH/PSS polyelectrolytes used as the alternating layers [343]. Silica nanoparticles also serve a similar role to PS and can be used with polyelectrolyte/metal oxide LbL techniques [344].

3.3.2. Lithography and stamping

Lithographic and stamp based methods are techniques that have been employed recently to template nanostructured materials. Advantages of this lithographic approach include a highly repeatable, uniform, and high yield production of the desired nanostructured material. Through stamping, nanoimprint, and interference lithography, a tremendous range of nanostructures can be obtained, as the master stamp or mask will dictate the final structure. However, several instances throughout literature emphasize specifically novel and unique methods involving lithography to produce nanostructured materials and are outlined here.

With vigorous nanoimprint lithography, high resolution, uniform nanostructures can be produced through selective masking and etching processes. A representative procedure is that nanostructured Si mold (template) was first fabricated through conversional etching process, and then transferred into nanopatterned films [345,346]. Recently, Aryal et al. [347] introduced a novel route to fabricate nanoporous Si mold using freestanding nanoporous anodic alumina membrane as a mask for etching. More recently, AAO membranes were directly used as templates through a thermal imprinting step to synthesis freestanding poly(3-hexylthiophene) (P3HT) nanopillars [348] and cross-linked divinyltriphenylamine (DVTPA) nanorods [349].

Interference lithography involves generating wavefunctions that cause an interference pattern onto a mask material which then transformed the pattern into a visible feature. Interference lithography provides excellent resolution and uniformity for templating nanoporous arrays but for higher dimensional and geometries, obtaining uniform symmetry requires a greater number of beam interactions and their corresponding algorithms. While a physical template is not used, establishing a method to produce three-dimensional nanostructures on planar substrates has been developed to produce structures beyond pores and pillars, and instead, unusual novel frameworks on the surface [350].

In addition to lithographic techniques, stamping allows for patterned materials that are directly transferred into substrates, which can be the final pattern or seeds from which other growth mechanisms can form the nanostructure. This approach allows for the elimination of

faults, anomalies, or other non-desirable features to be transferring during the process. Using direct stamping with a gold template produced from an AAO membrane, gold seeds were transferred onto a GaN/Si substrate, from which highly ordered and homogeneous ZnO nanowires of 90 nm diameter were grown through vapor deposition [351]. A combination of traditional lithography and stamping done by Park et al. [352] produced PDMS stamps with sub 20 nm features from the original SiO_2 nanostructures. As the nanostructure features approach these dimensions, to prevent incorrect features from transferring, a novel modification done by Huang et al. [353] incorporated a dual-stage stamping method to transfer hydrophobic features to the non-essential surfaces, thus preventing those non-patterned surfaces from transferring features to the substrate. Although only done with micron spacing between features, the approach allows for potential stamping of nanostructure with minimal flaws.

4. Applications

4.1. Solar cells

During the past decade, solar cells incorporating controlled nanostructures have drawn increasing attention due to their superior performance, processing flexibility, ease of tuning, etc. [354–357]. The most direct strategies to improve the absorption of solar radiation and increase efficiency are to enhance the optical path length and/or to increase light reflecting and scattering area in the cell. These can be achieved by engaging nanostructures e.g. spherical hollow nanoparticles. It is well known that when the dimension of the hollow nanoparticles is comparable to the wavelengths of UV and visible lights, multiple reflections are enhanced within their interior cavities [358]. In addition, spherical hollow nanoparticles can also provide a larger surface/volume ratio for scattering incident light compared with solid nanoparticles. Kondo et al. [359] used TiO_2 hollow spheres as the electrode to fabricate dye-sensitized solar cells (DSSC). The TiO_2 hollow spheres were synthesized by hydrolysis of titanium tetraisopropoxide (TTIP) in the presence of PS-bead template, followed by removing the PS cores. They demonstrated that the per-weight efficiency was 2.5 times higher than those of the conventional DSSCs of TiO_2. Similar and improved work has also been reported in other literature [360–362]. Besides TiO_2, ZnO was also utilized for preparation of hollow spheres. Outstanding work has been conducted by Dong et al. [363], where multi-shelled ZnO hollow spheres were produced through different heating processes. The DSSCs using these multi-shelled nanostructures as photoanodes show high energy conversion efficiency of 5.6%.

In addition to the above-mentioned hollow spheres that are normally engaged into electrode, metallic nanoparticles can also be employed in the cell architectures because of their plasmonic effects. The strong scattering from surface plasmon resonance is known to effectively enhance light absorption, which also sensitively depends on the size and shape of the nanoparticles [364–366]. Although various deposition methods exist, template-based synthesis provides a facile way to deposit controlled plasmonic nanoparticles. Nakayama et al. [367] decorated thin GaAs solar cells with Ag nanoparticles using AAO templates as deposition mask. The height of the nanoparticles can be controlled by varying the deposition thickness. They showed an 8% increase in the short circuit current density and at least 10% increase in the fill factor of the cells. Recently, Pryce et al. [368] used similar template masking process to deposit 100 nm Ag nanoparticles into InGaN quantum well solar cells, which leaded to enhancement of the external quantum efficiency by up to 54%.

On the same principle, enhanced light scattering and increased interfacial area were proven to be the simple and effective methods to improve the performance of solar cells. One-dimensional and two-dimensional nanostructures were introduced into device structures for these purposes [369]. As a matter of fact, 1D/2D nanostructures were more extensively studied for solar cell applications compared with nanoparticles due to additional advantage of enhanced charge carrier collection efficiency [370–372]. Normally, oriented one-dimensional nanostructures, such as nanowires or nanotubes, are aligned perpendicular to the substrates, which facilitates charge carrier transport as well as reduces recombination. For example, Martinson et al. [373] embedded ZnO nanotube arrays as working electrodes into the dye-sensitized solar cells. The nanotubes were synthesized using AAO templates by atomic layer deposition, and the resulting devices showed exceptional open circuit voltage, fill factors, and power efficiency. More recently, Kang et al. [374] synthesized highly ordered TiO_2 nanotube arrays using alumina templating method with modified sol–gel route, and then integrated into the DSSCs. The power conversion efficiencies of their devices were able to reach up to 3.5%. Fig. 9 represents a schematic of the architecture of this process and SEM-images of the TiO_2 nanotubes obtained.

As we mentioned earlier, efficient charge separation and reduced recombination are two key design elements in solar cells, which is particularly true for developing organic solar cells. Unlike the case in inorganic solar cells, organic solar cells generate excitons (electron–hole pairs with high bonding energy) at the donor/acceptor interfaces when absorbing light. Since the exciton diffusion length is typically ~10 nm before recombination [375,376], it is critical to limit the morphology of heterojunction to the nanoscale. An ideal bulk heterojunction solar cell structure, therefore, was proposed afterwards, which consists of vertically aligned conjugated polymer nanorods (donor) attached to the anode and surrounded by acceptor materials connected to the cathode [377,378]. Such well-organized nanostructures are extremely challenging to obtain due to disorder nature of polymers. Template-based synthesis method seems to be the most promising approach. Haberkorn et al. [349] fabricated highly ordered nanorod arrays of a hole-conducting cross-linked triphenylamine derivative using AAO templates, which can be potentially used in the solar cells due to their excellent electrochemical properties and their organic solvent resistance. It is also worth noting that the aspect ratio of the nanorods was optimized in order to prevent from aggregation and collapse. Recently, Kim et al. [379] fabricated organic photovoltaic devices using P3HT nanorod arrays obtained from similar AAO template-assisted method. The device yielded around 1.12% power conversion efficiency. More recently, Chen et al. [348] further increased the efficiency up to 2.4% by embedding freestanding P3HT nanopillar arrays.

4.2. Thermoelectrics

There has been a renewed interest in thermoelectric materials for small, scalable, and solid-state cooling and power generation applications. Thermoelectric materials and devices generate a potential gradient when a thermal gradient is applied, or vice-versa, allowing for the direct conversion of waste heat into electricity, or solid-state, reversible heating and cooling. The relationship between the thermal and potential gradients is given by the Seebeck coefficient, Eq. (1):

$$\alpha = -\frac{\Delta V}{\Delta T} \tag{1}$$

The performance of a thermoelectric material is quantified by its figure of merit zT, given by the Eq. (2)

$$zT = \frac{\sigma \alpha^2 T}{\kappa} \tag{2}$$

where σ is the electrical conductivity, α is the Seebeck coefficient, T is the operating temperature, and κ is the thermal conductivity. At a given operating temperature, the device efficiency approaches the Carnot efficiency as zT approaches infinity [380]. Current-generation materials have a zT around 1, though a zT of 4 or greater is desired for materials to reach broad commercial acceptance in the energy sector

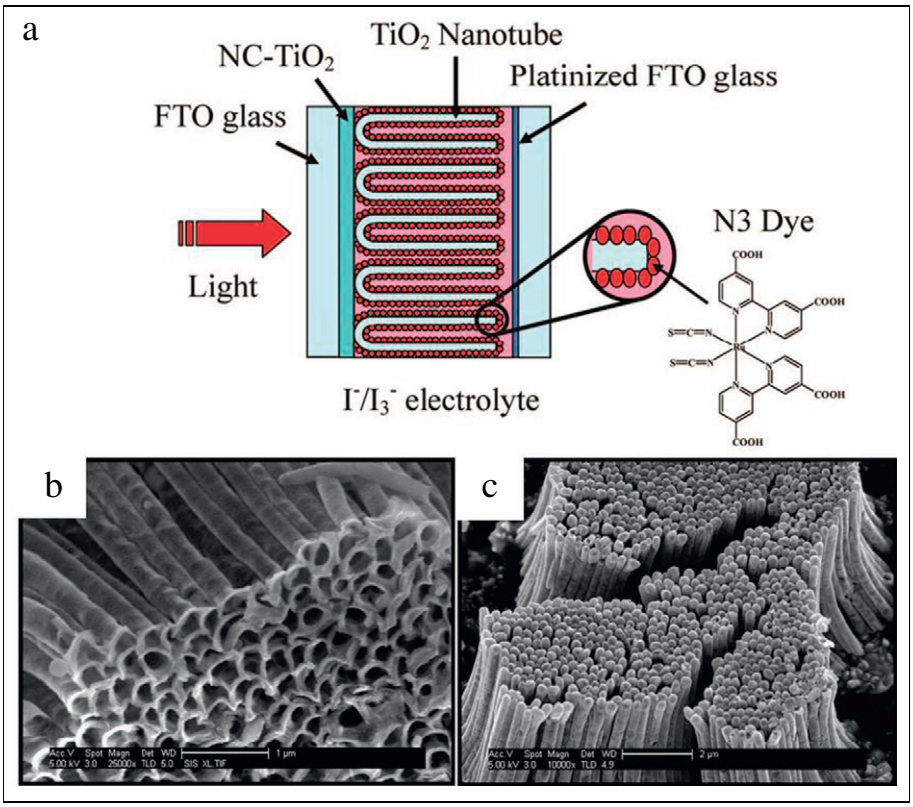

Fig. 9. a) Schematic representation of the architecture used to fabricate dye-sensitized solar cells utilizing the TiO_2 nanotube arrays. b) Field emission-SEM images of top-down of TiO_2 nanotube arrays after removal of the anodized alumina template. c) Field emission-SEM images of the TiO_2 nanotubes that have been transferred onto an adhesive carbon tape [374].

[381]. The thermal conductivity κ may further be expressed as $\kappa = \kappa_e + \kappa_l$ where κ_e is the contribution from mobile charge carriers and κ_l is the lattice thermal conductivity. The Wiedemann–Franz law indicates that κ_e scales linearly with σ; therefore the figure of merit may be increased by disproportionately scattering phonons in order to minimize kl, while simultaneously allowing charge carriers in the material to flow unimpeded. Such a combination of properties is described as "phonon glass-electron crystal" behavior [382].

Nanostructures may be used to tune the properties of a thermoelectric material via multiple pathways: the reduced size affects electronic structure, leading to novel reduced-dimension regimes in carrier transport; boundary scattering from structures smaller than the mean free path of phonons selectively decreased lattice thermal conductivity; and surface states which differ electronically from the bulk may provide beneficial properties as the ratio of surface to bulk increases with decreasing structure size.

Bismuth nanotube and nanowires [383] have been shown theoretically to undergo a semimetal-to-semiconductor transition below a critical radius, due to energy band quantization from quantum confinement effects as well as classical scattering. This modification in the electronic structure has been experimentally demonstrated, along with the corresponding zT enhancement [384]. Similar improvements in the zT of chalcogenides such as Bi_2Te_3 and $Bi_xSb_{2-x}Te_3$, some of the best bulk thermoelectric materials, have also been modeled [385, 386] and demonstrated experimentally [387,388]. These materials may be readily grown in nanowire morphology via templated electrodeposition [387,389–393], with Bi_2Te_3 nanowires also having been grown via galvanic displacement on DNA templates [394]. Increased zT has also been demonstrated in superlattice structures, such as PbTe/Te, PbTe/PbSe [395], and Bi_2Te_3 [396] superlattice structures may be combined with nanowire morphologies via templated electrodeposition for potentially even greater gains in zT.

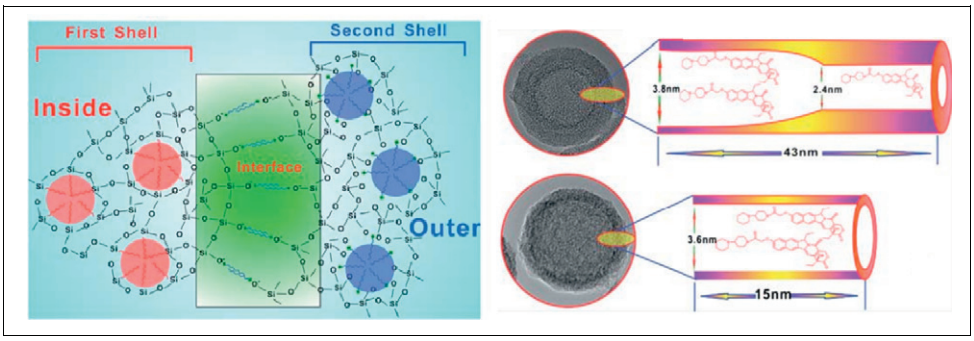

Fig. 10. Hollow MSNs with single and dual porous structures capable of tuning the release of hydrophobic and hydrophilic species [468].

Certain systems may utilize the difference in mean free path for electrons and phonons to selectively reduce κ_l while leaving σ unaffected. Hochbaum et al. demonstrated a 100-fold increase in the zT of Si nanowires for diameters under 50 nm [397]. The mean free path for phonons is 300 nm while it is only 100 nm for electrons; surface scattering therefore disproportionately affects the phonons. They furthermore showed that nanowires with rough surfaces, morphologically similar to those achieved through templated deposition, provided an even larger increase in zT, perhaps due to the multiple length scales on which phonon scattering occurs or the modification of phonon modes that do not contribute to thermal conductivity but improve the thermopower [398]. Si nanowires may be grown via VLS growth [399], where their growth diameter and location is templated on Au nanoparticles deposited on a Si substrate, or via templated electrodeposition [400]. Alloys and heterostructures of Si and Ge have also been shown to increase zT. Such structures may take the form of axial superlattice nanowires [401], core–shell nanowires [402,403], and alloyed nanowires [404,405].

An additional promising class of thermoelectric materials are skutterudites, most notably $CoSb_3$, which provide a lead-free alternative to PbTe-based thermoelectrics over the 200–600 °C temperature range [380]. Skutterudites have a large interstitial void that can play host to "rattler dopants" [406] which may be used to selectively scatter phonons; these materials therefore provide the opportunity to combine rattler scattering and confinement effects for a potentially significant increase in zT above the bulk value. The growth of $CoSb_3$ nanowires via electrodeposition has been demonstrated [163,407] and it is predicted that similar enhancement of zT from confinement effects should be observed [163,408], though this has yet to be experimentally verified. In all of the above classes of material, careful control of feature size is paramount to both understanding and controlling the size effects that lead to enhanced thermoelectric performance, be it quantum confinement and band structure modification, enhanced phonon scattering, or other effects. Template-based syntheses provide a powerful and scalable platform for determining the size of the nanostructures grown. This enhanced size control facilitates the systematic analysis of size effects in these materials, and provides a platform for the large-scale growth of such nanostructured materials for future device integration. Where nanostructured thermoelectrics may prove expensive when fabricated by other methods [409], templated growth may provide an inexpensive and easily scalable alternative for the production of next-generation thermoelectric materials.

4.3. Catalysis

Catalysis is a key tool for chemical sustainability and improved catalytic processes, which will make more efficient use of natural resources, reduce the amount of byproducts formed, and eliminate contaminant effluents, in addition to lowering energy requirements [6]. The high chemical, thermal, and mechanical stability, combined with the highly uniform pore distribution with tunable pore size gives MSNs high surface area and adsorption capabilities, thus allowing it to be excellent candidates for catalysis applications. Inorganic, organic and enzymatic catalysis fields have been revolutionized by introduction of MSNs as supports due to dramatic increase of contact area and thus contributing to overall reaction yield [410–412]. Mesoporous materials with narrow pore size distribution may replace zeolite catalysts in some commercial applications, and in many research applications they already now have a comparable or superior performance compared to conventional microporous zeolites or amorphous silica-alumina catalysts, although it is not always clear that the right zeolite catalyst had been chosen as a benchmark [413].

Mesoporous silica nanoparticles exhibit great potential in reactions, which require milder acidity and involve bulky reactants products, such as mild microcracking reactions. One of the most important features of ordered mesoporous oxides, as it was mentioned previously, is their exceptionally high surface area. This can be exploited to create highly dispersed active species on interacting and non-interacting support materials. Ordered mesoporous oxide have been used as supports for metals, metal oxides and as a host material for anchoring stereo- and enantioselective species, such as certain molecular catalysts [413]. Currently, zeolites are one of the most important materials used as catalyst. Most of the current large-scale commercial processes using zeolite-based catalyst are in the petroleum refining and petrochemical industry [414] but their implementation in chemical industry, environmental applications, non-conventional conversion processes of gas [415], oil, and coal, bio-mass transformation, and car exhaust treatment [416] is increasing rapidly [411].

Although the molecular dimensions of the pores size or shape selectivity of zeolites are beneficial for guest molecules in the reactions, it is known that because zeolites present a configurational regimen of diffusion, the micropores restrict the diffusion rates of reactant and product, limiting the activity of zeolite catalysts for certain reaction [417]. The diffusion rates of the reactants, products and intermediate can be restricted or improve by pores which depend on shape selectivity. Using templates such as carbon frameworks to obtain mesoporous zeolites the diffusion coefficient can be increased more than 2 times due to the diffusivity is proportional to the diameter. Since the point of view of large reactant molecules, the presence of mesoporous in the zeolite will increase the external surface and pore openings accessible to the reactant [417,418]. Mesoporous zeolites can be used for a number of industrial catalytic applications such as catalytic cracking, hydrocracking, aromatic alkylation and alkene hydroisomerization, as well as fine chemical synthesis [417,419,420].

4.3.1. Cracking

MSNs have been extensively investigated with regard to their use in cracking and hydrocracking reactions. Despite of the low acid strength and low hydrothermal stability of MCM-41 catalysts, the advantage of having larger pores improves the accessibility for larger molecules. MCM-41 catalysts show substantial cracking activity for bulky substances such as palm oil [421,422]. FSM-16 structured mesoporous silica nanoparticles are active in the thermal degradation of polyethylene to fuel oil [423].

In order to improve the activity of the silica or aluminosilicate MCM-41 in acid catalyzed reaction, this material can be modified. For example, Sun. et al. [424] sulfated ZrO_2 supported on MCM-41 shows similar activity with bulk sulfated ZrO_2 catalyst in reactions such as cumene, n-hexane or 1,3,5-triisopropylbenzene cracking, obtaining a slower catalyst deactivation for the supported catalyst compared to bulk sulfated ZrO_2. Sulfated tetragonal ZrO_2 supported on SBA-15, which is another type of MSN, shows about two times higher yield of methyl ter-butyl ether (MTBE) that bulk zirconia in agreement with the study of Landay et al. [425] $H_3PW_{12}O_{40}$ in the cracking of 1,3,5-triisopropylbenzene initially increased with increasing heteropoly acid loading, and reached a maximum at around 23 wt.% loading [426,427].

Zeolites are a typical catalysts used for the cracking of hydrocarbons. Some of the most important commercial processes, such as FCC, hydrocracking, aromatic alkylation, isomerization of sort chain alkanes and C8 alkylaromatics, or disproportionation of toluene, are based on zeolite catalyst [411]. ZSM-5 is one of the most important zeolites due to its high Si/Al ratio and its porous structure. Because of its properties, including large surface area, large selectivity and resistance to acidic conditions, it is well suited for catalytic applications such cracking. These properties are due to the use of OSDA template in the synthesis. ZSM-5 is used as catalyst for cracking of n-hexane. Specifically, ZSM-5 zeolite is one of the most efficient catalysts for the naphtha catalytic cracking process at high temperatures (873 K–923 K) [428–433]. One of the most important problems of the cracking process is the amount of coke which is produced over the zeolite. This coke fouls the catalytic surfaces and blocks the micropores. Therefore, the regeneration of HZSM-5 by calcination in air is necessary. However, a small amount of

steam generated in the hydrothermal atmosphere during the calcination results in permanent deactivation due to the introduction of aluminum in the zeolite framework. Zeolites with mesoporous structure have a beneficial effect in reactions such as slurry-phase reactions where the diffusion is much slower than for gas-phase reactions. Slurry-phase catalytic cracking and isomerization of n-hexadecane exhibits pronounced activity enhancement using mesoporous zeolite as catalyst than the conventional zeolite [417,434]. Also, an enhancement of cumene cracking was obtained using mesopororous ZSM-5 [435].

Cu-ZSM-5 and Ag-ZSM-5 were used as catalyst in the n-heptane cracking with various cation exchange degrees and P/H-ZSM-5 before and after steaming under various conditions. Whereas the P/H-ZSM-5 exhibited a lower n-heptane cracking activity that H-ZSM-5 due to a decrease in Bronsted acidity by phosphorous impregnation, the reduced Cu-ZSM-5 and Ag-ZSM-5 exhibited similar n-heptane cracking activities as H-ZSM-5 due to generation of Bronsted acid sites by reduction of metal cations [436].

Alkylation of benzene with ethylene is another example of the importance of the mesoporous in zeolites. This reaction is one of the most important industrial processes to produce ethylbenzene which in turn is the raw material for styrene manufacture. Mesoporous zeolite single crystal showed significantly improved catalytic activities and selectivity as compared to conventional zeolite [437]. The selectivity for ethylbenzene increases by 5–10% depending on the benzene conversion. The higher selectivity is due to improved mass transport in zeolites. By modifying mass transport, it is possible to obtain higher selectivity and higher product selectivity using mesoporous zeolite catalysts that can be obtained by template synthesis.

4.3.2. Fine chemical synthesis

The large pore openings of mesoporous materials offer the advantage of effective diffusion of bulky substances as they are often found in fine chemicals synthesis. One of the first examples of that is a Friedel-Crafts alkylation with mesoporous aluminosilicates. Friedel-Crafts alkylation is a special class of electrophilic aromatic substitution which uses a Lewis acid as catalyst. The reaction has wide applications in the preparation of substituted aromatics [438]. The Al-MCM-41 with a pore diameter of 3 nm is active in Friedel-Crafts alkylation of 2,4-di-tert-butylphenol with cinnamyl alcohol. The yield over Al-MCM-41 (35%) was higher than over HY zeolite (<1%) because of diffusion restrictions of the bulky 2,4-di-tert-butylphenol that there are in the zeolites [413,439]. Furthermore, Al-MCM-41 gave a much higher yield of dihydrobenzopyran than conventional catalysts, such as H_2SO_4 (12%) and amorphous silica-alumina (6%) catalysts. Al-MCM-41 is also used in the alkylation of unsubstituted phenol with methanol [413,440]. Friedel-Crafts alkylation of benzene with benzyl chloride in liquid phase uses Ga impregnated MCM-41 as well as Fe-impregnated MCM-41, Al-MCM-41, and La-MCM-41 [413,441].

Acetalization is an important reaction for the protection of carbonyl functional groups. This reaction does not require strong acidic conditions, and therefore, mesoporous silica with weak to intermediate acid tolerance is a suitable catalyst in this reaction [413,442,443]. Different MCM-41 are used as catalysts in different acetalization with: Al substituted MCM-41 being used in the acetalization of heptanal, 2-phenylpropanal, and acetaldehyde with trimethyl orthoformate [413,442]; Al-MCM-41 in the acetalization of jasminaldehyde [413,443]; and MCM-41 in the acetalization of cyclohexanone [413,444]. Aluminum substituted mesoporous silica exhibits better activity in Diels–Alder reactions with large organic molecules compared to conventional microporous zeolites or ion exchange resins. Mesoporous aluminosilicate, ion-exchanged with $ZnCl_2$, was found to be effective in the Diels–Alder reaction of cyclopentadiene and methylacrylate [413,445,446].

4.3.3. Reduction/oxidation reactions

Several liquid-phase oxidation processes are catalyzed by soluble oxometallic compounds. Their substitution by zeolites based oxidation catalyst presents several advantages, beyond the benefits of working with a solid catalyst. The zeolite structure contributes with steric and confinement effects, and the incorporation of the desired metal atom in the framework (Ti, Fe, and Sn) results in well-dispersed active sites, generally stable toward leaching [6,413].

Titanium-silicalite (TS-1) is presently the most employed zeolite-based oxidation catalyst. This Al-free MFI zeolite, which has the titanium atoms in tetrahedral framework positions, is commercially used for olefin epoxidation, hydroxylation of phenols and ammoxidation of ketones, or oxidation of sulfur compounds and ethers, using hydrogen peroxide as the oxidant [6,413,447,448]. Titanium modified MCM-41 was researched on ordered mesoporous materials studied as selective oxidation catalysts [413,449]. Such mesoporous materials present a clear advantage of a larger pore system than zeolites, enabling the oxidation of much larger hydrocarbons. Leaching is a particular problem of solid catalysts in liquid-phase processes, and especially in oxidation reactions with peroxides, which is attributed to the strong complexing and solvolytic properties of oxidant products [413,450]. Significant Ti-leaching has been reported for the liquid phase oxidation of crotylalcohol using Ti-β and Ti-MCM-41 served in all samples with the exception of TS-1, and the order of leaching was Ti-Alβ > Cp_2TiCl_2-grafted MCM-41 > Ti-MCM-41 > Ti-Al-MCM-41 ≫ TS-1, when hydrogen peroxide was used as an oxidant. If hydrogen peroxide was replaced with tert-butyl hydroperoxide (TBHP) as an oxidant, Ti-leaching was minimized and the selective epoxide formation was observed with Ti-β and Ti-MCM-41 [413,451].

4.4. Biomedical applications

Nanomaterials have been used for wide range of biomedical applications such as drug delivery, imaging and diagnostics, tissue engineering, and therapeutic functions [452]. Of the nanomaterials investigated for biological applications, MSNs and polymeric nanoparticles are the most commonly researched due to their biocompatibility and in some cases, biodegradability. Due to the abundance of thorough literature on MSNs [453–456] and polymers [457–460] documenting this, only a review of recent literature highlighting template-driven approaches will be outlined here. As MSNs serve primarily as the support for encapsulation, the surface modification through polymers, biomaterials, ligands, or other functional groups will not be touched upon here.

4.4.1. Drug delivery

When considering nanoparticles for drug delivery applications, the loading species or cargo is one of the most important criterions for designing the MSN. For smaller organic compounds, such as the widely used doxorubicin (DOX) for anticancer applications, typical MSN pore diameters on the order of 2–3 nm are capable of loading these or similarly sized compounds [461]. With most MSNs that have been unmodified, the pore size constrains the delivery species by size and often the loading capacity as well. Instead, a trend toward larger pore MSNs, HMSNs, and other pore-expanded MSNs that are capable of delivering larger compounds for genetic or peptide therapy applications have been shown to be more effective in targeting cancer resistant cells [462]. With pore expansion techniques, as those mentioned earlier with TMB, delivery of larger proteins [383,463–465] and even genetic material [207,391] are possible.

Due to the structure of HMSNs, they serve as excellent candidates for dual stage drug release where two or more species can be sequentially loaded and released due to the hollow interior and porous shell [466]. Advantages of such systems have been noted to increase circulation time within the system, as the release of a drug can be prolonged through steric or diffusion limitations of the second species within the porous network or at its surface. The empty voids of HMSNs also offer flexibility in encapsulating enzymes to interact with diffusing species, thus forming biological nanoreactors. Ortac et al. [467] demonstrated a polystyrene template approach to produce highly uniform HMSNs

that were capable of being loaded with various enzymes and then protected by additional, controlled silica formation around the porous shell. The resulting nanoparticles boast a long circulation time due to the preserved enzymatic activity and capability to still interact with its target. Hierarchal structures such as those developed by Chen et al. [468] and Fang et al. [469] have allowed for combinations of dual delivery featuring both hydrophobic and hydrophilic drugs, e.g. docetaxel/irinotecan and paclitaxel/cisplatin respectively. The modification was done through either structural variation in pore channel size or through compositing the core/shell with a hydrophobic/hydrophilic material (See Fig. 10).

4.4.2. Imaging and detection

Templating the MSNs or HMSNs with an inorganic core also allows for simultaneous imaging with drug delivery [56]. In many examples found throughout literature, simply precipitating mesoporous silica growth onto nanoparticles such as gold, iron oxide, or other semiconducting metals will yield core–shell structured MSNs with functional cores. However, in order to differentiate uniquely templated MSN examples for imaging and detection applications, such as confocal microscopy or magnetic resonance imaging (MRI), specific recent examples involving multi-templated, functional MSNs are presented here.

Cores such as iron oxide or gold have been incorporated as part of multifunctional MSNs for many years now. Due to the magnetic behavior, especially the superparamagnetic behavior, of Fe_3O_4, iron oxide is frequently used as dual purpose hyperthermic and MRI agent [470]. In one instance, Yang et al. [471] produces a gold scaffold from silver nanocube templates due to galvanic replacement in order to produce MSNs with a hollow gold cage-like structure as the core. This feature combined with the thermoresponsive polymer coating combines both a laser triggered release mechanism for the nanoparticle, in addition to the possibility of imaging in situ due to the presence of the gold cores. A similar concept with a Pd shell was combined with HMSNs template from solid SiO_2 cores [472]. Through inclusion of such materials, core–shell MSNs are capable of functioning both as drug delivery media and providing diagnostic feedback to assess their mobility and targeting capabilities.

4.4.3. Scaffolds and membranes

Besides MSNs and polymeric nanoparticles, planar nanostructures such as scaffolds and membranes also are widely used in biomedical applications. For topical treatments, tissue engineering, and separation/purification applications, a large porous matrix is desirable as opposed to nanoparticles. In a recent study by Chung et al. [473] the scaffold surface geometry and chemistry, as varied through material selection, was revealed to play a significant impact on cellular regeneration and growth. As such, optimal templates can be selected to address the dimensions and biocompatibility. Materials including poly(lactic-co-glycolic acid) (PLGA) [474], polycaprolactone (PCL) [475], polyethylene glycol (PEG)- poly(2-hydroxyethyl methacrylate) (pHEMA) [476], chitosan [477], hydroxyapatite [478], and bioglasses [479] with low content of SiO_2 are designed and prepared through templating.

Template selection varies but relies on either removing the template due to biocompatibility issues, or in the alternative instance that the template is permanent; it should not only be biocompatible, but stable with the scaffold material. Materials such as AAO membranes are highly effective, removable templates for many biocompatible polymer scaffolds, including PLGA [480] and PCL [152]. In the case of Wang et al. [474] AAO membranes were used to produce PLGA porous membranes but not incorporated into the scaffold whereas in Poinern et al. [481], pHEMA was coated onto AAO membranes as-is and also demonstrated strong biocompatibility with cellular adhesion. Hydroxyapatite scaffolds for regeneration and growth of bone can be produced from AAO templates as well [482]. In other instances, commercial, porous polymeric foams and sponges such as polyurethane [483,484] can be used to generate porous frameworks for hydroxyapatite precipitation and growth. In Soft templating through emulsion systems utilizing poly(L-lactic acid)-grafted hydroxyapatite (g-HAp) nanoparticle templates stabilized in PLGA [485] and foamed surfactant solutions [486] have also produced scaffolds with porosity on the order of micrometers in diameter. Facile template removal is illustrated using ice crystals done by Ko et al. [477] or PMMA microspheres [476] produced micrometer-sized, porous chitosan or PEG-pHEMA scaffolds, respectively.

4.5. Wetting of Surfaces

Droplet contact angles depend sensitively on both surface energy and surface morphology, and accordingly many techniques have been developed to alter either the energetic or morphological characteristics of a surface to obtain desired wetting behavior [487]. For example, precise fabrication of nanoscale features on a surface allows surfaces to be superhydrophobic [488] or even superoleophobic [489] by exploiting Cassie and/or Wenzel states [490–492]. Similarly, asymmetric nanofeatures guide spreading of droplets in preferred directions [493] or in preferred shapes [494]. Even without precise control of the nanoarchitecture, however, the surface energy and corresponding contact angle can be modified by application of a sufficiently strong external field. The most well-known example involves applied electric fields, which give rise to the electrowetting effect [495] that has found widespread application in optical lens [496] and lab-on-a-chip devices [497]. A key design constraint in electrowetting, however, is that there must be direct electrical contact between the substrate and droplet. In contrast, magnetic fields offer the possibility of non-intrusively modifying droplet contact angles, and indeed ferrofluids have been widely demonstrated to dramatically alter their contact angle and undergo a variety of instabilities in response to sufficiently strong magnetic fields [498,499].

Zhou et al. [500] used a porous template method in combination with the LbL deposition technique. The LbL process typically involves the sequential deposition of different species, such as polymers, nanoparticles, lipids, proteins, dyes or other small molecules into various porous templates, which are subsequently removed to yield free-standing nanotubes with tailored properties [501]. Zhou et al. followed the procedure similar to that used by Lee et al., who prepared freely suspended nanotubes with embedded magnetite nanoparticles [502], into a LbL structure of PAH and PSS using PCTE membrane as the template. Since the nanotubes were directly attached to a substrate, the fabrication yielded a nanostructured superparamagnetic surface.

Zhou et al. demonstrated that the contact angle of pure water droplets deposited on the nanostructured film is highly sensitive to the *ante situm* strength of an applied magnetic field, decreasing linearly from 117° at no applied field to 105° at an applied field of approximately 500 gauss. Importantly, this decrease in contact angle did not require an inordinately strong magnetic field: a fifteen-degree decrease in contact angle was observed even with a standard alnico bar magnet. Surfaces with improved wetting response have been devised by Grigoryev et al. [503], Zhu et al. [504] and Lee et al. [505]. Bernardi and Dietrich [506] have proposed a model to predict contact angle change for magnetic, nanostructured surfaces that are exposed to external magnetic fields.

5. Trends and conclusions

Templates are one of the effective strategies for better control on the size and shape of the synthesized nanostructures. In order to synthesize nanostructures with desired size and shape the first step is selection of the proper template. The next step is the synthesis method which is compatible with the selected template. Outlined in this review are several templates used across literature for various types of nanostructured materials, where template-based synthesis methods are typically crucial and fundamental to achieve their structure. Finally, the importance

of template synthesis in the properties of nanostructures for several applications has been reviewed.

As MSNs and zeolites in particular have been heavily researched for over two decades now and have been used as a platform for many applications, many of the template driven approaches for their syntheses have been well studied and are standards in the preparation of structures such as M41S or ZSM-5. Most of the templates used in this field are frequently used without much variation but in particular for MSNs, recent trends have been toward improving the biocompatibility and biodegradability of MSNs. This is important specifically for biomaterial applications where the toxicity of MSNs has been debated. Literature supporting both highly biocompatible [507–509] and toxic sides of the argument [510] has led toward recent attention toward to HMSNs and particularly, their functionalization. As the frequently used polystyrene core template is highly uniform and cleanly removed from the final product, the resulting MSN shells are highly monodisperse and homogeneous [467], which improves their biocompatibility. The hollow aspect of HMSNs has significant advantages over traditional MSNs, in addition to less silica material being present, which is the major concern about MSN toxicity.

Although zeolites have usually been synthesized in hydrothermal conditions, in basic aqueous media as we reported previously, different template synthesis methods have been approached in the last two decades. One of the most important zeolite in catalysis because of its structure is ZSM-5. This structure and a high Si/Al ratio are obtained using an OSDA such as template. Other types of templates such carbon frameworks, CNTs, CMK, and CAs, have been used in order to obtain mesoporous zeolites. This type of zeolites improve the diffusion through the porous due to the larger pores give them less diffusional limitations.

Nanowires, nanotubes, and nanocaps have been demonstrated to provide a wide range of unique functionalities, holding promise for applications in energy technologies, photonics, biological sensing, and other fields. Good control has been demonstrated over composition, size, and morphology across a wide range of materials. Templated deposition provides a powerful tool in controlling overall nanowire shape, including external and internal diameter control for nanotubes, and is compatible with well-understood synthesis methods such as electrodeposition, electroless deposition, and physical deposition. However challenges still exist in functionalizing individual nanowires for use in devices or interfacing with individual biological macromolecules; templated deposition shows promise in addressing these issues, both by allowing nanowire growth directly onto a functionalized substrate, as well as through the addressing of individual nanowires by utilizing mushroom cap overgrowth.

Acknowledgements

The University of California Office of the President (UCOP) Lab Fees Research Program funded this research.

References

[1] Liu Y, Goebl J, Yin Y. Templated synthesis of nanostructured materials. Chem Soc Rev 2013;42:2610–53.
[2] Kresge CT, Leonowicz ME, Roth WJ, Vartuli JC, Beck JS. Ordered mesoporous molecular sieves synthesized by a liquid–crystal template mechanism. Nature 1992;359:710–2.
[3] Zhu W, Zhou Y, Ma W, Li M, Yu J, Xie K. Using silica fume as silica source for synthesizing spherical ordered mesoporous silica. Mater Lett 2013;92:129–31.
[4] Le VH, Thuc CNH, Thuc HH. Synthesis of silica nanoparticles from Vietnamese rice husk by sol–gel method. Nanoscale Res Lett 2013;8:58.
[5] Lin Y-c, Lin L-Y, Gao M-Y, Fang Y-P. Mesoporous silica nanoparticles synthesized from liquid crystal display manufacturing extracts as a potential candidate for a drug delivery carrier: evaluation of their safety and biocompatibility. Int J Nanomedicine 2013;8:3833–42.
[6] Martínez C, Corma A. 5.05 — Zeolites. In: Poeppelmeier JR, editor. Comprehensive inorganic chemistry II. 2nd ed. Amsterdam: Elsevier; 2013. p. 103–31.
[7] J Martinez Sanches CCO, Wright Paul A, Lozinska Magdalena. Zeolies nd orered porous solids: fndamentals and pplications. Chapter 1: structural chemistry and properties of zeolites. 3rd FEZA School on Zeolites: fundamentals and applications. Valencia, Spain: Universidad Politécnica de Valencia; 2011 [Chapter 1].
[8] Reed TB, Breck DW. Crystalline zeolites. II. Crystal structure of synthetic zeolite, type A. J Am Chem Soc 1956;78:5972–7.
[9] Cundy CS, Cox PA. The hydrothermal synthesis of zeolites: history and development from the earliest days to the present time. Chem Rev 2003;103:663–702.
[10] Meng X, Xiao FS. Green routes for synthesis of zeolites. Chem Rev 2014;114:1521–43.
[11] Flanigen EM. Zeolites and molecular sieves: an historical perspective. In: van Bekkum EMFPAJ H, JC Jansen, editors. Studies in surface science and catalysis. Elsevier; 2001. p. 11–35 [Chapter 2].
[12] Cundy CS, Cox PA. The hydrothermal synthesis of zeolites: precursors, intermediates and reaction mechanism. Microporous Mesoporous Mater 2005;82:1–78.
[13] Cui Y, Lieber CM. Functional nanoscale electronic devices assembled using silicon nanowire building blocks. Science 2001;291:851–3.
[14] Gudiksen MS, Lauhon LJ, Wang J, Smith DC, Lieber CM. Growth of nanowire superlattice structures for nanoscale photonics and electronics. Nature 2002;415:617–20.
[15] Piraux L, George JM, Despres JF, Leroy C, Ferain E, Legras R, et al. Giant magnetoresistance in magnetic multilayered nanowires. Appl Phys Lett 1994;65:2484–6.
[16] Cui Y, Wei Q, Park H, Lieber CM. Nanowire nanosensors for highly sensitive and selective detection of biological and chemical species. Science 2001;293:1289–92.
[17] Routkevitch D, Bigioni T, Moskovits M, Xu JM. Electrochemical fabrication of CdS nanowire arrays in porous anodic aluminum oxide templates. J Phys Chem 1996;100:14037–47.
[18] Thurn-Albrecht T, Schotter J, Kästle GA, Emley N, Shibauchi T, Krusin-Elbaum L, et al. Ultrahigh-density nanowire arrays grown in self-assembled diblock copolymer templates. Science 2000;290:2126–9.
[19] Richter J, Mertig M, Pompe W, Mönch I, Schackert HK. Construction of highly conductive nanowires on a DNA template. Appl Phys Lett 2001;78:536–8.
[20] Wu W, DiMaria JB, Yoo HG, Pan S, Rothberg LJ, Zhang Y. In situ electrochemical fabrication of natural contacts on single nanowires. Appl Phys Lett 2004;84:966–8.
[21] RM Barrer, PJ Denny. 201. Hydrothermal chemistry of the silicates. Part IX. Nitrogenous aluminosilicates. J Chem Soc (Resumed) 1961:971–82.
[22] Jiang J, Yu J, Corma A. Extra-large-pore zeolites: bridging the gap between micro and mesoporous structures. Angew Chem Int Ed 2010;49:3120–45.
[23] Kokotailo GT, Lawton SL, Olson DH, Meier WM. Structure of synthetic zeolite ZSM-5. Nature 1978;272:437–8.
[24] Briscoe NA, Johnson DW, Shannon MD, Kokotailo GT, McCusker LB. The framework topology of zeolite EU-1. Zeolites 1988;8:74–6.
[25] Shannon MD, Casci JL, Cox PA, Andrews SJ. Structure of the two-dimensional medium-pore high-silica zeolite NU-87. Nature 1991;353:417–20.
[26] Fouad OA, Mohamed RM, Hassan MS, Ibrahim IA. Effect of template type and template/silica mole ratio on the crystallinity of synthesized nanosized ZSM-5. Catal Today 2006;116:82–7.
[27] Meng X, Xiao F-S. Green routes for synthesis of zeolites. Chem Rev 2014;114:1521–43.
[28] Da Silva RMP, Mano JF, Reis RL. Smart thermoresponsive coatings and surfaces for tissue engineering: switching cell-material boundaries. Trends Biotechnol 2007;25:577–83.
[29] Xu R, Pang W, Yu J, Huo Q, Chen J. Synthesis, structure, and characterization of mesoporous materials. Chem Zeolites Relat Porous Mater Synth Struct 2007:467–601.
[30] Wang J, Song J, Yin C, Ji Y, Zou Y, Xiao F-S. Tetramethylguanidine-templated synthesis of aluminophosphate-based microporous crystals with AFI-type structure. Microporous Mesoporous Mater 2009;117:561–9.
[31] Zones SI, Hwang SJ. Synthesis of high silica zeolites using a mixed quaternary ammonium cation, amine approach: discovery of zeolite SSZ-47. Chem Mater 2002;14:313–20.
[32] Vaughan DEW, Edwards GC, Michael GB. Preparation of Zeolites; 1982 Patent number US4340573-A.
[33] Liu S, Li L, Li C, Xiong X, Xiao F-S. Synthesis of EMT-rich faujasite in the presence of organic template of low-cost polyquaternium-6. J Porous Mater 2008;15:295–301.
[34] Kruk M, Jaroniec M, Sayari A. Application of large pore MCM-41 molecular sieves to improve pore size analysis using nitrogen adsorption measurements. Langmuir 1997;13:6267–73.
[35] Zhang K, Xu L-L, Jiang J-G, Calin N, Lam K-F, Zhang S-J, et al. Facile large-scale synthesis of monodisperse mesoporous silica nanospheres with tunable pore structure. J Am Chem Soc 2013;135:2427–30.
[36] Daniels RH, Kerr GT, Rollmann LD. Cationic polymers as templates in zeolite crystallization. J Am Chem Soc 1978;100:3097–100.
[37] Xiao FS, Wang LF, Yin CY, Lin KF, Di Y, Li JX, et al. Catalytic properties of hierarchical mesoporous zeolites templated with a mixture of small organic ammonium salts and mesoscale cationic polymers. Angew Chem Int Ed 2006;45:3090–3.
[38] Che S, Garcia-Bennett AE, Yokoi T, Sakamoto K, Kunieda H, Terasaki O, et al. A novel anionic surfactant templating route for synthesizing mesoporous silica with unique structure. Nat Mater 2003;2:801–5.
[39] Trewyn BG, Whitman CM, Lin VSY. Morphological control of room-temperature ionic liquid templated mesoporous silica nanoparticles for controlled release of antibacterial agents. Nano Lett 2004;4:2139–43.
[40] Zhou Y, Schattka JH, Antonietti M. Room-temperature ionic liquids as template to monolithic mesoporous silica with wormlike pores via a sol–gel nanocasting technique. Nano Lett 2004;4:477–81.
[41] Zhao D, Feng J, Huo Q, Melosh N, Fredrickson GH, Chmelka BF, et al. Triblock copolymer syntheses of mesoporous silica with periodic 50 to 300 Angstrom pores. Science 1998;279:548–52.

[42] Zhao D, Huo Q, Feng J, Chmelka BF, Stucky GD. Nonionic triblock and star diblock copolymer and oligomeric surfactant syntheses of highly ordered, hydrothermally stable, mesoporous silica structures. J Am Chem Soc 1998;120:6024–36.
[43] Monnier A, Schüth F, Huo Q, Kumar D, Margolese D, Maxwell RS, et al. Cooperative formation of inorganic–organic interfaces in the synthesis of silicate mesostructures. Science 1993;261:1299–303.
[44] Kim T-W, Chung P-W, Lin VSY. Facile synthesis of monodisperse spherical MCM-48 mesoporous silica nanoparticles with controlled particle size. Chem Mater 2010;22:5093–104.
[45] Liu S, Cool P, Collart O, Van Der Voort P, Vansant EF, Lebedev OI, et al. The influence of the alcohol concentration on the structural ordering of mesoporous silica: cosurfactant versus cosolvent. J Phys Chem B 2003;107:10405–11.
[46] Ryoo R, Kim JM, Ko CH, Shin CH. Disordered molecular sieve with branched mesoporous channel network. J Phys Chem 1996;100:17718–21.
[47] Bagshaw SA, Prouzet E, Pinnavaia TJ. Templating of mesoporous molecular sieves by nonionic polyethylene oxide surfactants. Science 1995;269:1242–4.
[48] Imhof A. Preparation and characterization of titania-coated polystyrene spheres and hollow titania shells. Langmuir 2001;17:3579–85.
[49] Lu Y, McLellan J, Xia Y. Synthesis and crystallization of hybrid spherical colloids composed of polystyrene cores and silica shells. Langmuir 2004;20:3464–70.
[50] Li G, Liu G, Kang ET, Neoh KG, Yang X. pH-Responsive hollow polymeric microspheres and concentric hollow silica microspheres from silica—polymer core—shell microspheres. Langmuir 2008;24:9050–5.
[51] Jang J, Ha H. Fabrication of hollow polystyrene nanospheres in microemulsion polymerization using triblock copolymers. Langmuir 2002;18:5613–8.
[52] Jang J, Ha H. Fabrication of carbon nanocapsules using PMMA/PDVB core/shell nanoparticles. Chem Mater 2003;15:2109–11.
[53] Tan B, Rankin SE. Dual latex/surfactant templating of hollow spherical silica particles with ordered mesoporous shells. Langmuir 2005;21:8180–7.
[54] Zhu G, Qiu S, Terasaki O, Wei Y. Polystyrene bead-assisted self-assembly of microstructured silica hollow spheres in highly alkaline media. J Am Chem Soc 2001;123:7723–4.
[55] Blas H, Save M, Pasetto P, Boissière C, Sanchez C, Charleux B. Elaboration of monodisperse spherical hollow particles with ordered mesoporous silica shells via dual latex/surfactant templating: radial orientation of mesopore channels. Langmuir 2008;24:13132–7.
[56] Chen Y, Chen H, Zeng D, Tian Y, Chen F, Feng J, et al. Core/shell structured hollow mesoporous nanocapsules: a potential platform for simultaneous cell imaging and anticancer drug delivery. ACS Nano 2010;4:6001–13.
[57] Chen Z, Gang T, Zhang K, Zhang J, Chen X, Sun Z, et al. Ag nanoparticles-coated silica–PMMA core–shell microspheres and hollow PMMA microspheres with Ag nanoparticles in the interior surfaces. Colloids Surf A Physicochem Eng Asp 2006;272:151–6.
[58] Zhang K, Zheng L, Zhang X, Chen X, Yang B. Silica-PMMA core–shell and hollow nanospheres. Colloids Surf A Physicochem Eng Asp 2006;277:145–50.
[59] Liu Y-L, Wu Y-H, Tsai W-B, Tsai C-C, Chen W-S, Wu C-S. Core–shell silica@chitosan nanoparticles and hollow chitosan nanospheres using silica nanoparticles as templates: preparation and ultrasound bubble application. Carbohydr Polym 2011;84:770–4.
[60] Han K, Zhao Z, Xiang Z, Wang C, Zhang J, Yang B. The sol–gel preparation of ZnO/silica core–shell composites and hollow silica structure. Mater Lett 2007;61:363–8.
[61] Wu X-J, Xu D. Formation of Yolk/SiO2 shell structures using surfactant mixtures as template. J Am Chem Soc 2009;131:2774–5.
[62] Liu J, Qiao SZ, Budi Hartono S, Lu GQM. Monodisperse yolk–shell nanoparticles with a hierarchical porous structure for delivery vehicles and nanoreactors. Angew Chem 2010;122:5101–5.
[63] Tao YS, Kanoh H, Abrams L, Kaneko K. Mesopore-modified zeolites: preparation, characterization, and applications. Chem Rev 2006;106:896–910.
[64] White RJ, Fischer A, Goebel C, Thomas A. A sustainable template for mesoporous zeolite synthesis. J Am Chem Soc 2014;136:2715–8.
[65] Jacobsen CJ, Madsen C, Houzvicka J, Schmidt I, Carlsson A. Mesoporous zeolite single crystals. J Am Chem Soc 2000;122:7116–7.
[66] Schmidt I, Boisen A, Gustavsson E, Stahl K, Pehrson S, Dahl S, et al. Carbon nanotube templated growth of mesoporous zeolite single crystals. Chem Mater 2001;13:4416.
[67] Schmidt I, Madsen C, Jacobsen CJH. Confined space synthesis. A novel route to nanosized zeolites. Inorg Chem 2000;39:2279–83.
[68] Sakthivel A, Huang SJ, Chen WH, Lan ZH, Chen KH, Kim TW, et al. Replication of mesoporous aluminosilicate molecular sieves (RMMs) with zeolite framework from mesoporous carbons (CMKs). Chem Mater 2004;16:3168–75.
[69] Yang ZX, Xia YD, Mokaya R. Zeolite ZSM-5 with unique supermicropores synthesized using mesoporous carbon as a template. Adv Mater 2004;16:727.
[70] Pekala RW, Alviso CT. Carbon aerogels and xerogels. In: Renschler CL, Pouch JJ, Cox DM, editors. Novel forms of carbon, Vol. 270. ; 1992. p. 3–14.
[71] Hulsey SS, Alviso CT, Kong FM, Pekala RW. The effect of pyrolysis temperature and formulation of pore-size distribution and surface-area of carbon aerogels. In: Renschler CL, Pouch JJ, Cox DM, editors. Novel forms of carbon, Vol. 270. ; 1992. p. 53–7.
[72] Hanzawa Y, Kaneko K. Lack of a predominant adsorption of water vapor on carbon mesopores. Langmuir 1997;13:5802–4.
[73] Hanzawa Y, Kaneko K, Yoshizawa N, Pekala RW, Dresselhaus MS. The pore structure determination of carbon aerogels. Adsorpt J Int Adsorpt Soc 1998;4:187–95.
[74] Bekyarova E, Kaneko K. Structure and physical properties of tailor-made Ce. Zr-doped Carbon Aerogels Adv Mater 2000;12:1625.
[75] Hanzawa Y, Hatori H, Yoshizawa N, Yamada Y. Structural changes in carbon aerogels with high temperature treatment. Carbon 2002;40:575–81.
[76] Tao YS, Tanaka H, Ohkubo T, Kanoh H, Kaneko K. Pore structures of ZSM-5 synthesized in the mesopore spaces of a carbon aerogel. Adsorpt Sci Technol 2003;21:199–203.
[77] Sing KSW. Reporting physisorption data for gas/solid systems with special reference to the determination of surface area and porosity (recommendations 1984). Pure Appl Chem 1985;57.
[78] Tao YS, Kanoh H, Kaneko K. ZSM-5 monolith of uniform mesoporous channels. J Am Chem Soc 2003;125:6044–5.
[79] Tao YS, Kanoh H, Kaneko K. Uniform mesopore-donated zeolite Y using carbon aerogel templating. J Phys Chem B 2003;107:10974–6.
[80] Mendelson NH. Helical growth of bacillus-subtilis — new model of cell-growth. Proc Natl Acad Sci U S A 1976;73:1740–4.
[81] Zhang B, Davis SA, Mendelson NH, Mann S. Bacterial templating of zeolite fibres with hierarchical structure. Chem Commun 2000;781-2.
[82] Davis SA, Burkett SL, Mendelson NH, Mann S. Bacterial templating of ordered macrostructures in silica and silica-surfactant mesophases. Nature 1997;385:420–3.
[83] Zhang B, Davis SA, Mann S. Starch gel templating of spongelike macroporous silicalite monoliths and mesoporous films. Chem Mater 2002;14:1369–75.
[84] Mbindyo JKN, Mallouk TE, Mattzela JB, Kratochvilova I, Razavi B, Jackson TN, et al. Template synthesis of metal nanowires containing monolayer molecular junctions. J Am Chem Soc 2002;124:4020–6.
[85] Penner RM, Martin CR. Preparation and electrochemical characterization of ultramicroelectrode ensembles. Anal Chem 1987;59:2625–30.
[86] Pan H, Liu B, Yi J, Poh C, Lim S, Ding J, et al. Growth of single-crystalline Ni and Co nanowires via electrochemical deposition and their magnetic properties. J Phys Chem B 2005;109:3094–8.
[87] Hurst SJ, Payne EK, Qin L, Mirkin CA. Multisegmented one-dimensional nanorods prepared by hard-template synthetic methods. Angew Chem Int Ed 2006;45:2672–92.
[88] Saedi A, Ghorbani M. Electrodeposition of Ni–Fe–Co alloy nanowire in modified AAO template. Mater Chem Phys 2005;91:417–23.
[89] Liang Z, Susha A, Caruso F. Gold nanoparticle-based core—shell and hollow spheres and ordered assemblies thereof. Chem Mater 2003;15:3176–83.
[90] Wang JX, Inada H, Wu L, Zhu Y, Choi Y, Liu P, et al. Oxygen reduction on well-defined core—shell nanocatalysts: particle size, facet, and Pt shell thickness effects. J Am Chem Soc 2009;131:17298–302.
[91] Wang J. Barcoded metal nanowires. J Mater Chem 2008;18:4017–20.
[92] Noginov MA, Li H, Barnakov YA, Dryden D, Nataraj G, Zhu G, et al. Controlling spontaneous emission with metamaterials. Opt Lett 2010;35:1863–5.
[93] Lal S, Hafner JH, Halas NJ, Link S, Nordlander P. Noble metal nanowires: from plasmon waveguides to passive and active devices. Acc Chem Res 2012;45:1887–95.
[94] Martin BR, Dermody DJ, Reiss BD, Fang M, Lyon LA, Natan MJ, et al. Orthogonal self-assembly on colloidal gold—platinum nanorods. Adv Mater 1999;11:1021–5.
[95] Quach DV, Vidu R, Groza JR, Stroeve P. Electrochemical deposition of Co–Sb thin films and nanowires. Ind Eng Chem Res 2010;49:11385–92.
[96] Vidu R, Li S, Quach DV, Stroeve P. Electrochemical deposition of Co–Sb thin films on nanostructured gold. J Appl Electrochem 2012;42:333–9.
[97] Vidu R. Electrochemical atomic force microscopy studies of Te, Cd and CdTe electrodeposition processes on Au single crystal. Osaka, JAPAN: Osaka University; 2000.
[98] Vidu R, Ku J, Stroeve P. Fabrication of multiscale nanostructures from polymeric membrane templates. In: Nalwa HS, editor. Polymeric nanostructures and their applications, Vol. 1. ; 2007. p. 124–49 [Chapter 3].
[99] Piraux L, Dubois S, Duvail JL, Radulescu A, Demoustier-Champagne S, Ferain E, et al. Fabrication and properties of organic and metal nanocylinders in nanoporous membranes. J Mater Res 1999;14:3042–50.
[100] Vidu R, Ku JR, Stroeve P. Growth of ultrathin films of cadmium telluride and tellurium as studied by electrochemical atomic force microscopy. J Colloid Interface Sci 2006;300:404–12.
[101] Ku JR, Vidu R, Talroze R, Stroeve P. Ion-mediated, smooth electrochemical deposition of nano thick tellurium and cadmium telluride films. Abstr Pap Am Chem Soc 2005;230 [U2255-U].
[102] Ku JR, Vidu R, Stroeve P. Mechanism of film growth of tellurium by electrochemical deposition in the presence and absence of cadmium ions. J Phys Chem B 2005;109:21779–87.
[103] Bercu B, Enculescu I, Spohr R. Copper tubes prepared by electroless deposition in ion track templates. Nucl Instrum Methods Phys Res, Sect B 2004;225:497–502.
[104] Bergquist J, Gobom J, Blomberg A, Roepstorff P, Ekman R. Identification of nuclei associated proteins by 2D-gel electrophoresis and mass spectrometry. J Neurosci Methods 2001;109:3–11.
[105] Hou ZZ, Abbott NL, Stroeve P. Electroless gold as a substrate for self-assembled monolayers. Langmuir 1998;14:3287–97.
[106] Yuan XY, Wu GS, Xie T, Lin Y, Meng GW, Zhang LD. Autocatalytic redox fabrication and magnetic studies of Co–Ni–P alloy nanowire arrays. Solid State Commun 2004;130:429–32.
[107] Yuan XY, Wu GS, Xie T, Lin Y, Zhang LD. Self-assembly synthesis and magnetic studies of Co–P alloy nanowire arrays. Nanotechnology 2004;15:59–61.
[108] Yuan XY, Xie T, Wu GS, Lin Y, Meng GW, Zhang LD. Fabrication of Ni–W–P nanowire arrays by electroless deposition and magnetic studies. Physica E 2004;23:75–80.

[109] Lebedev K, Mafe S, Stroeve P. Modeling electrochemical deposition inside nanotubes to obtain metal-semiconductor multiscale nanocables or conical nanopores. J Phys Chem B 2005;109:14523–8.
[110] Possin GE. A method for forming very small diameter wires. Rev Sci Instrum 1970; 41:772–4.
[111] Martin CR. Nanomaterials: a membrane-based synthetic approach. Science 1994; 266:1961–6.
[112] Preston CK, Moskovits M. Optical characterization of anodic aluminum oxide films containing electrochemically deposited metal particles. 1. Gold in phosphoric acid anodic aluminum oxide films. J Phys Chem 1993;97:8495–503.
[113] Walter EC, Zach MP, Favier F, Murray BJ, Inazu K, Hemminger JC, et al. Metal nanowire arrays by electrodeposition. Chemphyschem 2003;4:131–8.
[114] Stegmann C, Muench F, Rauber M, Hottes M, Brötz J, Kunz U, et al. Platinum nanowires with pronounced texture, controlled crystallite size and excellent growth homogeneity fabricated by optimized pulsed electrodeposition. RSC Adv 2014;4: 4804–10.
[115] Wang J-G, Tian M-L, Kumar N, Mallouk TE. Controllable template synthesis of superconducting Zn nanowires with different microstructures by electrochemical deposition. Nano Lett 2005;5:1247–53.
[116] Djokić SS, Cavallotti PL. Electroless deposition: theory and applications, Vol. 48, Springer; 2010 251–89.
[117] Sharma NC, Kainthla RC, Pandya DK, Chopra KL. Electroless deposition of semiconductor films. Thin Solid Films 1979;60:55–9.
[118] Ye Y-H, Badilescu S, Truong V-V, Rochon P, Natansohn A. Self-assembly of colloidal spheres on patterned substrates. Appl Phys Lett 2001;79:872–4.
[119] Yi DK, Kim MJ, Kim D-Y. Surface relief grating induced colloidal crystal structures†. Langmuir 2002;18:2019–23.
[120] Yi DK, Seo E-M, Kim D-Y. Surface-modulation-controlled three-dimensional colloidal crystals. Appl Phys Lett 2002;80:225–7.
[121] Yi DK, Yoo SJ, Kim DY. Spin-on-based fabrication of titania nanowires using a sol–gel process. Nano Lett 2002;2:1101–4.
[122] Masuda H, Fukuda K. Ordered metal nanohole arrays made by a two-step replication of honeycomb structures of anodic alumina. Science 1995;268:1466–8.
[123] Kovtyukhova NI, Kelley BK, Mallouk TE. Coaxially gated in-wire thin-film transistors made by template assembly. J Am Chem Soc 2004;126:12738–9.
[124] Shi J-B, Chen C-J, Lin Y-T, Hsu W-C, Chen Y-C, Wu P-F. Anodic aluminum oxide membrane-assisted fabrication of β-in2s3nanowires. Nanoscale Res Lett 2009;4: 1059.
[125] Karim S, Toimil-Molares ME, Maurer F, Miehe G, Ensinger W, Liu J, et al. Synthesis of gold nanowires with controlled crystallographic characteristics. Appl Phys A 2006;84:403–7.
[126] Wang J. Adaptive nanowires for on-demand control of electrochemical microsystems. Electroanalysis 2008;20:611–5.
[127] Chen M, Chien CL, Searson PC. Potential modulated multilayer deposition of multisegment Cu/Ni nanowires with tunable magnetic properties. Chem Mater 2006;18:1595–601.
[128] Ku JR, Vidu R, Talroze R, Stroeve P. Fabrication of nanocables by electrochemical deposition inside metal nanotubes. J Am Chem Soc 2004;126:15022–3.
[129] Wirtz M, Martin CR. Template-fabricated gold nanowires and nanotubes. Adv Mater 2003;15:455–8.
[130] Wirtz M, Parker M, Kobayashi Y, Martin CR. Molecular sieving and sensing with gold nanotube membranes. Chem Rec 2002;2:259–67.
[131] Wirtz M, Yu S, Martin CR. Template synthesized gold nanotube membranes for chemical separations and sensing. Analyst 2002;127:871–9.
[132] Ikemiya N, Iwai D, Yamada K, Vidu R, Hara S. Atomic structures and growth morphologies of electrodeposited Te film on Au(100) and Au(111) observed by in situ atomic force microscopy. Surf Sci 1996;369:199–208.
[133] Ding LX, Li GR, Wang ZL, Liu ZQ, Liu H, Tong YX. Porous Ni@Pt core–shell nanotube array electrocatalyst with high activity and stability for methanol oxidation. Chemistry 2012;18:8386–91.
[134] Rahman M, Tajabadi F, Shooshtari L, Taghavinia N. Nanoparticulate hollow TiO2 fibers as light scatterers in dye-sensitized solar cells: layer-by-layer self-assembly parameters and mechanism. Chemphyschem 2011;12:966–73.
[135] Li Z, Yao C, Yu Y, Cai Z, Wang X. Highly efficient capillary photoelectrochemical water splitting using cellulose nanofiber-templated TiO(2) photoanodes. Adv Mater 2014;26:2262–7 [110].
[136] Guo H, Mao R, Yang X, Wang S, Chen J. Hollow nanotubular SnO2 with improved lithium storage. J Power Sources 2012;219:280–4.
[137] Huang J, Matsunaga N, Shimanoe K, Yamazoe N, Kunitake T. Nanotubular SnO2 templated by cellulose fibers: synthesis and gas sensing. Chem Mater 2005;17:3513–8.
[138] Liu S, Zhang L, Zhou J, Xiang J, Sun J, Guan J. Fiberlike Fe2O3 macroporous nanomaterials fabricated by calcinating regenerate cellulose composite fibers. Chem Mater 2008;20:3623–8.
[139] Guo H, Mao R, Yang X, Chen J. Hollow nanotubular SiOx templated by cellulose fibers for lithium ion batteries. Electrochim Acta 2012;74:271–4.
[140] Ghadiri E, Taghavinia N, Zakeeruddin SM, Gratzel M, Moser JE. Enhanced electron collection efficiency in dye-sensitized solar cells based on nanostructured TiO(2) hollow fibers. Nano Lett 2010;10:1632–8.
[141] Rahman M, Tajabadi F, Shooshtari L, Taghavinia N. Nanoparticulate hollow TiO2 fibers as light scatterers in dye-sensitized solar cells: layer-by-layer self-assembly parameters and mechanism. Chemphyschem 2011;12:966–73.
[142] Zhang Y, Liu X, Huang J. Hierarchical mesoporous silica nanotubes derived from natural cellulose substance. ACS Appl Mater Interfaces 2011;3:3272–5.
[143] Korhonen JT, Hiekkataipale P, Malm J, Karppinen M, Ikkala O, Ras RH. Inorganic hollow nanotube aerogels by atomic layer deposition onto native nanocellulose templates. ACS Nano 2011;5:1967–74.
[144] Melone L, Altomare L, Alfieri I, Lorenzi A, De Nardo L, Punta C. Ceramic aerogels from TEMPO-oxidized cellulose nanofibre templates: synthesis, characterization, and photocatalytic properties. J Photochem Photobiol A Chem 2013; 261:53–60.
[145] Tkalya E, Ghislandi M, Thielemans W, van der Schoot P, de With G, Koning C. Cellulose nanowhiskers templating in conductive polymer nanocomposites reduces electrical percolation threshold 5-fold. ACS Macro Lett 2013;2:157–63.
[146] Ogihara H, Sadakane M, Nodasaka Y, Ueda W. Shape-controlled synthesis of ZrO2, Al2O3, and SiO2 nanotubes using carbon nanofibers as templates. Chem Mater 2006;18:4981–3.
[147] Xing Z, Asiri AM, Obaid AY, Sun X, Ge X. Carbon nanofiber-templated mesoporous TiO2 nanotubes as a high-capacity anode material for lithium-ion batteries. RSC Adv 2014;4:9061.
[148] Greiner A, Wendorff JH. Electrospinning: a fascinating method for the preparation of ultrathin fibers. Angew Chem Int Ed Engl 2007;46:5670–703.
[149] Xu L, Lee HK. Zirconia hollow fiber: preparation, characterization, and microextraction application. Anal Chem 2007;79:5241–8.
[150] Yuwono VM, Hartgerink JD. Peptide amphiphile nanofibers template and catalyze silica nanotube formation. Langmuir 2007;23:5033–8.
[151] Ahmed S, Mondal JH, Behera N, Das D. Self-assembly of peptide-amphiphile forming helical nanofibers and in situ template synthesis of uniform mesoporous single wall silica nanotubes. Langmuir 2013;29:14274–83.
[152] Jeon H, Kim G. Preparation and characterization of an electrospun polycaprolactone (PCL) fibrous mat and multi-layered PCL scaffolds having a nanosized pattern-surface for tissue regeneration. J Mater Chem B 2014;2:171–80.
[153] Li S, Lu X, Li X, Xue Y, Zhang C, Lei J, et al. Preparation of bamboo-like PPy nanotubes and their application for removal of Cr(VI) ions in aqueous solution. J Colloid Interface Sci 2012;378:30–5.
[154] Su Z, Yan C, Tang D, Sun K, Han Z, Liu F, et al. Fabrication of Cu2ZnSnS4 nanowires and nanotubes based on AAO templates. CrystEngComm 2012;14:782–5.
[155] Mazur M. Template synthesis of polyaniline and poly(2-methoxyaniline) nanotubes: comparison of the formation mechanisms. Electrochem Commun 2003;5: 403–7.
[156] Jin S, Lee Y, Jeon S-M, Sohn B-H, Chae W-S, Lee J-K. Simple fabrication of single- and multi-layer polymer nanotubes by spin-casting method within anodized aluminum oxide (AAO) templates. J Mater Chem 2012;22:23368.
[157] Wang H, Song Y, Liu W, Yao S, Zhang W. Template synthesis and characterization of TiO2 nanotube arrays by the electrodeposition method. Mater Lett 2013;93: 319–21.
[158] Maas MG, Rodijk EJB, Wouter Maijenburg A, Blank DHA, ten Elshof JE. Microstructure development in zinc oxide nanowires and iron oxohydroxide nanotubes by cathodic electrodeposition in nanopores. J Mater Res 2011;26:2261–7.
[159] Chon Chen C, Cheng C-H, Lin C-K. Template assisted fabrication of TiO2 and WO3 nanotubes. Ceram Int 2013;39:6631–6.
[160] Pathak S, Singh S, Sharma M. Synthesis of cobalt nanotubules and characterization of magnetization dynamics. Int J Nanosci 2011;10:641–6.
[161] Jirage KB. Nanotubule-based molecular-filtration membranes. Science 1997;278: 655–8.
[162] Hou S, Harrell CC, Trofin L, Kohli P, Martin CR. Layer-by-layer nanotube template synthesis. J Am Chem Soc 2004;126:5674–5.
[163] Quach DV, Vidu R, Groza JR, Stroeve P. Electrochemical deposition of Co—Sb thin films and nanowires. Ind Eng Chem Res 2010;49:11385–92.
[164] Luo F, Li J, Lei Y, Yang W, Yuan H, Xiao D. Three-dimensional enoki mushroom-like Co3O4 hierarchitectures constructed by one-dimension nanowires for high-performance supercapacitors. Electrochim Acta 2014;135:495–502.
[165] Shen Y, Zhou J, Liu T, Tao Y, Jiang R, Liu M, et al. Plasmonic gold mushroom arrays with refractive index sensing figures of merit approaching the theoretical limit. Nat Commun 2013;4.
[166] Vlad A, Dutu CA, Jedrasik P, Södervall U, Gohy JF, Melinte S. Vertical single nanowire devices based on conducting polymers. Nanotechnology 2012;23:025302.
[167] Hu J, Liu Y, Ning CZ, Dutton R, Kang S-M. Fringing field effects on electrical resistivity of semiconductor nanowire-metal contacts. Appl Phys Lett 2008;92: 083503.
[168] Shin S, Cho HH. Self-formed platform for in situ measurement of electrical transport of individual copper nanowires. Electrochim Acta 2014;117:120–6.
[169] Li Q, Lin Y, Creighton JR, Figiel JJ, Wang GT. Nanowire-templated lateral epitaxial growth of low-dislocation density nonpolar a-plane GaN on r-plane sapphire. Adv Mater 2009;21:2416–20.
[170] Hao E, Kelly KL, Hupp JT, Schatz GC. Synthesis of silver nanodisks using polystyrene mesospheres as templates. J Am Chem Soc 2002;124:15182–3.
[171] Chi MH, Kao YH, Wei TH, Lee CW, Chen JT. Curved polymer nanodiscs by wetting nanopores of anodic aluminum oxide templates with polymer nanospheres. Nanoscale 2014;6:1340–6.
[172] Kubota T, Hashimoto T, Takeguchi M, Nishioka K, Uraoka Y, Fuyuki T, et al. Coulomb-staircase observed in silicon-nanodisk structures fabricated by low-energy chlorine neutral beams. J Appl Phys 2007;101:124301.
[173] Igarashi M, Fairuz Budiman M, Pan W, Hu W, Usami N, Samukawa S. Quantum dot solar cells using 2-dimensional array of 6.4-nm-diameter silicon nanodisks fabricated using bio-templates and neutral beam etching. Appl Phys Lett 2012;101:063121.
[174] Yoshikawa K, Higo A, Lee CY, Tamura Y, Thomas C, Kiba T, et al. Fabrication of InGaAs quantum nanodisks array by using bio-template and top-down etching processes. Procedings of the 14th IEEE International Conference of Nanotechnology, Toronto, Canada; 2014. p. 211–4.
[175] Shen Y, Wang J, Kuhlmann U, Hildebrandt P, Ariga K, Mohwald H, et al. Supramolecular templates for nanoflake-metal surfaces. Chemistry 2009;15: 2763–7.

[176] Chen C-C, Chen C-F, Lee IH, Lin C-L. Fabrication of high surface area graphitic nanoflakes on carbon nanotubes templates. Diamond Relat Mater 2005;14:1897–900.
[177] Xu C, Zeng Y, Rui X, Xiao N, Zhu J, Zhang W, et al. Controlled soft-template synthesis of ultrathin C@FeS nanosheets with high-Li-storage performance. ACS Nano 2012;6:4713–21.
[178] Fan Z, Liu Y, Yan J, Ning G, Wang Q, Wei T, et al. Template-directed synthesis of pillared-porous carbon nanosheet architectures: high-performance electrode materials for supercapacitors. Adv Energy Mater 2012;2:419–24.
[179] Son JS, Wen X-D, Joo J, Chae J, Baek S-i, Park K, et al. Large-scale soft colloidal template synthesis of 1.4 nm thick CdSe nanosheets. Angew Chem 2009;121:6993–6.
[180] Lu Z, Zhu J, Sim D, Zhou W, Shi W, Hng HH, et al. Synthesis of ultrathin silicon nanosheets by using graphene oxide as template. Chem Mater 2011;23:5293–5.
[181] Caruso F. Hollow capsule processing through colloidal templating and self-assembly. Chem – Eur J 2000;6:413–9.
[182] Zhang J, Sun L, Liao C, Yan C. Size control and photoluminescence enhancement of CdS nanoparticles prepared via reverse micelle method. Solid State Commun 2002;124:45–8.
[183] Fulton JL, Smith RD. Reverse micelle and microemulsion phases in supercritical fluids. J Phys Chem 1988;92:2903–7.
[184] Wang J, Xiao Q, Zhou H, Sun P, Yuan Z, Li B, et al. Budded, mesoporous silica hollow spheres: hierarchical structure controlled by kinetic self-assembly. Adv Mater 2006;18:3284–8.
[185] Yao L, Liu C, Chong WH, Wang H, Chen L, Chen H. Understanding the phase emergence of mesoporous silica. Small 2015;11:232–8.
[186] Pochert A, Ziller S, Kapetanovic S, Neusser G, Kranz C, Linden M. Intermediate pickering emulsion formation as a means for synthesizing hollow mesoporous silica nanoparticles. New J Chem 2016. http://dx.doi.org/10.1039/C5NJ02855H.
[187] Teng Z, Han Y, Li J, Yan F, Yang W. Preparation of hollow mesoporous silica spheres by a sol–gel/emulsion approach. Microporous Mesoporous Mater 2010;127:67–72.
[188] Tsou C-J, Hung Y, Mou C-Y. Hollow mesoporous silica nanoparticles with tunable shell thickness and pore size distribution for application as broad-ranging pH nanosensor. Microporous Mesoporous Mater 2014;190:181–8.
[189] Curri ML, Agostiano A, Mavelli F, Della Monica M. Reverse micellar systems: self organised assembly as effective route for the synthesis of colloidal semiconductor nanocrystals. Mater Sci Eng C 2002;22:423–6.
[190] Zimmermann C, Feldmann C, Wanner M, Gerthsen D. Nanoscale gold hollow spheres through a microemulsion approach. Small 2007;3:1347–9.
[191] Wang Z, Chen M, Wu L. Synthesis of monodisperse hollow silver spheres using phase-transformable emulsions as templates. Chem Mater 2008;20:3251–3.
[192] Eun TH, Kim S-H, Jeong W-J, Jeon S-J, Kim S-H, Yang S-M. Single-step fabrication of monodisperse TiO2 hollow spheres with embedded nanoparticles in microfluidic devices. Chem Mater 2009;21:201–3.
[193] Zoldesi CI, van Walree CA, Imhof A. Deformable hollow hybrid silica/siloxane colloids by emulsion templating. Langmuir 2006;22:4343–52.
[194] Ye F, Guo H, Zhang H, He X. Polymeric micelle-templated synthesis of hydroxyapatite hollow nanoparticles for a drug delivery system. Acta Biomater 2010;6:2212–8.
[195] Li Y, Shi J. Hollow-structured mesoporous materials: chemical synthesis. Functionalization Appl Adv Mater 2014;26:3176–205.
[196] Ma X, Zhao Y, Ng KW, Zhao Y. Integrated hollow mesoporous silica nanoparticles for target drug/siRNA Co-delivery. Chem – Eur J 2013;19:15593–603.
[197] Fang X, Zhao X, Fang W, Chen C, Zheng N. Self-templating synthesis of hollow mesoporous silica and their applications in catalysis and drug delivery. Nanoscale 2013;5:2205–18.
[198] Schmidt-Winkel P, Glinka CJ, Stucky GD. Microemulsion templates for mesoporous silica. Langmuir 2000;16:356–61.
[199] Li W, Sha X, Dong W, Wang Z. Synthesis of stable hollow silica microspheres with mesoporous shell in nonionic W/O emulsion. Chem Commun 2002:2434–5.
[200] Yang M, Wang G, Yang Z. Synthesis of hollow spheres with mesoporous silica nanoparticles shell. Mater Chem Phys 2008;111:5–8.
[201] Li Y, Bastakoti BP, Imura M, Tang J, Aldalbahi A, Torad NL, et al. Dual soft-template system based on colloidal chemistry for the synthesis of hollow mesoporous silica nanoparticles. Chem – Eur J 2015;21:6375–80.
[202] Fang X, Chen C, Liu Z, Liu P, Zheng N. A cationic surfactant assisted selective etching strategy to hollow mesoporous silica spheres. Nanoscale 2011;3:1632–9.
[203] Chen F, Hong H, Shi S, Goel S, Valdovinos HF, Hernandez R, et al. Engineering of hollow mesoporous silica nanoparticles for remarkably enhanced tumor active targeting efficacy. Sci Rep 2014;4:5080.
[204] Botterhuis NE, Sun Q, Magusin PCMM, van Santen RA, Sommerdijk NAJM. Hollow silica spheres with an ordered pore structure and their application in controlled release studies. Chem – Eur J 2006;12:1448–56.
[205] Yu C, Tian B, Fan J, Stucky GD, Zhao D. Synthesis of siliceous hollow spheres with ultra large mesopore wall structures by reverse emulsion templating. Chem Lett 2002;31:62–3.
[206] Wang X, Miao X, Li Z, Deng W. Fabrication of mesoporous silica hollow spheres using triblock copolymer PEG–PPG–PEG as template. J Non Cryst Solids 2010;356:898–905.
[207] Kim M-H, Na H-K, Kim Y-K, Ryoo S-R, Cho HS, Lee KE, et al. Facile synthesis of monodispersed mesoporous silica nanoparticles with ultralarge pores and their application in gene delivery. ACS Nano 2011;5:3568–76.
[208] Chen D, Li Z, Wan Y, Tu X, Shi Y, Chen Z, et al. Anionic surfactant induced mesophase transformation to synthesize highly ordered large-pore mesoporous silica structures. J Mater Chem 2006;16:1511–9.
[209] Du X, He J. Spherical silica micro/nanomaterials with hierarchical structures: synthesis and applications. Nanoscale 2011;3:3984–4002.
[210] Iskandar F, Mikrajuddin, Okuyama K. Controllability of pore size and porosity on self-organized porous silica particles. Nano Lett 2002;2:389–92.
[211] Nandiyanto ABD, Kim S-G, Iskandar F, Okuyama K. Synthesis of spherical mesoporous silica nanoparticles with nanometer-size controllable pores and outer diameters. Microporous Mesoporous Mater 2009;120:447–53.
[212] Du X, Shi B, Liang J, Bi J, Dai S, Qiao SZ. Developing functionalized dendrimer-like silica nanoparticles with hierarchical pores as advanced delivery nanocarriers. Adv Mater 2013;25:5981–5.
[213] Moon D-S, Lee J-K. Tunable synthesis of hierarchical mesoporous silica nanoparticles with radial wrinkle structure. Langmuir 2012;28:12341–7.
[214] Yang H, Liao S, Huang C, Du L, Chen P, Huang P, et al. Facile one-pot approach to the synthesis of spherical mesoporous silica nanoflowers with hierarchical pore structure. Appl Surf Sci 2014;314:7–14.
[215] Wang C, Yan J, Cui X, Cong D, Wang H. Preparation and characterization of magnetic hollow PMMA nanospheres via in situ emulsion polymerization. Colloids Surf A Physicochem Eng Asp 2010;363:71–7.
[216] He, Ge, Liu, Wang, Zhang. Synthesis of cagelike polymer microspheres with hollow core/porous shell structures by self-assembly of latex particles at the emulsion droplet interface. Chem Mater 2005;17:5891–2.
[217] Marinakos SM, Novak JP, Brousseau LC, House AB, Edeki EM, Feldhaus JC, et al. Gold particles as templates for the synthesis of hollow polymer capsules. Control of capsule dimensions and guest encapsulation. J Am Chem Soc 1999;121:8518–22.
[218] Fu G, Zhao J, Sun Y, Kang E, Neoh K. Conductive hollow nanospheres of polyaniline via surface-initiated atom transfer radical polymerization of 4-vinylaniline and oxidative graft copolymerization of aniline. Macromolecules 2007;40:2271–5.
[219] Feng X, Mao C, Yang G, Hou W, Zhu J-J. Polyaniline/Au composite hollow spheres: synthesis, characterization, and application to the detection of dopamine. Langmuir 2006;22:4384–9.
[220] Cheng D, Xia H, Chan HSO. Facile fabrication of AgCl@ polypyrrole-chitosan core–shell nanoparticles and polymeric hollow nanospheres. Langmuir 2004;20:9909–12.
[221] Cheng D, Zhou X, Xia H, Chan HSO. Novel method for the preparation of polymeric hollow nanospheres containing silver cores with different sizes. Chem Mater 2005;17:3578–81.
[222] Wang W, Luo C, Shao S, Zhou S. Chitosan hollow nanospheres fabricated from biodegradable poly-D,L-lactide-poly(ethylene glycol) nanoparticle templates. Eur J Pharm Biopharm 2010;76:376–83.
[223] Shu S, Sun C, Zhang X, Wu Z, Wang Z, Li C. Hollow and degradable polyelectrolyte nanocapsules for protein drug delivery. Acta Biomater 2010;6:210–7.
[224] White RJ, Tauer K, Antonietti M, Titirici M-M. Functional hollow carbon nanospheres by latex templating. J Am Chem Soc 2010;132:17360–3.
[225] Wei Z, Wan M. Hollow microspheres of polyaniline synthesized with an aniline emulsion template. Adv Mater 2002;14:1314–7.
[226] Lee D, Weitz DA. Double emulsion-templated nanoparticle colloidosomes with selective permeability. Adv Mater 2008;20:3498–503.
[227] Yanagishita T, Fujimura R, Nishio K, Masuda H. Fabrication of monodisperse polymer nanoparticles by membrane emulsification using ordered anodic porous alumina. Langmuir 2010;26:1516–9.
[228] Talapin DV, Rogach AL, Kornowski A, Haase M, Weller H. Highly luminescent monodisperse CdSe and CdSe/ZnS nanocrystals synthesized in a hexadecylamine—trioctylphosphine oxide—trioctylphospine mixture. Nano Lett 2001;1:207–11.
[229] Chen X, Dobson PJ. Synthesis of semiconductor nanoparticles. Methods Mol Biol 2012;906:103–23.
[230] Murray CB, Norris DJ, Bawendi MG. Synthesis and characterization of nearly monodisperse CDE (E = S, SE, TE) semiconductor nanocrystallites. J Am Chem Soc 1993;115:8706–15.
[231] Kudera S, Carbone L, Manna L, Parak W. Growth mechanism, shape and composition control of semiconductor nanocrystals. In: Rogach A, editor. Semiconductor nanocrystal quantum dots. Springer Vienna; 2008. p. 1–34 [Chapter 1].
[232] Liu L, Wu QS, Ding YP, Liu HJ, Zhang BQ. Synthesis of HgSe quantum dots through templates controlling and gas–liquid transport with emulsion liquid membrane system. Colloids Surf A Physicochem Eng Asp 2004;240:135–9.
[233] Sun SQ, Li T. Synthesis and characterization of CdS nanoparticles and nanorods via solvo-hydrothermal route. Cryst Growth Des 2007;7:2367–71.
[234] Entezari MH, Ghows N. Micro-emulsion under ultrasound facilitates the fast synthesis of quantum dots of CdS at low temperature. Ultrason Sonochem 2011;18:127–34.
[235] Caponetti E, Martino DC, Leone M, Pedone L, Saladino ML, Vetri V. Microwave-assisted synthesis of anhydrous CdS nanoparticles in a water–oil microemulsion. J Colloid Interface Sci 2006;304:413–8.
[236] Whitney TM, Searson PC, Jiang JS, Chien CL. Fabrication and magnetic Properties of arrays of metallic nanowires. Science 1993;261:1316–9.
[237] Lakshmi BB, Patrissi CJ, Martin CR. Sol–gel template synthesis of semiconductor oxide micro- and nanostructures. Chem Mater 1997;9:2544–50.
[238] Hulteen JC, Martin CR. A general template-based method for the preparation of nanomaterials. J Mater Chem 1997;7:1075–87.
[239] Dasgupta NP, Sun J, Liu C, Brittman S, Andrews SC, Lim J, et al. 25th anniversary article: semiconductor nanowires — synthesis, characterization, and applications. Adv Mater 2014;26:2137–84.
[240] Xia Y, Yang P, Sun Y, Wu Y, Mayers B, Gates B, et al. One-dimensional nanostructures: synthesis, characterization, and applications. Adv Mater 2003;15:353–89.
[241] Martin CR. Template synthesis of electronically conductive polymer nanostructures. Acc Chem Res 1995;28:61–8.

[242] Steinhart M, Wendorff JH, Greiner A, Wehrspohn RB, Nielsch K, Schilling J, et al. Polymer nanotubes by wetting of ordered porous templates. Science 2002;296:1997.
[243] Martin CR. Membrane-based synthesis of nanomaterials. Chem Mater 1996;8:1739–46.
[244] Furneaux RC, Rigby WR, Davidson AP. The formation of controlled-porosity membranes from anodically oxidized aluminium. Nature 1989;337:147–9.
[245] Tonucci RJ, Justus BL, Campillo AJ, Ford CE. Nanochannel array glass. Science 1992;258:783–5.
[246] Beck JS, Vartuli JC, Roth WJ, Leonowicz ME, Kresge CT, Schmitt KD, et al. A new family of mesoporous molecular sieves prepared with liquid crystal templates. J Am Chem Soc 1992;114:10834–43.
[247] Clark TD, Ghadiri MR. Supramolecular design by covalent capture. Design of a peptide cylinder via hydrogen-bond-promoted intermolecular olefin metathesis. J Am Chem Soc 1995;117:12364–5.
[248] Ajayan PM, Lijima S. Capillarity-induced filling of carbon nanotubes. Nature 1993;361:333–4.
[249] Ugarte D, Châtelain A, de Heer WA. Nanocapillarity and chemistry in carbon nanotubes. Science 1996;274:1897–9.
[250] Cao G, Liu D. Template-based synthesis of nanorod, nanowire, and nanotube arrays. Adv Colloid Interface Sci 2008;136:45–64.
[251] Nakano H, Matsuno M, Oue S, Yano M, Kobayashi S, Fukushima H. Mechanism of anomalous type electrodeposition of Fe–Ni alloys from sulfate solutions. Mater Trans 2004;45:3130–5.
[252] Bentley AK, Trethewey JS, Ellis AB, Crone WC. Magnetic manipulation of copper—tin nanowires capped with nickel ends. Nano Lett 2004;4:487–90.
[253] Blythe HJ, Fedosyuk VM, Kasyutich OI, Schwarzacher W. SQUID studies of Co–Cu heterogeneous alloy nanowires. J Magn Magn Mater 2000;208:251–4.
[254] Wang YW, Zhang LD, Meng GW, Peng XS, Jin YX, Zhang J. Fabrication of ordered ferromagnetic—nonmagnetic alloy nanowire arrays and their magnetic property dependence on annealing temperature. J Phys Chem B 2002;106:2502–7.
[255] Xiao Y, Yu G, Yuan J, Wang J, Chen Z. Fabrication of Pd–Ni alloy nanowire arrays on HOPG surface by electrodeposition. Electrochim Acta 2006;51:4218–27.
[256] Yuan XY, Xie T, Wu GS, Lin Y, Meng GW, Zhang LD. Fabrication of Ni–W–P nanowire arrays by electroless deposition and magnetic studies. Phys E 2004;23:75–80.
[257] Chen Z, Zhan P, Wang ZL, Zhang JH, Zhang WY, Ming NB, et al. Two- and three-dimensional ordered structures of hollow silver spheres prepared by colloidal crystal templating. Adv Mater 2004;16:417–22.
[258] Tierno P, Goedel WA. Using electroless deposition for the preparation of micron sized polymer/metal core/shell particles and hollow metal spheres. J Phys Chem B 2006;110:3043–50.
[259] Dickerson MB, Sandhage KH, Naik RR. Protein- and peptide-directed syntheses of inorganic materials. chem rev 2008;108:4935–78.
[260] Lee S-Y, Choi J, Royston E, Janes DB, Culver JN, Harris MT. Deposition of platinum clusters on surface-modified tobacco mosaic virus. J Nanosci Nanotechnol 2006;6:974–81.
[261] Valenzuela K, Raghavan S, Deymier PA, Hoying J. Formation of copper nanowires by electroless deposition using microtubules as templates. J Nanosci Nanotechnol 2008;8:3416–21.
[262] Watson SMD, Pike AR, Pate J, Houlton A, Horrocks BR. DNA-templated nanowires: morphology and electrical conductivity. Nanoscale 2014;6:4027–37.
[263] Habas SE, Lee H, Radmilovic V, Somorjai GA, Yang P. Shaping binary metal nanocrystals through epitaxial seeded growth. Nat Mater 2007;6:692–7.
[264] Kim Y-T, Han JH, Hong BH, Kwon Y-U. Electrochemical synthesis of CdSe quantum-dot arrays on a graphene basal plane using mesoporous silica thin-film templates. Adv Mater 2010;22:515.
[265] Jana Drbohlavova JC, Hrdy Radim, Prasek Jan, Mravec Filip, Cudek Pavel, Ryvolova Marketa, et al. Templated based frabrication of titania quentum dots array. NanoCon 2011;9:21–3.
[266] Cho SI, Lee SB. Fast electrochemistry of conductive polymer nanotubes: synthesis, mechanism, and application. Acc Chem Res 2008;41:699–707.
[267] Xia L, Wei Z, Wan M. Conducting polymer nanostructures and their application in biosensors. J Colloid Interface Sci 2010;341:1–11.
[268] Pan L, Qiu H, Dou C, Li Y, Pu L, Xu J, et al. Conducting polymer nanostructures: template synthesis and applications in energy storage. Int J Mol Sci 2010;11:2636–57.
[269] Schönenberger C, van der Zande BMI, Fokkink LGJ, Henny M, Schmid C, Krüger M, et al. Template synthesis of nanowires in porous polycarbonate membranes: electrochemistry and morphology. J Phys Chem B 1997;101:5497–505.
[270] Van Dyke LS, Martin CR. Electrochemical investigations of electronically conductive polymers. 4. Controlling the supermolecular structure allows charge transport rates to be enhanced. Langmuir 1990;6:1118–23.
[271] Jérôme C, Jérôme R. Electrochemical synthesis of polypyrrole nanowires. Angew Chem Int Ed 1998;37:2488–90.
[272] Xiao R, Cho SI, Liu R, Lee SB. Controlled electrochemical synthesis of conductive polymer nanotube structures. J Am Chem Soc 2007;129:4483–9.
[273] Liu R, Lee SB. MnO2/poly(3,4-ethylenedioxythiophene) coaxial nanowires by one-step coelectrodeposition for electrochemical energy storage. J Am Chem Soc 2008;130:2942–3.
[274] Luo Q, Liu Z, Li L, Xie S, Kong J, Zhao D. Creating highly ordered metal, alloy, and semiconductor macrostructures by electrodeposition, ion spraying, and laser spraying. Adv Mater 2001;13:286–9.
[275] Sun F, Cai WP, Li Y, Cao B, Lu F, Duan G, et al. Morphology control and transferability of ordered through-pore arrays based on the electrodeposition of a colloidal monolayer. Adv Mater 2004;16:1116–21.
[276] Xia XH, Tu JP, Zhang J, Xiang JY, Wang XL, Zhao XB. Cobalt oxide ordered bowl-like array films prepared by electrodeposition through monolayer polystyrene sphere template and electrochromic properties. ACS Appl Mater Interfaces 2010;2:186–92.
[277] Fu M, Zhou J, Xiao Q, Li B, Zong R, Chen W, et al. ZnO nanosheets with ordered pore periodicity via colloidal crystal template assisted electrochemical deposition. Adv Mater 2006;18:1001–4.
[278] Nakayama M, Kanaya T, Inoue R. Anodic deposition of layered manganese oxide into a colloidal crystal template for electrochemical supercapacitor. Electrochem Commun 2007;9:1154–8.
[279] Yeo SH, Teh LK, Wong CC. Fabrication & characterization of macroporous CdSe nanostructure via colloidal crystal templating with electrodeposition method. J Porous Mater 2006;13:281–5.
[280] Takahashi K, Limmer SJ, Wang Y, Cao G. Synthesis and electrochemical properties of single-crystal V2O5 nanorod arrays by template-based electrodeposition. J Phys Chem B 2004;108:9795–800.
[281] Zhang H, Cao G, Wang Z, Yang Y, Shi Z, Gu Z. Growth of manganese oxide nanoflowers on vertically-aligned carbon nanotube arrays for high-rate electrochemical capacitive energy storage. Nano Lett 2008;8:2664–8.
[282] Aziz NSA, Nishiyama T, Rusli NI, Mahmood MR, Yasui K, Hashim AM. Seedless growth of zinc oxide flower-shaped structures on multilayer graphene by electrochemical deposition. Nanoscale Res Lett 2014;9:1–9.
[283] Kazemi SH, Asghari A, Kiani MA. High performance supercapacitors based on the electrodeposited Co3O4 nanoflakes on electro-etched carbon fibers. Electrochim Acta 2014;138:9–14.
[284] Zhang Q, Xu T, Butterfield D, Misner MJ, Ryu DY, Emrick T, et al. Controlled placement of CdSe nanoparticles in diblock copolymer templates by electrophoretic deposition. Nano Lett 2005;5:357–61.
[285] Wang YC, Leu IC, Hon MH. Dielectric property and structure of anodic alumina template and their effects on the electrophoretic deposition characteristics of ZnO nanowire arrays. J Appl Phys 2004;95:1444–9.
[286] Lin Y, Sun FQ, Yuan XY, Geng BY, Zhang LD. Sol–gel electrophoretic deposition and optical properties of Fe2O3 nanowire arrays. J Appl Phys A 2003;78:1197–9.
[287] Dziomkina NV, Hempenius MA, Vancso GJ. Symmetry control of polymer colloidal monolayers and crystals by electrophoretic deposition on patterned surfaces. Adv Mater 2005;17:237–40.
[288] Huang ML, Gu CD, Ge X, Wang XL, Tu JP. NiO nanoflakes grown on porous graphene frameworks as advanced electrochemical pseudocapacitor materials. J Power Sources 2014;259:98–105.
[289] Ma J, Wang C, Peng KW. Electrophoretic deposition of porous hydroxyapatite scaffold. Biomaterials 2003;24:3505–10.
[290] Limmer SJ, Seraji S, Forbess MJ, Wu Y, Chou TP, Nguyen C, et al. Electrophoretic growth of lead zirconate titanate nanorods. Adv Mater 2001;13:1269–72.
[291] Limmer SJ, Seraji S, Wu Y, Chou TP, Nguyen C, Cao GZ. Template-based growth of various oxide nanorods by sol–gel electrophoresis. Adv Funct Mater 2002;12:59–64.
[292] Limmer SJ, Cao G. Sol–gel electrophoretic deposition for the growth of oxide nanorods. Adv Mater 2003;15:427–31.
[293] Miao Z, Xu D, Ouyang J, Guo G, Zhao X, Tang Y. Electrochemically induced sol–gel preparation of single-crystalline TiO2 nanowires. Nano Lett 2002;2:717–20.
[294] Lu Y, Ganguli R, Drewien CA, Anderson MT, Brinker CJ, Gong W, et al. Continuous formation of supported cubic and hexagonal mesoporous films by sol–gel dip-coating. Nature 1997;389:364–8.
[295] Cheng JP, Zhang XB, Luo ZQ. Oriented growth of ZnO nanostructures on Si and Al substrates. Surf Coat Technol 2008;202:4681–6.
[296] Sarkar K, Rawolle M, Herzig EM, Wang W, Buffet A, Roth SV, et al. Custom-made morphologies of ZnO nanostructured films templated by a poly(styrene-block-ethylene oxide) diblock copolymer obtained by a sol–gel technique. ChemSusChem 2013;6:1414–24.
[297] Mu C, Yu Y, Liao W, Zhao X, Xu D, Chen X, et al. Controlling growth and field emission properties of silicon nanotube arrays by multistep template replication and chemical vapor deposition. Appl Phys Lett 2005;87:113104.
[298] Zhao Q, Wen G, Liu Z, Fan Y, Zou G, Li L, et al. Synthesis of dense, single-crystalline CrO2 nanowire arrays using AAO template-assisted chemical vapor deposition. Nanotechnology 2011;22:125603.
[299] Liu CH, Zapien JA, Yao Y, Meng XM, Lee CS, Fan SS, et al. High-density, ordered ultraviolet light-emitting ZnO nanowire arrays. Adv Mater 2003;15:838–41.
[300] Ge JP, Li YD. Selective atmospheric pressure chemical vapor deposition route to CdS arrays, nanowires, and nanocombs. Adv Funct Mater 2004;14:157–62.
[301] Liu JZ, Yan PX, Yue GH, Kong LB, Zhuo RF, Qu DM. Synthesis of doped ZnS one-dimensional nanostructures via chemical vapor deposition. Mater Lett 2006;60:3471–6.
[302] Dickey MD, Weiss EA, Smythe EJ, Chiechi RC, Capasso F, Whitesides GM. Fabrication of arrays of metal and metal oxide nanotubes by shadow evaporation. ACS Nano 2008;2:800–8.
[303] Li F, Li L, Liao X, Wang Y. Precise pore size tuning and surface modifications of polymeric membranes using the atomic layer deposition technique. J Membr Sci 2011;385–386:1–9.
[304] Li Y-L, Kinloch IA, Windle AH. Direct spinning of carbon nanotube fibers from chemical vapor deposition synthesis. Science 2004;304:276–8.
[305] Che G, Lakshmi BB, Martin CR, Fisher ER, Ruoff RS. Chemical vapor deposition based synthesis of carbon nanotubes and nanofibers using a template method. Chem Mater 1998;10:260–7.

[306] Jang J, Oh JH. A facile synthesis of polypyrrole nanotubes using a template-mediated vapor deposition polymerization and the conversion to carbon nanotubes. Chem Commun 2004:882–3.
[307] Lee KJ, Oh JH, Kim Y, Jang J. Fabrication of photoluminescent dyes/poly(acrylonitrile) coaxial nanotubes using vapor deposition polymerization. Chem Mater 2006;18:5002–8.
[308] Zhao YS, Xiao D, Yang W, Peng A, Yao J. 2,4,5-Triphenylimidazole nanowires with fluorescence narrowing spectra prepared through the adsorbent-assisted physical vapor deposition method. Chem Mater 2006;18:2302–6.
[309] Sokolov AN, Yap FL, Liu N, Kim K, Ci L, Johnson OB, et al. Direct growth of aligned graphitic nanoribbons from a DNA template by chemical vapour deposition. Nat Commun 2013;4.
[310] Suresh V, Huang MS, Srinivasan MP, Krishnamoorthy S. In situ synthesis of high density sub-50 nm ZnO nanopatterned arrays using diblock copolymer templates. ACS Appl Mater Interfaces 2013;5:5727–32.
[311] Huber CA, Huber TE, Sadoqi M, Lubin JA, Manalis S, Prater CB. Nanowire array composites. Science 1994;263:800–2.
[312] Zhang Z, Ying JY, Dresselhaus MS. Bismuth quantum-wire arrays fabricated by a vacuum melting and pressure injection process. J Mater Res 1998;13:1745–8.
[313] Zhang Z, Gekhtman D, Dresselhaus MS, Ying JY. Processing and characterization of single-crystalline ultrafine bismuth nanowires. Chem Mater 1999;11:1659–65.
[314] Govindaraj A, Satishkumar BC, Nath M, Rao CNR. Metal nanowires and intercalated metal layers in single-walled carbon nanotube bundles. Chem Mater 2000;12:202–5.
[315] Kiang C-H, Choi J-S, Tran TT, Bacher AD. Molecular nanowires of 1 nm diameter from capillary filling of single-walled carbon nanotubes. J Phys Chem B 1999;103:7449–51.
[316] Ajayan PM, Stephan O, Redlich P, Colliex C. Carbon nanotubes as removable templates for metal oxide nanocomposites and nanostructures. Nature 1995;375:564–7.
[317] Chen YK, Chu A, Cook JLH, Green MJF, Harris P, Heesom R, et al. Synthesis of carbon nanotubes containing metal oxides and metals of the d-block and f-block transition metals and related studies. J Mater Chem 1997;7:545–9.
[318] Han Y-J, Kim JM, Stucky GD. Preparation of noble metal nanowires using hexagonal mesoporous silica SBA-15. Chem Mater 2000;12:2068–9.
[319] Parthasarathy RV, Martin CR. Template-synthesized polyaniline microtubules. Chem Mater 1994;6:1627–32.
[320] Koopal CGJ, de Ruiter B, Nolte RJM. Amperometric biosensor based on direct communication between glucose oxidase and a conducting polymer inside the pores of a filtration membrane. J Chem Soc Chem Commun 1991;1691-2.
[321] Martin CR. Template synthesis of polymeric and metal microtubules. Adv Mater 1991;3:457–9.
[322] Martin CR, Van Dyke LS, Cai Z, Liang W. Template synthesis of organic microtubules. J Am Chem Soc 1990;112:8976–7.
[323] Cai Z, Martin CR. Electronically conductive polymer fibers with mesoscopic diameters show enhanced electronic conductivities. J Am Chem Soc 1989;111:4138–9.
[324] Cepak VM, Hulteen JC, Che G, Jirage KB, Lakshmi BB, Fisher ER, et al. Chemical strategies for template syntheses of composite micro- and nanostructures. Chem Mater 1997;9:1065–7.
[325] Berdichevsky Y, Lo YH. Polypyrrole nanowire actuators. Adv Mater 2006;18:122–5.
[326] Lee JI, Cho SH, Park S-M, Kim JK, Kim JK, Yu J-W, et al. Highly aligned ultrahigh density arrays of conducting polymer nanorods using block copolymer templates. Nano Lett 2008;8:2315–20.
[327] Park DH, Kim BH, Jang MG, Bae KY, Joo J. Characteristics and photoluminescence of nanotubes and nanowires of poly (3-methylthiophene). Appl Phys Lett 2005;86:113116.
[328] Parthasarathy RV, Phani KLN, Martin CR. Template synthesis of graphitic nanotubules. Adv Mater 1995;7:896–7.
[329] Hulteen JC, Chen HX, Chambliss CK, Martin CR. Template synthesis of carbon nanotubule and nanofiber arrays. Nanostruct Mater 1997;9:133–6.
[330] Cho SI, Kwon WJ, Choi SJ, Kim P, Park SA, Kim J, et al. Nanotube-based ultrafast electrochromic display. Adv Mater 2005;17:171–5.
[331] Wang Y, Angelatos AS, Caruso F. Template synthesis of nanostructured materials via layer-by-layer assembly. Chem Mater 2008;20:848–58.
[332] Srivastava S, Kotov NA. Composite layer-by-layer (LBL) assembly with inorganic nanoparticles and nanowires. Acc Chem Res 2008;41:1831–41.
[333] Artyukhin AB, Bakajin O, Stroeve P, Noy A. Layer-by-layer electrostatic self-assembly of polyelectrolyte nanoshells on individual carbon nanotube templates. Langmuir 2004;20:1442–8.
[334] Koo W-T, Choi S-J, Kim N-H, Jang J-S, Kim I-D. Catalyst-decorated hollow WO3 nanotubes using layer-by-layer self-assembly on polymeric nanofiber templates and their application in exhaled breath sensor. Sens Actuators B 2016;223:301–10.
[335] Donath E, Sukhorukov GB, Caruso F, Davis SA, Möhwald H. Novel hollow polymer shells by colloid-templated assembly of polyelectrolytes. Angew Chem Int Ed 1998;37:2201–5.
[336] Shi X, Briseno AL, Sanedrin RJ, Zhou F. Formation of uniform polyaniline thin shells and hollow capsules using polyelectrolyte-coated microspheres as templates. Macromolecules 2003;36:4093–8.
[337] Correa-Duarte MA, Liz-Marzan LM. Carbon nanotubes as templates for one-dimensional nanoparticle assemblies. J Mater Chem 2006;16:22–5.
[338] Du N, Zhang H, Chen BD, Ma XY, Liu ZH, Wu JB, et al. Porous indium oxide nanotubes: layer-by-layer assembly on carbon-nanotube templates and application for room-temperature NH3 gas sensors. Adv Mater 2007;19:1641–5.
[339] Liang Z, Susha AS, Yu A, Caruso F. Nanotubes prepared by layer-by-layer coating of porous membrane templates. Adv Mater 2003;15:1849–53.
[340] Ma R, Sasaki T, Bando Y. Layer-by-layer assembled multilayer films of titanate nanotubes, Ag- or Au-loaded nanotubes, and nanotubes/nanosheets with polycations. J Am Chem Soc 2004;126:10382–8.
[341] Lou X, Chen J, Wang M, Gu J, Wu P, Sun D, et al. Carbon nanotubes supported cerium dioxide and platinum nanohybrids: layer-by-layer synthesis and enhanced electrocatalytic activity for methanol oxidation. J Power Sources 2015;287:203–10.
[342] Huang W, Shen J, Wan L, Chang Y, Ye M. Y2O3:Yb/Er nanotubes: layer-by-layer assembly on carbon-nanotube templates and their upconversion luminescence properties. Mater Res Bull 2012;47:3875–80.
[343] Caruso RA, Susha A, Caruso F. Multilayered titania, silica, and laponite nanoparticle coatings on polystyrene colloidal templates and resulting inorganic hollow spheres. Chem Mater 2001;13:400–9.
[344] Du N, Zhang H, Chen J, Sun J, Chen B, Yang D. Metal oxide and sulfide hollow spheres: layer-by-layer synthesis and their application in lithium-ion battery. J Phys Chem B 2008;112:14836–42.
[345] He X, Gao F, Tu G, Hasko DG, Hüttner S, Greenham NC, et al. Formation of well-ordered heterojunctions in polymer:PCBM photovoltaic devices. Adv Funct Mater 2011;21:139–46.
[346] He X, Gao F, Tu G, Hasko D, Hüttner S, Steiner U, et al. Formation of nanopatterned polymer blends in photovoltaic devices. Nano Lett 2010;10:1302–7.
[347] Aryal M, Buyukserin F, Mielczarek K, Zhao X-M, Gao J, Zakhidov A, et al. Imprinted large-scale high density polymer nanopillars for organic solar cells. J Vac Sci Technol B 2008;26:2562–6.
[348] Chen D, Zhao W, Russell TP. P3HT nanopillars for organic photovoltaic devices nanoimprinted by AAO templates. ACS Nano 2012;6:1479–85.
[349] Haberkorn N, Gutmann JS, Theato P. Template-assisted fabrication of free-standing nanorod arrays of a hole-conducting cross-linked triphenylamine derivative: toward ordered bulk-heterojunction solar cells. ACS Nano 2009;3:1415–22.
[350] Jang JH, Ullal CK, Maldovan M, Gorishnyy T, Kooi S, Koh C, et al. 3D micro- and nanostructures via interference lithography. Adv Funct Mater 2007;17:3027–41.
[351] Fan HJ, Lee W, Scholz R, Dadgar A, Krost A, Nielsch K, et al. Arrays of vertically aligned and hexagonally arranged ZnO nanowires: a new template-directed approach. Nanotechnology 2005;16:913.
[352] Park HJ, Kang M-G, Guo LJ. Large area high density sub-20 nm SiO2 nanostructures fabricated by block copolymer template for nanoimprint lithography. ACS Nano 2009;3:2601–8.
[353] Huang Y-H, Wu J-T, Yang S-Y. Direct fabricating patterns using stamping transfer process with PDMS mold of hydrophobic nanostructures on surface of microcavity. Microelectron Eng 2011;88:849–54.
[354] Kamat PV. Quantum dot solar cells. Semiconductor nanocrystals as light harvesters. J Phys Chem C 2008;112:18737–53.
[355] Gonzalez-Valls I, Lira-Cantu M. Vertically-aligned nanostructures of ZnO for excitonic solar cells: a review. Energy Environ Sci 2009;2:19–34.
[356] Toivola M, Halme J, Miettunen K, Aitola K, Lund PD. Nanostructured dye solar cells on flexible substrates—review. Int J Energy Res 2009;33:1145–60.
[357] Zhang Q, Cao G. Nanostructured photoelectrodes for dye-sensitized solar cells. Nano Today 2011;6:91–109.
[358] Li H, Bian Z, Zhu J, Zhang D, Li G, Huo Y, et al. Mesoporous titania spheres with tunable chamber stucture and enhanced photocatalytic activity. J Am Chem Soc 2007;129:8406–7.
[359] Kondo Y, Yoshikawa H, Awaga K, Murayama M, Mori T, Sunada K, et al. Preparation, photocatalytic activities, and dye-sensitized solar-cell performance of submicron-scale TiO2 hollow spheres. Langmuir 2008;24:547–50.
[360] Yang SC, Yang DJ, Kim J, Hong JM, Kim HG, Kim ID, et al. Hollow TiO2 hemispheres obtained by colloidal templating for application in dye-sensitized solar cells. Adv Mater 2008;20:1059–64.
[361] Wu X, Lu GQ, Wang L. Shell-in-shell TiO2 hollow spheres synthesized by one-pot hydrothermal method for dye-sensitized solar cell application. Energy Environ Sci 2011;4:3565–72.
[362] Qian J, Liu P, Xiao Y, Jiang Y, Cao Y, Ai X, et al. TiO2-coated multilayered SnO2 hollow microspheres for dye-sensitized solar cells. Adv Mater 2009;21:3663–7.
[363] Dong Z, Lai X, Halpert JE, Yang N, Yi L, Zhai J, et al. Accurate control of multishelled ZnO hollow microspheres for dye-sensitized solar cells with high efficiency. Adv Mater 2012;24:1046–9.
[364] Stuart HR, Hall DG. Absorption enhancement in silicon-on-insulator waveguides using metal island films. Appl Phys Lett 1996;69:2327–9.
[365] Pillai S, Catchpole KR, Trupke T, Green MA. Surface plasmon enhanced silicon solar cells. J Appl Phys 2007;101:093105.
[366] Atwater HA, Polman A. Plasmonics for improved photovoltaic devices. Nat Mater 2010;9:205–13.
[367] Nakayama K, Tanabe K, Atwater HA. Plasmonic nanoparticle enhanced light absorption in GaAs solar cells. Appl Phys Lett 2008;93:121904.
[368] Pryce IM, Koleske DD, Fischer AJ, Atwater HA. Plasmonic nanoparticle enhanced photocurrent in GaN/InGaN/GaN quantum well solar cells. Appl Phys Lett 2010;96:153501.
[369] Garnett E, Yang P. Light trapping in silicon nanowire solar cells. Nano Lett 2010;10:1082–7.
[370] Zhu K, Neale NR, Miedaner A, Frank AJ. Enhanced charge-collection efficiencies and light scattering in dye-sensitized solar cells using oriented TiO2 nanotubes arrays. Nano Lett 2007;7:69–74.
[371] Yu M, Long Y-Z, Sun B, Fan Z. Recent advances in solar cells based on one-dimensional nanostructure arrays. Nanoscale 2012;4:2783–96.
[372] Li L, Zhai T, Bando Y, Golberg D. Recent progress of one-dimensional ZnO nanostructured solar cells. Nano Energy 2012;1:91–106.
[373] Martinson ABF, Elam JW, Hupp JT, Pellin MJ. ZnO nanotube based dye-sensitized solar cells. Nano Lett 2007;7:2183–7.

[374] Kang T-S, Smith AP, Taylor BE, Durstock MF. Fabrication of highly-ordered TiO2 nanotube arrays and their use in dye-sensitized solar cells. Nano Lett 2009;9:601–6.
[375] Pettersson LAA, Roman LS, Inganäs O. Modeling photocurrent action spectra of photovoltaic devices based on organic thin films. J Appl Phys 1999;86:487–96.
[376] Shaw PE, Ruseckas A, Samuel IDW. Exciton diffusion measurements in poly(3-hexylthiophene). Adv Mater 2008;20:3516–20.
[377] Mayer AC, Scully SR, Hardin BE, Rowell MW, McGehee MD. Polymer-based solar cells. Mater Today 2007;10:28–33.
[378] Günes S, Neugebauer H, Sariciftci NS. Conjugated polymer-based organic solar cells. Chem Rev 2007;107:1324–38.
[379] Kim JS, Park Y, Lee DY, Lee JH, Park JH, Kim JK, et al. Poly(3-hexylthiophene) nanorods with aligned chain orientation for organic photovoltaics. Adv Funct Mater 2010;20:540–5.
[380] Snyder GJ, Toberer ES. Complex thermoelectric materials. Nat Mater 2008;7:105–14.
[381] Vining CB. An inconvenient truth about thermoelectrics. Nat Mater 2009;8:83–5.
[382] Rowe DM. CRC handbook of thermoelectrics. One ed. Boca Raton, FL: CRC Press; 1995.
[383] Kim J, Lee S, Brovman YM, Kim P, Lee W. Diameter-dependent thermoelectric figure of merit in single-crystalline Bi nanowires. Nanoscale 2015;7:5053–9.
[384] Keskar G, Iyyamperumal E, Hitchcock DA, He J, Rao AM, Pfefferle LD. Significant improvement of thermoelectric performance in nanostructured bismuth networks. Nano Energy 2012;1:706–13.
[385] Qi Y, Wang Z, Zhang M, Yang F, Wang X. Thermoelectric devices based on one-dimensional nanostructures. J Mater Chem A 2013;1:6110–24.
[386] Lv HY, Liu HJ, Shi J, Tang XF, Uher C. Optimized thermoelectric performance of Bi2Te3 nanowires. J Mater Chem A 2013;1:6831–8.
[387] Xu EZ, Li Z, Martinez JA, Sinitsyn N, Htoon H, Li N, et al. Diameter dependent thermoelectric properties of individual SnTe nanowires. Nanoscale 2015;7:2869–76.
[388] Lin Y-M, Rabin O, Cronin SB, Ying JY, Dresselhaus MS. Semimetal–semiconductor transition in Bi[1 − x]Sb[x] alloy nanowires and their thermoelectric properties. Appl Phys Lett 2002;81:2403.
[389] Prieto AL, Sander MS, Martín-González MS, Gronsky R, Sands T, Stacy AM. Electrodeposition of ordered Bi2Te3 nanowire arrays. J Am Chem Soc 2001;123:7160–1.
[390] Li L, Xu S, Li G. Enhancement of thermoelectric properties in Bi–Sb–Te alloy nanowires by pulsed electrodeposition. Energy Technol 2015;3:828–9.
[391] Picht O, Müller S, Alber I, Rauber M, Lensch-Falk J, Medlin DL, et al. Tuning the geometrical and crystallographic characteristics of Bi2Te3 nanowires by electrodeposition in ion-track membranes. J Phys Chem C 2012;116:5367–75.
[392] Töllner W, Bäßler S, Peranio N, Pippel E, Eibl O, Nielsch K. Electrodeposition of Bi2Te3-based thin films and nanowires. In: Eibl O, Nielsch K, Peranio N, Völklein F, editors. Thermoelectric Bi2Te3 nanomaterials. Wiley-VCH Verlag GmbH & Co; 2015. p. 11–32 [KGaA].
[393] Trahey L, Becker CR, Stacy AM. Electrodeposited bismuth telluride nanowire arrays with uniform growth fronts. Nano Lett 2007;7:2535–9.
[394] Liu J, Uprety B, Gyawali S, Woolley AT, Myung NV, Harb JN. Fabrication of DNA-templated Te and Bi2Te3 nanowires by galvanic displacement. Langmuir 2013;29:11176–84.
[395] Vineis CJ, Shakouri A, Majumdar A, Kanatzidis MG. Nanostructured thermoelectrics: big efficiency gains from small features. Adv Mater 2010;22:3970–80.
[396] Venkatasubramanian R, Siivola E, Colpitts T, O'Quinn B. Thin-film thermoelectric devices with high room-temperature figures of merit. Nature 2001;413:597–602.
[397] Hochbaum AI, Chen R, Delgado RD, Liang W, Garnett EC, Najarian M, et al. Enhanced thermoelectric performance of rough silicon nanowires. Nature 2008;451:163–7.
[398] Boukai AI, Bunimovich Y, Tahir-Kheli J, Yu J-K, Goddard III WA, Heath JR. Silicon nanowires as efficient thermoelectric materials. Nature 2008;451:168–71.
[399] Hochbaum AI, Fan R, He R, Yang P. Controlled growth of Si nanowire arrays for device integration. Nano Lett 2005;5:457–60.
[400] Al-Salman R, Mallet J, Molinari M, Fricoteaux P, Martineau F, Troyon M, et al. Template assisted electrodeposition of germanium and silicon nanowires in an ionic liquid. Phys Chem Chem Phys 2008;10:6233–7.
[401] Shelley M, Mostofi AA. Prediction of high zT in thermoelectric silicon nanowires with axial germanium heterostructures. Europhys Lett 2011;94:67001.
[402] Hu M, Giapis KP, Goicochea JV, Zhang X, Poulikakos D. Significant reduction of thermal conductivity in Si/Ge core—shell nanowires. Nano Lett 2011;11:618–23.
[403] Chen X, Wang Y, Ma Y. High thermoelectric performance of Ge/Si core—shell nanowires: first-principles prediction. J Phys Chem C 2010;114:9096–100.
[404] Martinez JA, Provencio PP, Picraux ST, Sullivan JP, Swartzentruber BS. Enhanced thermoelectric figure of merit in SiGe alloy nanowires by boundary and hole-phonon scattering. J Appl Phys 2011;110:074317.
[405] Lee EK, Yin L, Lee Y, Lee JW, Lee SJ, Lee J, et al. Large thermoelectric figure-of-merits from SiGe nanowires by simultaneously measuring electrical and thermal transport properties. Nano Lett 2012;12:2918–23.
[406] Shi X, Yang J, Salvador JR, Chi M, Cho JY, Wang H, et al. Multiple-filled skutterudites: high thermoelectric figure of merit through separately optimizing electrical and thermal transports. J Am Chem Soc 2011;133:7837–46.
[407] Chen L, Hu H, Li Y, Chen G, Yu S, Wu G. Ordered CoSb < SUB > 3</SUB > nanowire arrays synthesized by electrodeposition. Chem Lett 2006;35:170–1.
[408] Behnke JF, Prieto AL, Stacy AM, Sands T. Electrodeposition of CoSb/sub 3/ nanowires. Eighteenth International Conference on Thermoelectrics; 1999. p. 451–3.
[409] LeBlanc S, Yee SK, Scullin ML, Dames C, Goodson KE. Material and manufacturing cost considerations for thermoelectrics. Renew Sustain Energy Rev 2014;32:313–27.
[410] Corma A, Garcia H. Lewis acids: from conventional homogeneous to green homogeneous and heterogeneous catalysis. Chem Rev 2003;103:4307–65.
[411] Martinez C, Corma A. Inorganic molecular sieves: preparation, modification and industrial application in catalytic processes. Coord Chem Rev 2011;255:1558–80.
[412] White RJ, Luque R, Budarin VL, Clark JH, Macquarrie DJ. Supported metal nanoparticles on porous materials. Methods Appl Chem Soc Rev 2009;38:481–94.
[413] Taguchi A, Schüth F. Ordered mesoporous materials in catalysis. Microporous Mesoporous Mater 2005;77:1–45.
[414] Di Renzo F, Fajula F. Introduction to molecular sieves: trends of evolution of the zeolite community. In: Čejka J, Bekkum Hv, editors. Studies in surface science and catalysis. Elsevier; 2005. p. 1–12.
[415] Yilmaz B, Müller U. Catalytic applications of zeolites in chemical industry. Top Catal 2009;52:888–95.
[416] Forzatti P, Lietti L, Tronconi E. Catalytic removal of NOx under lean conditions from stationary and mobile sources. Catalysis for sustainable energy production. Wiley-VCH Verlag GmbH & Co; 2009. p. 393–438 [KGaA].
[417] Tao Y, Kanoh H, Abrams L, Kaneko K. Mesopore-modified zeolites: preparation, characterization, and applications. Chem Rev 2006;106:896–910.
[418] Corma A. From microporous to mesoporous molecular sieve materials and their use in catalysis. Chem Rev 1997;97:2373–420.
[419] van Donk S, Broersma A, Gijzeman OLJ, van Bokhoven JA, Bitter JH, de Jong KP. Combined diffusion, adsorption, and reaction studies of n-hexane hydroisomerization over Pt/H–mordenite in an oscillating microbalance. J Catal 2001;204:272–80.
[420] Corma A, Martínez A, Arroyo PA, Monteiro JLF, Sousa-Aguiar EF. Isobutane/2-butene alkylation on zeolite beta: influence of post-synthesis treatments. Appl Catal Gen 1996;142:139–50.
[421] Byambajav E, Ohtsuka Y. Cracking behavior of asphaltene in the presence of iron catalysts supported on mesoporous molecular sieve with different pore diameters. Fuel 2003;82:1571–7.
[422] Twaiq FA, Mohamed AR, Bhatia S. Liquid hydrocarbon fuels from palm oil by catalytic cracking over aluminosilicate mesoporous catalysts with various Si/Al ratios. Microporous Mesoporous Mater 2003;64:95–107.
[423] Azhar Uddin M, Sakata Y, Muto A, Shiraga Y, Koizumi K, Kanada Y, et al. Catalytic degradation of polyethylene and polypropylene into liquid hydrocarbons with mesoporous silica. Microporous Mesoporous Mater 1998;21:557–64.
[424] Sun YY, Zhu L, Lu HJ, Wang RW, Lin S, Jiang DZ, et al. Sulfated zirconia supported in mesoporous materials. Appl Catal Gen 2002;237:21–31.
[425] Landau MV, Titelman L, Vradman L, Wilson P. Thermostable sulfated 2–4 nm tetragonal ZrO2 with high loading in nanotubes of SBA-15: a superior acidic catalytic material. Chem Commun 2003:594–5.
[426] Ghanbari-Siahkali A, Philippou A, Dwyer J, Anderson MW. The acidity and catalytic activity of heteropoly acid on MCM-41 investigated by MAS NMR, FTIR and catalytic tests. Appl Catal Gen 2000;192:57–69.
[427] Xia QH, Hidajat K, Kawi S. Structure, acidity, and catalytic activity of mesoporous acid catalysts for the gas-phase synthesis of MTBE from MeOH and (BuOH)-O-t. J Catal 2002;209:433–44.
[428] Yoshimura Y, Kijima N, Hayakawa T, Murata K, Suzuki K, Mizukami F, et al. Catalytic cracking of naphtha to light olefins. Catal Surv Jpn 2000;4:157–67.
[429] Mochizuki H, Yokoi T, Imai H, Watanabe R, Namba S, Kondo JN, et al. Facile control of crystallite size of ZSM-5 catalyst for cracking of hexane. Microporous Mesoporous Mater 2011;145:165–71.
[430] Mochizuki H, Yokoi T, Imai H, Namba S, Kondo JN, Tatsumi T. Effect of desilication of H-ZSM-5 by alkali treatment on catalytic performance in hexane cracking. Appl Catal Gen 2012;449:188–97.
[431] Kubo K, Iida H, Namba S, Igarashi A. Selective formation of light olefin by n-heptane cracking over HZSM-5 at high temperatures. Microporous Mesoporous Mater 2012;149:126–33.
[432] Kubo K, Iida H, Namba S, Igarashi A. Effect of steaming on acidity and catalytic performance of H-ZSM-5 and P/H-ZSM-5 as naphtha to olefin catalysts. Microporous Mesoporous Mater 2014;188:23–9.
[433] Konno H, Tago T, Nakasaka Y, Ohnaka R, J-i Nishimura, Masuda T. Effectiveness of nano-scale ZSM-5 zeolite and its deactivation mechanism on catalytic cracking of representative hydrocarbons of naphtha. Microporous Mesoporous Mater 2013;175:25–33.
[434] Tromp M, vab Bokhoven JA, Garriga Oostenbrink MT, Bitter JH, de Jong KP, Koningsberger DC. Influence of the generation of mesopores on the hydroisomerization activity and selectivity of n-hexane over Pt/mordenite. J Catal 2000;190:209–14.
[435] Ogura M, Shinomiya S-y, Tateno J, Nara Y, Nomura M, Kikuchi E, et al. Alkali-treatment technique — new method for modification of structural and acid-catalytic properties of ZSM-5 zeolites. Appl Catal Gen 2001;219:33–43.
[436] Kubo K, Iida H, Namba S, Igarashi A. Comparison of steaming stability of Cu-ZSM-5 with those of Ag-ZSM-5, P/H-ZSM-5, and H-ZSM-5 zeolites as naphtha cracking catalysts to produce light olefin at high temperatures. Appl Catal Gen 2015;489:272–9.
[437] Christensen CH, Johannsen K, Schmidt I, Christensen CH. Catalytic benzene alkylation over mesoporous zeolite single crystals: improving activity and selectivity with a new family of porous materials. J Am Chem Soc 2003;125:13370–1.
[438] Friedel–Crafts alkylation; 2010.
[439] Armengol E, Cano ML, Corma A, Garcia H, Navarro MT. Mesoporous aluminosilicate MCM-41 as a convenient acid catalyst for friedel-crafts alkylation of a bulky aromatic compound with cinnamyl alcohol. J Chem Soc Chem Commun 1995:519–20.
[440] Landau MV, Dafa E, Kaliya ML, Sen T, Herskowitz M. Mesoporous alumina catalytic, material prepared by grafting wide-pore MCM-41 with an alumina multilayer. Microporous Mesoporous Mater 2001;49:65–81.

[441] Niwa M, Okumura K, Matsumoto S, Nishiaki N. Catalytic oxidation of methane on the Pd-mordenite with adjusted aluminum concentration. Abstr Pap Am Chem Soc 2001;222 [U363-U].
[442] Climent MJ, Corma A, Iborra S, Navarro MC, Primo J. Use of mesoporous MCM-41 aluminosilicates as catalysts in the production of fine chemicals: preparation of dimethylacetals. J Catal 1996;161:783–9.
[443] Climent MJ, Corma A, Guil-Lopez R, Iborra S, Primo J. Use of mesoporous MCM-41 aluminosilicates as catalysts in the preparation of fine chemicals - A new route for the preparation of Jasminaldehyde with high selectivity. J Catal 1998;175:70–9.
[444] Iwamoto M, Tanaka Y, Sawamura N, Namba S. Remarkable effect of pore size on the catalytic activity of mesoporous silica for the acetalization of cyclohexanone with methanol. J Am Chem Soc 2003;125:13032–3.
[445] Onaka M, Hashimoto N, Kitabata Y, Yamasaki R. Aluminum-rich mesoporous aluminosilicate (Al-HMS) as a solid acid catalyst for the Diels–Alder reaction of acrylates with 1,3-dienes. Appl Catal Gen 2003;241:307–17.
[446] Kugita T, Jana SK, Owada T, Hashimoto N, Onaka M, Namba S. Mesoporous Al-containing MCM-41 molecular sieves: highly active catalysts for Diels–Alder reaction of cyclopentadiene with α,β-unsaturated aldehydes. Appl Catal Gen 2003; 245:353–62.
[447] Gontier S, Tuel A. Oxidation of aniline over TS-1, the titanium substituted silicalite-1. Appl Catal Gen 1994;118:173–86.
[448] Huybrechts DRC, Bruycker LD, Jacobs PA. Oxyfunctionalization of alkanes with hydrogen peroxide on titanium silicalite. Nature 1990;345:240–2.
[449] Corma A, Navarro MT. Pariente JPr. Synthesis of an ultralarge pore titanium silicate isomorphous to MCM-41 and its application as a catalyst for selective oxidation of hydrocarbons. J Chem Soc Chem Commun 1994;147-8.
[450] Arends IWCE, Sheldon RA. Activities and stabilities of heterogeneous catalysts in selective liquid phase oxidations: Recent developments. Appl Catal Gen 2001; 212:175–87.
[451] Davies LJ, McMorn P, Bethell D, Bulman Page PC, King F, Hancock FE, et al. Oxidation of crotyl alcohol using Ti-β and Ti-MCM-41 catalysts. J Mol Catal A Chem 2001;165:243–7.
[452] Das S, Mitra S, Khurana SMP, Debnath N. Nanomaterials for biomedical applications. Front Life Sci 2014;7:90–8.
[453] Slowing II, Vivero-Escoto JL, Wu C-W, Lin VS-Y. Mesoporous silica nanoparticles as controlled release drug delivery and gene transfection carriers. Adv Drug Deliv Rev 2008;60:1278–88.
[454] Tang F, Li L, Chen D. Mesoporous silica nanoparticles: synthesis, biocompatibility and drug delivery. Adv Mater 2012;24:1504–34.
[455] Slowing II, Trewyn BG, Giri S, Lin VY. Mesoporous silica nanoparticles for drug delivery and biosensing applications. Adv Funct Mater 2007;17:1225–36.
[456] Rahman M, Yu E, Forman E, Roberson-Mailloux C, Tung J, Tringe J, et al. Modified release from lipid bilayer coated mesoporous silica nanoparticles using PEO–PPO–PEO triblock copolymers. Colloids Surf B Biointerfaces 2014; 122:818–22.
[457] Elsabahy M, Wooley KL. Design of polymeric nanoparticles for biomedical delivery applications. Chem Soc Rev 2012;41:2545–61.
[458] Oh JK, Park JM. Iron oxide-based superparamagnetic polymeric nanomaterials: design, preparation, and biomedical application. Prog Polym Sci 2011;36:168–89.
[459] Danhier F, Ansorena E, Silva JM, Coco R, Le Breton A, Preat V. PLGA-based nanoparticles: an overview of biomedical applications. J Control Release 2012; 161:505–22.
[460] Otsuka H, Nagasaki Y, Kataoka K. PEGylated nanoparticles for biological and pharmaceutical applications. Adv Drug Deliv Rev 2012;64:246–55.
[461] Chen AM, Zhang M, Wei D, Stueber D, Taratula O, Minko T, et al. Co-delivery of doxorubicin and Bcl-2 siRNA by mesoporous silica nanoparticles enhances the efficacy of chemotherapy in multidrug-resistant cancer cells. Small 2009;5: 2673–7.
[462] Gao Y, Chen Y, Ji X, He X, Yin Q, Zhang Z, et al. Controlled intracellular release of doxorubicin in multidrug-resistant cancer cells by tuning the shell-pore sizes of mesoporous silica nanoparticles. ACS Nano 2011;5:9788–98.
[463] Kao K-C, Lin T-S, Mou C-Y. Enhanced activity and stability of lysozyme by immobilization in the matching nanochannels of mesoporous silica nanoparticles. J Phys Chem C 2014;118:6734–43.
[464] Shin H-S, Hwang Y-K, Huh S. Facile preparation of ultra-large pore mesoporous silica nanoparticles and their application to the encapsulation of large guest molecules. ACS Appl Mater Interfaces 2014;6:1740–6.
[465] Slowing II, Trewyn BG, Lin VSY. Mesoporous silica nanoparticles for intracellular delivery of membrane-impermeable proteins. J Am Chem Soc 2007;129:8845–9.
[466] Jiao Y, Shen S, Sun Y, Jiang X, Yang W. A functionalized hollow mesoporous silica nanoparticles-based controlled dual-drug delivery system for improved tumor cell cytotoxicity. Part Part Syst Charact 2015;32:222–33.
[467] Ortac I, Simberg D, Yeh Y-s, Yang J, Messmer B, Trogler WC, et al. Dual-porosity hollow nanoparticles for the immunoprotection and delivery of nonhuman enzymes. Nano Lett 2014;14:3023–32.
[468] Chen Y, Chen H, Ma M, Chen F, Guo L, Zhang L, et al. Double mesoporous silica shelled spherical/ellipsoidal nanostructures: synthesis and hydrophilic/hydrophobic anticancer drug delivery. J Mater Chem 2011;21:5290–8.
[469] Fang Y, Zheng G, Yang J, Tang H, Zhang Y, Kong B, et al. Dual-pore mesoporous carbon@silica composite core–shell nanospheres for multidrug delivery. Angew Chem 2014;126:5470–4.
[470] Ma M, Chen H, Chen Y, Wang X, Chen F, Cui X, et al. Au capped magnetic core/mesoporous silica shell nanoparticles for combined photothermo-/chemo-therapy and multimodal imaging. Biomaterials 2012;33:989–98.
[471] Yang J, Shen D, Zhou L, Li W, Li X, Yao C, et al. Spatially confined fabrication of core–shell gold nanocages@mesoporous silica for near-infrared controlled photothermal drug release. Chem Mater 2013;25:3030–7.
[472] Fang W, Tang S, Liu P, Fang X, Gong J, Zheng N. Pd nanosheet-covered hollow mesoporous silica nanoparticles as a platform for the chemo-photothermal treatment of cancer cells. Small 2012;8:3816–22.
[473] Chung IC, Li C-W, Wang G-J. The influence of different nanostructured scaffolds on fibroblast growth. Sci Technol Adv Mater 2013;14:044401.
[474] Wang G-J, Lin Y-C, Li C-W, Hsueh C-C, S-h Hsu, Hung H-S. Fabrication of orderly nanostructured PLGA scaffolds using anodic aluminum oxide templates. Biomed Microdevices 2009;11:843–50.
[475] Izquierdo R, Garcia-Giralt N, Rodriguez MT, Cáceres E, García SJ, Gómez Ribelles JL, et al. Biodegradable PCL scaffolds with an interconnected spherical pore network for tissue engineering. J Biomed Mater Res Part A 2008;85A:25–35.
[476] LaNasa SM, Hoffecker IT, Bryant SJ. Presence of pores and hydrogel composition influence tensile properties of scaffolds fabricated from well-defined sphere templates. J Biomed Mater Res B Appl Biomater 2011;96B:294–302.
[477] Ko Y-G, Kawazoe N, Tateishi T, Chen G. Preparation of chitosan scaffolds with a hierarchical porous structure. J Biomed Mater Res B Appl Biomater 2010;93B:341–50.
[478] Ehrlich H, Krajewska B, Hanke T, Born R, Heinemann S, Knieb C, et al. Chitosan membrane as a template for hydroxyapatite crystal growth in a model dual membrane diffusion system. J Membr Sci 2006;273:124–8.
[479] Li X, Wang X, Chen H, Jiang P, Dong X, Shi J. Hierarchically porous bioactive glass scaffolds synthesized with a PUF and P123 cotemplated approach. Chem Mater 2007;19:4322–6.
[480] Wang GJ, Lin YC, Li CW, Hsueh CC, Hsu SH, Hung HS. Fabrication of orderly nanostructured PLGA scaffolds using anodic aluminum oxide templates. Biomed Microdevices 2009;11:843–50.
[481] Poinern GEJ, Le X, Loomes C, Fawcett D. Biocompatibility of composite membranes composed of anodic aluminium oxide (AAO) and Poly (2-hydroxyethylmethacrylate) for use as a cell culture substrate. Mater Lett 2014;131:182–5.
[482] Chandanshive BB, Rai P, Rossi AL, Ersen O, Khushalani D. Synthesis of hydroxyapatite nanotubes for biomedical applications. Mater Sci Eng C 2013;33:2981–6.
[483] Ramay HR, Zhang M. Preparation of porous hydroxyapatite scaffolds by combination of the gel-casting and polymer sponge methods. Biomaterials 2003;24: 3293–302.
[484] Jo I-H, Shin K-H, Soon Y-M, Koh Y-H, Lee J-H, Kim H-E. Highly porous hydroxyapatite scaffolds with elongated pores using stretched polymeric sponges as novel template. Mater Lett 2009;63:1702–4.
[485] Hu Y, Gu X, Yang Y, Huang J, Hu M, Chen W, et al. Facile fabrication of poly(L-lactic acid)-grafted hydroxyapatite/poly(lactic-co-glycolic acid) scaffolds by pickering high internal phase emulsion templates. ACS Appl Mater Interfaces 2014;6: 17166–75.
[486] Montufar EB, Traykova T, Gil C, Harr I, Almirall A, Aguirre A, et al. Foamed surfactant solution as a template for self-setting injectable hydroxyapatite scaffolds for bone regeneration. Acta Biomater 2010;6:876–85.
[487] Quéré D. Wetting and roughness. Annu Rev Mater Res 2008;38:71–99.
[488] Lau KKS, Bico J, Teo KBK, Chhowalla M, Amaratunga GAJ, Milne WI, et al. Superhydrophobic carbon nanotube Forests. Nano Lett 2003;3:1701–5.
[489] Tuteja A, Choi W, Ma M, Mabry JM, Mazzella SA, Rutledge GC, et al. Designing superoleophobic surfaces. Science 2007;318:1618–22.
[490] McHale G. Cassie and Wenzel: were they really so wrong? Langmuir 2007;23: 8200–5.
[491] Li XM, Reinhoudt D, Crego-Calama M. What do we need for a superhydrophobic surface? A review on the recent progress in the preparation of superhydrophobic surfaces. Chem Soc Rev 2007;36:1350–68.
[492] Koishi T, Yasuoka K, Fujikawa S, Ebisuzaki T, Zeng XC. Coexistence and transition between Cassie and Wenzel state on pillared hydrophobic surface. Proc Natl Acad Sci U S A 2009;106:8435–40.
[493] Chu KH, Xiao R, Wang EN. Uni-directional liquid spreading on asymmetric nanostructured surfaces. Nat Mater 2010;9:413–7.
[494] Courbin L, Denieul E, Dressaire E, Roper M, Ajdari A, Stone HA. Imbibition by polygonal spreading on microdecorated surfaces. Nat Mater 2007;6:661–4.
[495] Mugele F, Baret J-C. Electrowetting: from basics to applications. J Phys Condens Matter 2005;17 [R705-R74].
[496] Berge B, Peseux J. Variable focal lens controlled by an external voltage: an application of electrowetting. Eur Phys J E 2000;3:159–63.
[497] Pollack MG, Fair RB, Shenderov AD. Electrowetting-based actuation of liquid droplets for microfluidic applications. Appl Phys Lett 2000;77:1725.
[498] Chen C-Y, Cheng ZY. An experimental study on Rosensweig instability of a ferrofluid droplet. Phys Fluids 2008;20:054105.
[499] Nguyen NT, Zhu G, Chua YC, Phan VN, Tan SH. Magnetowetting and sliding motion of a sessile ferrofluid droplet in the presence of a permanent magnet. Langmuir 2010;26:12553–9.
[500] Zhou Q, Ristenpart WD, Stroeve P. Magnetically induced decrease in droplet contact angle on nanostructured surfaces. Langmuir 2011;27:11747–51.
[501] Wang Y, Angelatos AS, Caruso F. Template synthesis of nanostructured materials via layer-by-layer assembly. Chem Mater 2008;20:848–58.
[502] Lee D, Cohen RE, Rubner MF. Heterostructured magnetic nanotubes. Langmuir 2007;23:123–9.
[503] Grigoryev A, Tokarev I, Kornev KG, Luzinov I, Minko S. Superomniphobic magnetic microtextures with remote wetting control. J Am Chem Soc 2012;134:12916–9.
[504] Zhu Y, Xiao R, Wang EN. Design and fabrication of magnetically tunable microstructured surfaces. IEEE Explore 2013:1557–60.
[505] Lee S, Yim C, Kim W, Jeon S. Magnetorheological Elastomer Films with Tunable Wetting and Adhesion Properties. ACS Appl Mater Interfaces 2015;7(35):19853–6.

[506] Bernardino NR, Dietrich S. Complete wetting of elastically responsive substrates. Phys Rev E 2012;85.
[507] Lu J, Liong M, Li Z, Zink JI, Tamanoi F. Biocompatibility, biodistribution, and drug-delivery efficiency of mesoporous silica nanoparticles for cancer therapy in animals. Small 2010;6:1794–805.
[508] Zhang Q, Wang X, Li P-Z, Nguyen KT, Wang X-J, Luo Z, et al. Biocompatible, uniform, and redispersible mesoporous silica nanoparticles for cancer-targeted drug delivery in vivo. Adv Funct Mater 2014;24:2450–61.
[509] Fu C, Liu T, Li L, Liu H, Chen D, Tang F. The absorption, distribution, excretion and toxicity of mesoporous silica nanoparticles in mice following different exposure routes. Biomaterials 2013;34:2565–75.
[510] Lee S, Kim M-S, Lee D, Kwon TK, Khang D, Yun H-S, et al. The comparative immunotoxicity of mesoporous silica nanoparticles and colloidal silica nanoparticles in mice. Int J Nanomedicine 2013;8:147–58.
[511] Wu S-H, Mou C-Y, Lin H-P. Synthesis of mesoporous silica nanoparticles. Chem Soc Rev 2013;42:3862–75.